On Enhancing Air Quality Model Predictions of Particulate Matter From Aircraft Emissions

Matthew Woody

A dissertation submitted to the faculty at the University of North Carolina at Chapel Hill in partial fulfillment of the requirements for the degree of Doctor of Philosophy in the Department of Environmental Sciences and Engineering.

Chapel Hill
2014

Approved by:

J. Jason West

Saravanan Arunachalam

Sergey Napelenok

Jason Surratt

William Vizuete

ABSTRACT

MATTHEW WOODY: On Enhancing Air Quality Model Predictions of Particulate Matter From Aircraft Emissions
(Under the direction of J. Jason West and Saravanan Arunachalam)

Aviation is an important mode of transportation and usage is expected to continually grow. However, aircraft emit numerous pollutants that adversely impact air quality. The goal of this work is to provide additional certainty in air quality estimates of one of those pollutants, aircraft-attributable $PM_{2.5}$, during landing and takeoff cycles, using the Community Air Quality (CMAQ) Model and its enhancements.

First, CMAQ's response to secondary organic aerosol (SOA) concentrations, a component of $PM_{2.5}$, formed from aircraft emissions was examined. It was determined that at coarser model resolutions (36-km and 12-km), aircraft NO_x emissions lowered free radical concentrations and thereby reduced SOA precursor oxidation. This directly resulted in the reduction of SOA concentrations, primarily biogenic SOA. At a finer grid resolution (4-km), aircraft primary organic aerosol (POA) emissions provided additional mass for SOA to partition onto, promoting semi-volatile organic carbon species to partition from the particle phase to the gas phase, increasing SOA concentrations.

Secondly, a new formation pathway for modeled $PM_{2.5}$ (based on recent sampling and smog chamber data) was incorporated into CMAQ to account for non-traditional SOA (NTSOA), SOA formed from aircraft emissions of semi and intermediate volatile organic compounds. This new pathway added 1.7% in January and 7.4% in July to aircraft-attributable $PM_{2.5}$ at the Hartsfield-Jackson Atlanta International Airport. Downwind of the Atlanta airport, NTSOA averaged 4.6–17.9% of aircraft-attributable $PM_{2.5}$. These contributions were generally low compared to smog chamber results due to considerably lower ambient organic aerosol concentrations in CMAQ versus those in the smog chamber experiments.

Thirdly, alternative aircraft PM emission estimates based on a 1-D plume model were coupled with a plume in grid (PinG) treatment for aircraft in CMAQ. This treatment increased grid-based

monthly and contiguous U.S. average aircraft-attributable $PM_{2.5}$ by 40% (from 1.9 ng m^{-3} to 2.7 ng m^{-3}) in a winter month and 12% (from 2.4 ng m^{-3} to 2.6 ng m^{-3}) in a summer month. Maximum modeled hourly subgrid scale aircraft-attributable $PM_{2.5}$ concentrations were 23.7 μg m^{-3} in a winter month and 59.3 μg m^{-3} in a summer month, considerably higher than typical grid-based aircraft contributions (0.1 μg m^{-3}).

ACKNOWLEDGMENTS

I would like to thank my advisors, Jason West and Sarav Arunachalam, for their continued support, guidance, patience and mentorship.

I would also like to thank the members of my committee for their time and insights that helped to improve this work.

Finally, I'd like to thank my wife and daughter for their patience and support throughout this process.

TABLE OF CONTENTS

LIST OF TABLES

LIST OF FIGURES

LIST OF ABBREVIATIONS

A25	Other Unspeciated Particulate Matter or Crustal Material
ACRP	Airport Cooperative Research Program
ADSC	Aerosol Dynamics Simulation Code
AE6	Aerosol 6 Module
AEC	Elemental Carbon Aerosol
AEDT	Aviation Environmental Design Tool
AERO	Aerosols Model Process
ANH3	Ammonium Aerosol
ANO3	Nitrate Aerosol
AORGA	Anthropogenic Secondary Organic Aerosol
AORGB	Biogenic Secondary Organic Aerosol
APT	Advanced Plume Treatment
AQM	Air Quality Model
ASO4	Sulfate Aerosol
ATL	Hartsfield-Jackson Atlanta International Airport
CB05	Chemical Bond 2005
CHEM	Chemistry Model Process
CLDS	Cloud and Aqueous Chemistry Model Process
CMAQ	Community Multiscale Air Quality model
CO	Carbon Monoxide
DDEP	Dry Deposition Model Process
EC	Elemental Carbon
EDMS	Emissions and Dispersion Modeling System
EF	Emission Factor
EMIS	Emissions Model Process
EPA	Environmental Protection Agency

FAA	Federal Aviation Administration
FF2	Boeing Fuel Flow Method2
FOA3	First Order Approximation Version 3
FOA3a	First Order Approximation Version 3a
HADV	Horizontal Advection Model Process
HC	Hydrocarbon
HDIF	Horizontal Diffusion Model Process
ICAO	International Civil Aviation Organization
IRP	Integrated Process Rate
IRR	Integrated Reaction Rate
LTO	Landing and Takeoff
MM5	Pennsylvania State University/NCAR Mesoscale Model
NAAQS	National Ambient Air Quality Standards
NEI	National Emission Inventory
NO_3^-	Nitrate Radical
NO_x	Nitrogen Oxides
NTSOA	Non-Traditional Secondary Organic Aerosol
O_3	Ozone
OA	Organic Aerosol
OC	Organic Carbon
OH	Hydroxyl Radical
IVOC	Intermediate Volatility Organic Compound
PBL	Planetary Boundary Layer
PinG	Plume-in-Grid
POA	Primary Organic Aerosol
PERMM	Python-based Environment for Reaction Mechanisms/Mathematics
pyPA	Python-based Process Analysis
PM	Particulate Matter

$PM_{2.5}$	Fine Particulate Matter
SCICHEM	Second-order Closure Integrated puff model with CHEMistry
SAPRC-07	Statewide Air Pollution Research Center 2007
SERDP	Strategic Environmental Research and Development Program
SMOKE	Sparse Matrix Operator Kernel Emissions
SO_2	Sulfur Dioxide
SOA	Secondary Organic Aerosol
SVOC	Semi-Volatile Organic Compound
TOG	Total Organic Gases
TSOA	Traditional Secondary Organic Aerosol
VBS	Volatility Basis Set
VDIF	Vertical Diffusion Model Process
VOC	Volatile Organic Compound
ZADV	Vertical Advection Model Process

CHAPTER 1 INTRODUCTION

Aviation is a vital mode of transportation, rapidly transporting passengers and cargo long distances. In 2013, there were 739.3 million enplanements (passenger boardings) on domestic U.S. flights (Federal Aviation Administration, 2014a), which is equivalent to everyone in the U.S. taking at least one round trip flight ($\sim$2.5 flights per person). U.S. domestic enplanements are projected to grow by 2.3% per year over the next 20 years, reaching an expected 1.15 billion in 2034. Passenger growth on international flights to and from the U.S. is projected to be even greater, increasing at a rate of 4.1% per year over the next 20 years (from 176 million enplanements in 2013 to 403 million in 2033). In terms of cargo, aviation transported 67.8 million short tons in the U.S. in 2013. Compared to other transportation sources, aircraft transport less than 1% of the total weight both domestically and internationally (imports and exports), moving less weight than ships, trucks, rail, and pipelines (U.S. Department of Transportation, 2006). However, due to the high speeds at which aircraft operate, they commonly transport high priority cargo. Therefore, aircraft transport 4% domestically and 27% internationally of the total cargo value, second to trucks domestically and ships internationally.

While aircraft are an important mode of transportation, aircraft directly emit four of the six criteria air pollutants [carbon monoxide (CO), nitrogen dioxide (NO_2), fine particulate matter ($PM_{2.5}$), and sulfur dioxide (SO_2)] set by the National Ambient Air Quality Standards (NAAQS) under the Clean Air Act. Aircraft emissions also contribute to the production of a fifth criteria air pollutant, ozone (O_3), produced by the chemical processing of aircraft emissions of nitrogen oxides [NO_x, or nitrogen oxide (NO) + NO_2] and volatile organic compounds (VOCs) in the atmosphere. However, only aircraft NO_x emissions are currently regulated by the U.S. Environmental Protection Agency (EPA) (U.S. Environmental Protection Agency, 2005) while other transportation sources are generally more heavily regulated. For example, EPA regulations currently limit emissions of 5 pollutants (VOCs, NO_x, CO, formaldehyde, and PM) from light-duty vehicles (cars and light trucks) (http://www.epa.gov/otaq/standards/light-duty/ld-cff.htm).

Of the criteria air pollutants emitted and/or formed from aircraft emissions, aircraft contributions to $PM_{2.5}$ are likely the most uncertain due to multiple components (i.e. primary and secondary, multiple chemical constituents, varying size) and formation pathways. Exposure to $PM_{2.5}$ adversely effects cardiovascular and pulmonary health due to its small size and ability to penetrate deep into the lungs (Dockery and Pope, 1994). $PM_{2.5}$ also impairs visibility (Sisler and Malm, 2000) and impacts climate change (Bauer and Menon, 2012). Emission mitigation and control strategies across all emission sectors have led to a 33% reduction in total national average $PM_{2.5}$ concentrations between 2000 and 2012 (U.S. Environmental Protection Agency, 2013). However, over this same 12 year span, the number of total passengers traveling by aircraft in the U.S. increased by 10% and is expected to continue growing (Federal Aviation Administration, 2014a). Furthermore, the Federal Aviation Administration (FAA) indicates 43 hub (major) airports are located in $PM_{2.5}$ non-attainment areas, exceeding any of the 1997 or 2006 annual/daily average $PM_{2.5}$ standards (Figure 1.1) (Federal Aviation Administration, 2014b). Given the opposing trends in U.S. $PM_{2.5}$ concentrations and aviation activity, the current absence of $PM_{2.5}$ emission control policies for aircraft, and occurrence of airports in non-attainment areas, it is critical to accurately quantify aviation-attributable $PM_{2.5}$ to provide estimates of aviation's current impacts on surface air quality as well help to inform future policies and possible emission control strategies.

$PM_{2.5}$ is defined as particles in the atmosphere smaller than 2.5 micrometers in diameter. It is comprised of seven major components: elemental carbon (EC), sulfate, nitrate, ammonium, secondary organic aerosols (SOA), primary organic aerosols (POA), and crustal material. Of these seven, aircraft directly emit EC, sulfate and POA (primary $PM_{2.5}$ species) as well as emit precursors of sulfate (as SO_2), nitrate (as NO_x), and SOA (as VOCs) (secondary $PM_{2.5}$ species). A sixth component, ammonium, is generally emitted from agricultural activities as ammonia and neutralizes precursors of sulfate and nitrate to form the inorganic $PM_{2.5}$ species ammonium sulfate and ammonium nitrate. Therefore, of the seven major components of $PM_{2.5}$, only crustal material is neither emitted nor formed from aircraft emissions.

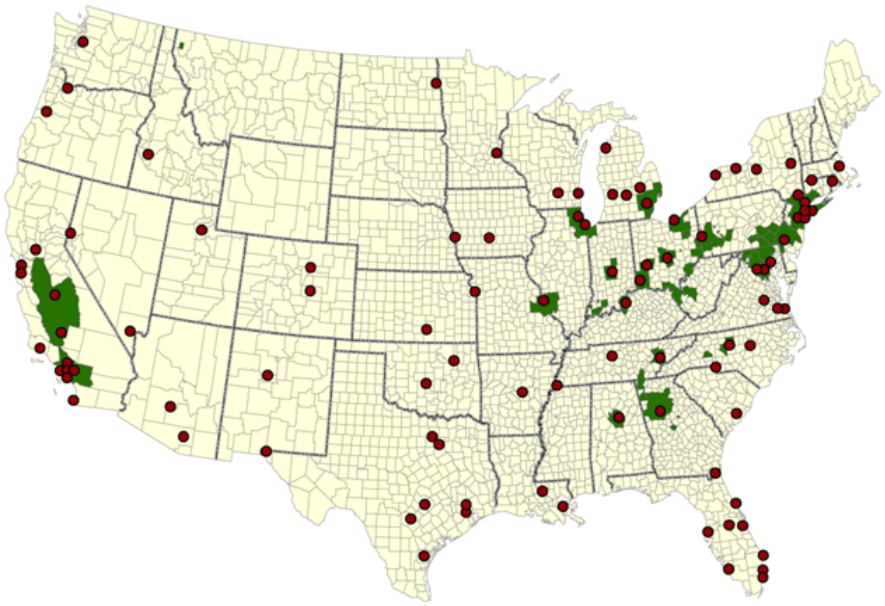

Figure 1.1: $PM_{2.5}$ non-attainment areas (green) and locations of the top 99 airports in the contiguous U.S. (red).

One method to quantify aircraft-attributable $PM_{2.5}$ is by direct measurements, such as those collected during the Aircraft Particle Emissions eXperiment (APEX) 1–3 measurement campaigns (Kinsey et al., 2010). However, these types of measurements only provide a portion of the total picture. They generally only capture primary $PM_{2.5}$ emitted by a single aircraft and often miss secondary $PM_{2.5}$ formed downwind of the aircraft. It is also difficult to scale measurements at an engine level up to determine impacts for in-use aircraft at larger scales (e.g. airport level to regional scales). Furthermore, no standardized sampling methodology currently exists for $PM_{2.5}$ from aircraft. That said, these types of measurements provide useful information for understanding and quantifying aircraft emissions.

Alternatively, measurements can provide emission estimates for aircraft to use in air quality models, such as the Community Multiscale Air Quality (CMAQ) model (Byun and Schere, 2006), which are commonly used to provide source specific predictions of total and speciated $PM_{2.5}$. CMAQ is a 3-dimensional regional air quality model developed and maintained by the U.S. EPA and frequently utilized in research and regulatory applications. CMAQ simulates the major processes in the atmosphere relevant to air quality (e.g. chemistry, transport, emissions) to provide predictions of both

gaseous and particle-phase pollutants. Furthermore, model processes in CMAQ are able to represent the complex nature of $PM_{2.5}$ (comprised of multiple components which include both primary and secondary, formed from multiple pathways, etc.).

CMAQ model estimates have shown that aircraft-attributable $PM_{2.5}$ range from 3.2 ng m^{-3} (0.05% of total $PM_{2.5}$) on an annual average basis in the contiguous U.S. (Woody et al., 2011) to as high as 0.9 μg m^{-3} (9.4% of total $PM_{2.5}$) at the Hartsfield-Jackson Atlanta International Airport (ATL) on a daily average basis (Arunachalam et al., 2011). However, due to uncertainties both inherent to air quality models and associated with the treatment of aircraft emissions in the model, studies have produced a wide range of aircraft-attributable $PM_{2.5}$ estimates. For example, air quality model estimates of aircraft-attributable $PM_{2.5}$ range from less than 1% in winter and statistically insignificant impacts in summer from full flight emissions globally (Lee et al., 2013) to approximately 1.3% of annual average $PM_{2.5}$ from aircraft LTO activities at ATL (Arunachalam et al., 2011). Furthermore, aviation-attributable premature mortality estimates from $PM_{2.5}$ based on air quality results range from 620 per year (Jacobson et al., 2013) to as high as 12,600 (Barrett et al., 2010) for full-flight global aircraft emissions and from 75 (Levy et al., 2012) to 210 (Brunelle-Yeung et al., 2014) for landing and takeoff (LTO) emissions in the U.S.

Traditionally, aircraft emissions in AQMs are treated on an airport level. In this treatment, aircraft emissions are instantaneously diluted into the grid cell containing the airport. However, this over-simplifies the 3-D spatial resolution of aircraft emissions. Unal et al. (2005) sought to improve this approach in an AQM by allocating aircraft emissions in three dimensions and found that the improved treatment lowered ozone and $PM_{2.5}$ impacts from aircraft by 75–80% at ATL. Furthermore, the instantaneous dilution of aircraft emissions into a grid cell can lead to non-linearities in AQM results. For example, Arunachalam et al. (2011) indicated that aircraft contributions to SOA concentrations at ATL varied significantly depending on the modeled grid resolutions. At coarser model grid resolutions (36-km and 12-km), $PM_{2.5}$ concentrations of most species increased in the immediate vicinity of the ATL airport. However, nitrate and SOA concentrations decreased near the airport but increased downwind (Arunachalam et al., 2011). This is in contrast to results at a finer grid resolution (4-km), where aircraft emissions increased SOA concentrations both at and downwind of the ATL airport.

Similarly, uncertainty exists in organic aerosols from aircraft (as well as other emission sources), due to the large number of organic compounds and multiple pathways involved, many of which are not fully understood and some are possibly yet to be discovered (Kroll and Seinfeld, 2008; Miracolo et al., 2011). Recent sampling and smog chamber results have found that a missing formation pathway for aircraft-attributable SOA in air quality models (AQMs) includes SOA formed from semi-volatile and intermediate volatility organic compounds (S/IVOCs) (Miracolo et al., 2012). S/IVOCs are unresolved organic compounds, difficult to measure, and have volatilities between POA (low volatility) and VOCs (relatively high volatility). Also, they are generally considered missing from traditional emission inventory estimates and are believed to form a significant amount of SOA from emissions of combustion sources (Jathar et al., 2014). For aircraft, Miracolo et al. (2012) measured a significant amount of SOA formed from emissions in a smog chamber and were unable to reproduce the results using traditional modeling approaches. They concluded that the gap in measurements and the model was attributable to SOA formed from S/IVOCs emitted by aircraft.

Jathar et al. (2012), utilizing the smog chamber measurements of Miracolo et al. (2012), developed a parameterization for use in AQMs to estimate non-typical SOA (NTSOA) formed from aircraft emissions of S/IVOCs using the volatility basis set (VBS) (Donahue et al., 2006). With the newly developed parameterization, Jathar et al. (2012) was able to better reproduce smog chamber measurements of SOA formed from aircraft emissions in a box model.

Additional uncertainty in AQM estimates of aircraft related impacts is introduced by the methodology to estimate aircraft PM emissions, which typically involves the First Order Approximation (FOA3) (Wayson et al., 2009). However, FOA3 has known limitations. For example, two versions of FOA3 are currently in use, FOA3 (Wayson et al., 2009) and FOA3a (Ratliff et al., 2009), where FOA3a accounts for uncertainties in PM emissions science and characterization at the time it was developed and estimates five times more PM emissions than FOA3. FOA3 organic PM emissions are estimated using measurements obtained from a single engine type (CFM56-2C1), which may or may not be representative of organic PM emissions from the 500+ International Civil Aviation Organization (ICAO) certified engines. Furthermore, comparisons against measurements have shown FOA3 estimates of POA and EC vary by an order of magnitude for 40% of aircraft engines (Stettler et al.,

2011). FOA3 assumes POA emissions are non-volatile (and similarly CMAQ traditionally treats POA as non-volatile) and does not account for variations in POA emissions due to changes in ambient temperature. However, measurements have shown that POA is, in fact, semi-volatile and organic aerosol formation 30 meters downwind of an aircraft engine is highly dependent on ambient temperature due to its volatility (Beyersdorf et al., 2014).

The goal of this work is to reduce uncertainty in predictions of aircraft-attributable $PM_{2.5}$ in an AQM. This task is accomplished in three ways:

1. by investigating the non-linearity of SOA produced from aircraft emissions at the ATL airport from Arunachalam et al. (2011), examining the model processes responsible for the changes in SOA concentrations using process analysis, an advanced diagnostic modeling tool (Chapter 2);

2. by updating CMAQ to include predictions of SOA formed from aircraft emissions of S/IVOC emissions using a parameterization developed by Jathar et al. (2012) based on smog chamber data (Miracolo et al., 2012) (Chapter 3); and

3. by combining plume-in-grid model techniques to remove spatial uncertainty introduced from modeled grid resolution with alternative emission estimates based on a 1-D plume scale model, while simultaneously quantifying both fine scale (subgrid) and regional scale aviation-attributable $PM_{2.5}$ (Chapter 4).

CHAPTER 2 SECONDARY ORGANIC AEROSOL PRODUCED FROM AIRCRAFT EMISSIONS AT THE ATLANTA AIRPORT – AN ADVANCED DIAGNOSTIC INVESTIGATION USING PROCESS ANALYSIS

2.1 Abstract

Efforts using the Community Multiscale Air Quality (CMAQ) model to investigate the impacts of aircraft emissions from the Hartsfield-Jackson Atlanta International Airport have previously shown aircraft emissions increased total daily $PM_{2.5}$ concentrations by up to 9.4% (0.94 μg m^{-3}) with overall impacts varying by modeled grid resolution. However, those results also indicated that secondary organic aerosol (SOA) concentrations in the airport grid cell were reduced due to aircraft emissions at coarser grid resolutions (36-km and 12-km) but not at a finer resolution (4-km). To investigate this anomaly, this study instruments the CMAQ model with process analysis, an advanced diagnostic modeling tool, and focuses on changes to SOA concentrations due to aircraft emissions in the grid cells containing the Atlanta airport at grid resolutions of 36-km, 12-km, and 4-km. Model results indicated aircraft emissions reduced hourly anthropogenic and biogenic SOA concentrations at the 36-km and 12-km grid resolutions by up to 6.2% (0.052 μg m^{-3}) by removing nitrate, hydroxyl, and hydroperoxy radicals through chemistry. At the 4-km resolution, however, hourly modeled SOA concentrations increased (primarily due to changes in biogenic SOA) by up to 11.5% (0.081 μg m^{-3}) due to primary organic aerosol emissions from aircraft, with the additional organic mass shifting partitioning of SOA semi-volatile gas phase species into the particle phase.

2.2 Introduction

Aviation is an integral part of daily global activities, transporting approximately 725 million passengers and 67 million tons of cargo in the U.S. in 2011 over approximately 18 million flights (Federal Aviation Administration, 2012a). The number of passengers flying is expected to grow by 3.1% per year through 2032 and eclipse 1 billion passengers in 2024 (Federal Aviation Administration, 2012b). While important to transportation, aircraft contribute to both noise and air pollution. Aircraft are the third largest producer of greenhouse gas emissions (11.6% of the total) within the U.S. transportation

sector behind light duty vehicles (58.7%) and freight trucks (19.2%) (U.S. Department of Transportation, 2010) and account for 3.5% of global anthropogenic radiative forcing (Lee et al., 2009). Furthermore, aviation activities have known emissions of CO, NO_x, volatile organic compounds (VOCs), SO_x, $PM_{2.5}$, and numerous hazardous air pollutants which adversely affect air quality (Brasseur et al., 1998; U.S. EPA, 1999; Wilkerson et al., 2010). In 2006, global commercial aircraft activities emitted approximately 2.7 Tg of NO_x (as NO_2-equivalent), 0.68 Tg of CO, 0.10 Tg of hydrocarbons (as CH_4-equivalent), 0.038 Tg of black carbon, 0.0041 Tg of primary sulfate aerosols, and 0.0028 Tg of primary organic aerosols (Wilkerson et al., 2010; Olsen et al., 2013). Ambient measurements have indicated that aircraft emit nanoparticles, with emissions (on the order of 10^{15}–10^{17} particles per kg of fuel burn) comparable on a per unit fuel burn basis to the number of particles generated from ship emissions, biomass burning and forest fires (Kumar et al., 2013) and which increase background particle number concentrations by up to 100 times, or 10^7 particles cm^{-3} (Zhu et al., 2011). Measurements have also shown aircraft emit secondary organic aerosol (SOA) precursors and the formation of SOA from those precursors can surpass primary aircraft PM emissions at idle (4% thrust), taxing (7% thrust), and approach (30% thrust) engine power settings (Miracolo et al., 2011). In this study, the focus is on the effects of aircraft emissions to fine particulate matter ($PM_{2.5}$) concentrations, and more specifically the SOA component of $PM_{2.5}$ at the Hartsfield-Jackson Atlanta International (ATL) airport.

Organic compounds as a whole make up 20%–90% of aerosol mass in the lower troposphere (Kanakidou et al., 2005). Kroll and Seinfeld (2008) suggest that the pathways leading to the formation and evolution of SOA are likely the area with the largest uncertainties concerning organic aerosols in the atmosphere and while scientific understanding of SOA continues to evolve, it is believed there are still additional undiscovered as well as not yet fully understood precursors and pathways of SOA formation. Currently, the most widely accepted pathway is the oxidation of VOCs (primarily monoterpenes and aromatics) by free radicals—mainly the hydroxyl (OH) radical, ozone (O_3), and nitrate (NO_3^-) radical—to form semi-volatile products of lower volatility which partition between the gas and particle phase (Kroll and Seinfeld, 2008).

Specific to aircraft emissions, only a limited number of studies have examined air quality impacts

(Moussiopoulos et al., 1997; Brasseur et al., 1998; Pison and Menut, 2004; Carslaw et al., 2006) in an air quality model (AQM), none of which explicitly examine SOA production due to aircraft emissions. Woody et al. (2011) modeled air quality impacts to speciated $PM_{2.5}$ from aviation in a current and future year scenario from 99 major U.S. airports. Impacts to SOA near airports were insignificant, while inorganic species and elemental carbon comprised the majority of impacts. In fact, Woody et al. (2011) reported that despite aircraft emissions containing SOA precursors (e.g. xylene, toluene, benzene), they lowered total SOA concentrations at the Atlanta airport. Recent sampling and experimental results from Miracolo et al. (2011) suggest otherwise. Aircraft emissions from a CFM56-2B engine formed significant amounts of secondary PM after 3 hours of photooxidation in a smog chamber (SOA at low engine power settings and sulfate aerosol at high engine power settings). The formation of relatively significant amounts of SOA at low engine power settings suggests that there are possible missing precursors from aircraft emission estimates currently used in AQMs.

At Atlanta, Unal et al. (2005) was one of the first to model aircraft impacts to $PM_{2.5}$, treating aircraft as line sources as opposed to the traditional point source treatment. However, only total $PM_{2.5}$ was considered. Subsequently, air quality and health impacts from commercial aircraft emissions were studied at the Atlanta, Chicago O'Hare, and Providence T.F. Green airports using a multiscale (36-km, 12-km, and 4-km) modeling approach (Arunachalam et al., 2011). A three-dimensional and realistic representation of aircraft emissions was developed using the EDMS2Inv tool (Baek et al., 2007), an interface between the FAA's Emissions and Dispersion Modeling System (EDMS) (Federal Register Notice, 1998), the required model for assessing air quality impacts from aviation sources in the U.S., and the Sparse Matrix Operator Kernel Emissions (SMOKE) model (Houyoux et al., 2000). Commercial aircraft emissions were included up to 3,000 m and based on landing and take-off (LTO) cycles, which include startup, taxiing, queuing, takeoff, climb-out, and approach (Arunachalam et al., 2011). Aircraft emissions increased total $PM_{2.5}$ contributions overall both at and downwind of the three airports and grid resolutions considered. While the concentrations of most $PM_{2.5}$ species increased in the immediate vicinity of the ATL airport, nitrate and SOA concentrations decreased near the airport but increased downwind of it at the 36-km and 12-km resolutions (Arunachalam et al., 2011), consistent with the SOA results reported by Woody et al. (2011) for ATL. At the 4-km

grid resolution however, aircraft increased SOA concentrations both at and downwind of the ATL airport.

This work serves as an extension of the Arunachalam et al. (2011) study, and investigates the unexpected reduction of SOA concentrations near the airport due to aircraft emissions in the coarser grid resolutions despite SOA precursors contained in aircraft emissions. The overall objective is to determine model sensitivities of SOA concentrations from aircraft emissions at the ATL airport when using various model grid resolutions, and to determine the primary model processes responsible for this sensitivity.

2.3 Methodology

The Pennsylvania State University/NCAR mesoscale model (MM5) (Grell et al., 1994), SMOKE model, and Community Multiscale Air Quality (CMAQ) (Byun and Ching, 1999; Byun and Schere, 2006) v4.7 model were used to estimate the effects of aircraft emissions from the ATL airport on SOA. CMAQ treats PM formation through a trimodal approach (Binkowski and Roselle, 2003). $PM_{2.5}$ particles are represented by two lognormal distributions for the Aitken and accumulation modes; a third lognormal distribution represents coarse particles up to PM_{10}. CMAQ treats the following components of $PM_{2.5}$ explicitly in each of these modes: sulfate (ASO4), nitrate (ANO3), ammonium (ANH4), primary organic aerosol (POA), anthropogenic secondary organic aerosol (AORGA), biogenic secondary organic aerosol (AORGB) (total SOA = AORGA + AORGB), elemental carbon (AEC), and other unspeciated PM or crustal (A25). CMAQ v4.7 includes several updates in its treatment of $PM_{2.5}$ and SOA, including high/low-NO_x SOA pathways; the incremental evaluation of the updates is available elsewhere (Carlton et al., 2010; Foley et al., 2010).

Two emissions scenarios were considered: a base case with emissions estimated using the EPA's 2002 National Emissions Inventory (NEI) (U.S. EPA, 2004) and excluding the reported commercial aircraft emissions and a sensitivity case which included the base case plus commercial aircraft emission estimates for ATL. Both emission scenarios were modeled at three grid resolutions, 36-km and nested 12-km and 4-km [for additional details, see Figure 2.1 of Arunachalam et al. (2011)]. The vertical resolution consisted of 22 layers of variable height from the surface to 50 mbar (about 18 km) in the 36-km and 12-km grid resolutions and 19 layers from the surface to 100 mbar (about 15 km) in

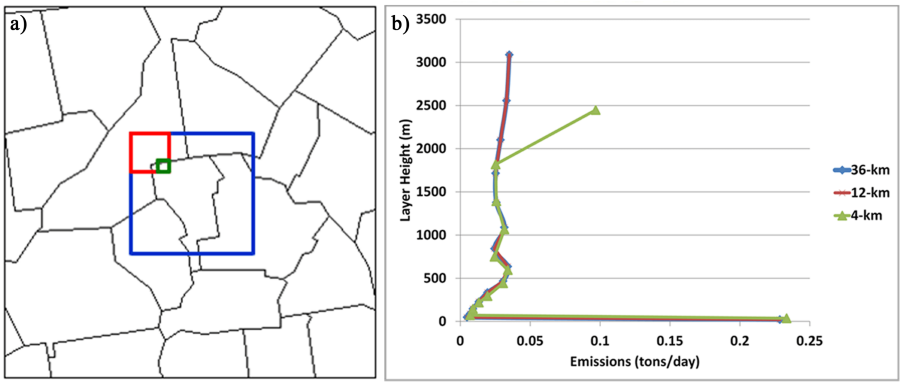

Figure 2.1: (a) The grid cell containing the ATL airport at the 36-km (blue), 12-km (red), and 4-km (green) grid resolutions with counties outlined in black. (b) The vertical profile for modeled $PM_{2.5}$, aircraft emissions at the ATL airport on June 6, 2002 for the 36-km, 12-km, and 4-km grid resolutions. Note the difference in emissions in the uppermost layer of the 4-km grid resolution was due to differences in vertical structure between the 36 and 12-km resolutions and the 4-km resolution.

the 4-km grid resolution. Meteorological input, based on 2002 data, was generated using MM5 with the 12-km resolution derived from a nested simulation of the 36-km while the 4-km meteorology was generated using separate inputs. Aircraft LTO emissions were modeled up to 3,000 m, corresponding to the lowest 15 layers in each grid resolution. With the exception of the horizontal and vertical grid resolutions and corresponding meteorological inputs, the modeling configuration and emissions inventories used were identical for each of the 3 grid resolutions. Figure 2.1a shows the location of the grid cell containing the ATL airport in the 36-km, 12-km, and 4-km grid resolutions. Though the inputs represent 2002 emissions and meteorology, the methodologies to generate them, including the aircraft emission inventories, remain mostly unchanged. Therefore, inputs based on a more recent year would likely produce similar results [e.g. Woody et al. (2011)].

Commercial aircraft emissions data, based on LTO cycles up to 3,000 m, were generated from a research version of EDMS, processed through the EDMS2Inv tool, and finally input into SMOKE. These emission estimates included VOCs (which include SOA precursors), CO, NO_x, SO_x, and $PM_{2.5}$ from 2005 aircraft flight activity at ATL. Speciated primary $PM_{2.5}$ emissions from aircraft were included for sulfate, elemental carbon (EC), and organic carbon (OC) using a conservative extension of the International Civil Aviation Organization Council's Committee on Aviation Environmental Protection's endorsed First Order Approximation v3 (FOA3) (Wayson et al., 2009). Figure 2.1b illustrates

the vertical profile of ATL aircraft emissions of $PM_{2.5}$ on June 6, 2002 in the lowest 15 layers of the model (3,000 m) at each grid resolution. The emission profile indicates that aircraft emissions are highest at the surface due to long aircraft idle times and max thrust during takeoff. Note that the overall vertical emission profile for the three grid resolutions was essentially identical with the exception of the highest layer (layer 15) in the 4-km resolution and attributable to differences in vertical grid structures. Additional details regarding aircraft emission estimates are located in Appendix A and elsewhere (Arunachalam et al., 2011).

From the June and July modeling already performed by Arunachalam et al. (2011), June 6 and 7 were selected as the two-day episode exhibiting the largest reduction in daily average SOA concentrations attributed to aircraft emissions for the 12-km and 36-km grid resolutions at ATL (0.005 μg m^{-3} and 0.014 μg m^{-3} reductions at the 36-km resolution, 0.011 μg m^{-3} and 0.003 μg m^{-3} reductions at the 12-km resolution, and 0.015 μg m^{-3} and 0.002 μg m^{-3} increases at the 4-km resolution). This two-day period was characterized with generally high aircraft emissions (although not the highest for the 2 months) and below average nighttime wind speeds when compared to other days in June and July (additional details on the modeled winds for the two-day episode and June and July are available in Appendix A). Given that the overall objective of this study is to perform a diagnostic investigation of modeled SOA formation due to aircraft emissions, we feel justified in focusing on the two-day episode out of the two months that were modeled, and still be able to obtain adequate new information that may be relevant for both scientific and policy assessments. Additionally, while we are unaware of similar studies focusing on SOA, other studies using process analysis to investigate changes in O_3 and $PM_{2.5}$ have similarly examined results over one to two day episodes (Xu et al., 2008; Yu et al., 2008).

The CMAQ configuration used in Arunachalam et al. (2011) was reconfigured with CMAQ v4.7 and to include process analysis (Jeffries and Tonnesen, 1994; Jang et al., 1995; Hogrefe et al., 2007; Liu et al., 2011) over this two-day period. Process analysis is an advanced diagnostic tool available within CMAQ to provide hourly integrated process rates (IPR) and integrated reaction rates (IRR) data for each of the scientific processes and reactions responsible for changes in concentrations in the model. It follows then, that the incremental contributions of aircraft emissions on concentrations,

Table 2.1: Number of modeled days in June and July that aircraft emissions in the grid cell containing the ATL airport increased $PM_{2.5}$ concentrations by at least 0.1 μg m^{-3} and decreased (increased) SOA concentrations by at least 1 ng m^{-3} at the 36-km and 12-km (4-km) grid resolutions based on results from Arunachalam et al. (2011).

Species	Change in Concentration	36-km (days)	12-km (days)	4-km (days)
$PM_{2.5}$	> 0.1 μg m^{-3}	32	60	61
SOA	> 1 ng m^{-3}	—	—	59
	< -1 ng m^{-3}	50	54	—

Table 2.2: Average modeled change in $PM_{2.5}$ and SOA concentrations due to aircraft emissions at the ATL airport on June 6 and 7, 2002.

Grid Resolution	Change in $PM_{2.5}$		Change in SOA	
	Absolute (μg m^{-3})	Percent (%)	Absolute (μg $^{-3}$)	Percent (%)
36-km	0.182	1.8	-0.009	-2.4
12-km	0.55	5.5	-0.007	-1.7
4-km	0.943	9.4	0.009	2.3

IPR, and IRR can be computed by taking the difference between CMAQ simulations with and without aircraft emissions. The model simulation included one day of spin-up, June 5, 2002, and initial conditions for each resolution were provided by the previous day's output (June 4, 2002) from the 2-month modeling performed by Arunachalam et al. (2011). The 12-km and 4-km episodes were nested simulations from the coarser domains with boundary conditions provided by 36-km and 12-km results, respectively. While modeling a short episode limits the amount of model results, doing so helps focus on those model processes responsible for the reduction of SOA concentrations at the 36 and 12-km grid resolutions at a greater detail. In fact, in the grid cell containing the airport, aircraft emissions decreased daily average SOA concentrations by at least 1 ng m^{-3} in the 36-km and 12-km grid resolutions and increased SOA concentrations by at least 1 ng m^{-3} in the 4-km grid resolution for the majority of modeled days in June and July as indicated by Table 2.1. Therefore, while the magnitude of change in SOA concentrations due to aircraft emissions was higher during this two-day period, the underlying model processes leading to these results were not unique. For comparison, $PM_{2.5}$ concentrations increased by at least 0.1 μg m^{-3} for the majority of days in each of the modeled grid resolutions (Table 2.1).

Using the Python-based Process Analysis (pyPA) (Henderson et al., 2011) and the Python-based

Environment for Reaction Mechanisms/Mathematics (PERMM) (Henderson et al., 2009) to post process and analyze CMAQ process analysis output, respectively, we analyzed model outputs from each grid resolution for each of the three single grid cells containing the airport (Figure 2.1). Additional analysis for the 9 grid cells at the 12-km resolution and the 81 grid cells at the 4-km resolution that match the spatial extent of the single 36-km grid cell can be found in Appendix A.

2.4 Results

Table 2.2 indicates the model results for the changes in average ground-level $PM_{2.5}$ and SOA concentrations over the two-day episode due to aircraft emissions in the grid cell containing the airport. Figure 2.2 indicates the spatial impacts of aircraft emissions on both average $PM_{2.5}$ and SOA concentrations over the two-day period in the area surrounding the airport. The largest impacts of aviation emissions on $PM_{2.5}$ and SOA occurred in the grid cell containing the airport, but also extended to downwind grid cells, for $PM_{2.5}$ sometimes stretching beyond the 180-km x 180-km box centered on the airport, albeit at lesser magnitudes.

Figure 2.3 indicates the modeled speciated daily average $PM_{2.5}$ contributions from aircraft emissions at the grid cell containing the airport on June 6 and 7, 2002. The largest contributions from aircraft emissions were from aerosol EC and ASO4, with negative contributions from SOA at the 36-km and 12-km grid resolutions and ANO3 at all three grid resolutions with the exception of the 36-km grid resolution on June 6 (see Appendix A for further discussion on this result).

Ground-level SOA IPR time series data, which include concentrations (Conc) and the various science processes modeled by CMAQ: horizontal (HADV) and vertical advection (ZADV), horizontal (HDIF) and vertical diffusion (VDIF), chemistry (CHEM), emissions (EMIS), cloud processes and aqueous chemistry (CLDS), aerosols (AERO), and dry deposition (DDEP), were examined for the grid cell containing the airport at each modeled grid resolution. Results indicated aircraft emissions lowered the rate of formation of aerosol mass (AERO process) in the coarser resolutions and increased it in the finer resolution (Figure 2.4a). In the 36-km and 12-km resolutions, the most apparent reduction in AERO process rate attributable to aircraft emissions (and responsible for reductions of SOA concentrations) occurred primarily during nighttime hours [and correspond to reductions in biogenic SOA (Figure 2.6a)], with the most significant reductions occurring between 0300 – 0500 GMT (2300

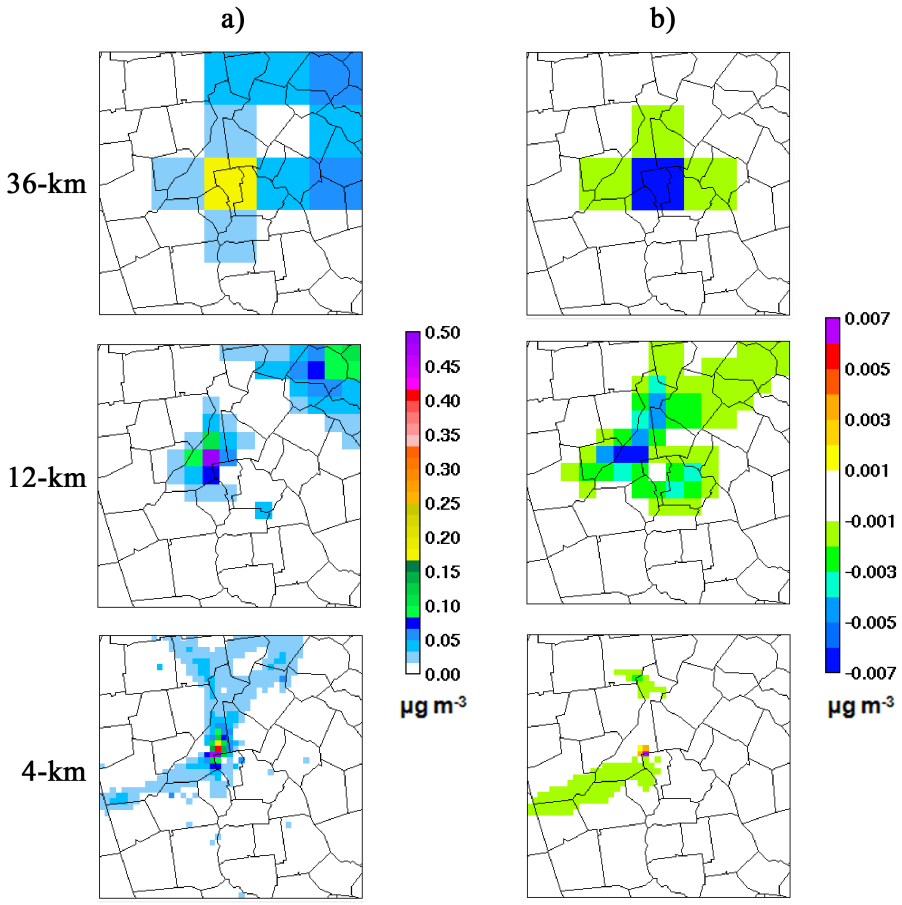

Figure 2.2: Two-day average model results for June 6 and 7, 2002 indicating the impacts of aviation emissions on average (a) $PM_{2.5}$ and (b) SOA concentrations at 36-km, 12-km, and 4-km grid resolutions. Note the highest $PM_{2.5}$ impacts occur in the grid cell containing the ATL airport.

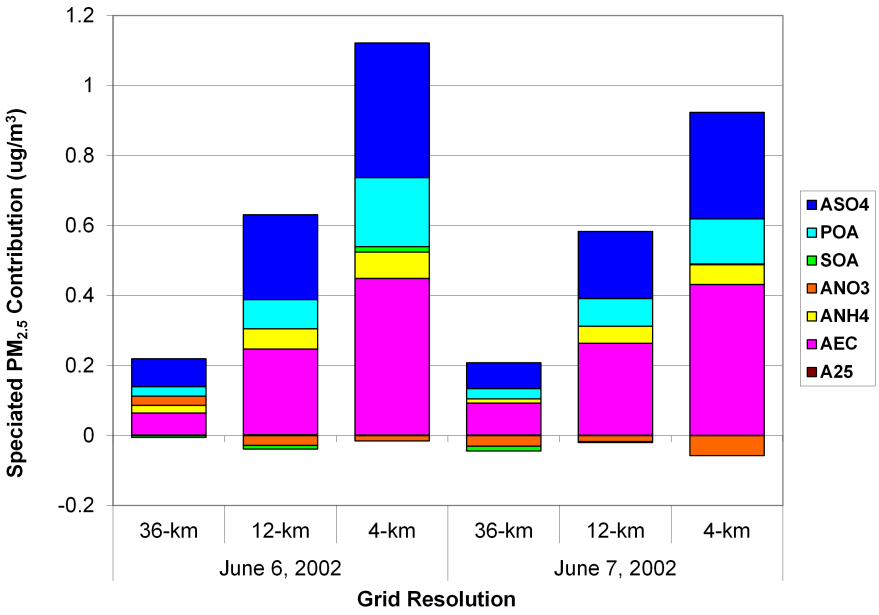

Figure 2.3: Modeled speciated daily average $PM_{2.5}$ contributions by mass from aircraft emissions at the grid cell containing the ATL airport on June 6 and 7, 2002 for sulfate (ASO4), primary organics (POA), secondary organics (SOA), nitrate (ANO3), ammonium (ANH4), elemental carbon (AEC), and crustal (A25) aerosols.

– 0100 LST) on June 6 and 0600 – 0700 GMT (0200 – 0300 LST) on June 7. It is worth noting that the changes in SOA concentrations due to aircraft emissions from processes associated with meteorology (HADV, ZADV, and CLDS), while important for aerosol formation in general, were minor. Examination of the SOA precursor and radical concentration time series data indicated that only NO_3 radical concentrations (of all the radicals in CMAQ which oxidize SOA precursors) exhibited significant changes due to aircraft emissions during these time periods, and were therefore responsible for the reduction in SOA concentrations. Note, only biogenic SOA precursors (monoterpene, isoprene, and sesquiterpene) undergo oxidation reactions with NO_3^- in CMAQ v4.7, and therefore reductions of NO_3^- concentrations have a larger impact on biogenic SOA (see Reactions A.4 and A.7 of Appendix A). This is particularly relevant since ATL is situated in the Southeastern U.S., which is dominated by biogenic VOC emissions, and hence forms higher levels of biogenic SOA (Morris et al., 2006). The change in ground-level nitrate radical IPR time series data in the grid cell containing the airport indicated that the ground-level reduction in radical concentrations from aircraft emissions were attributed

to changes in the vertical diffusion transport process. Additionally, process rates and concentrations for both SOA and nitrate radical integrated over the well-mixed volume of air within the planetary boundary layer (PBL) in the grid cell containing the airport indicated similar results when compared to the surface layer, suggesting the processes responsible for the reduction of nitrate radicals and SOA concentrations occurred above the PBL. Further details and discussion regarding the PBL heights at each of the three grid resolutions can be found in Appendix A.

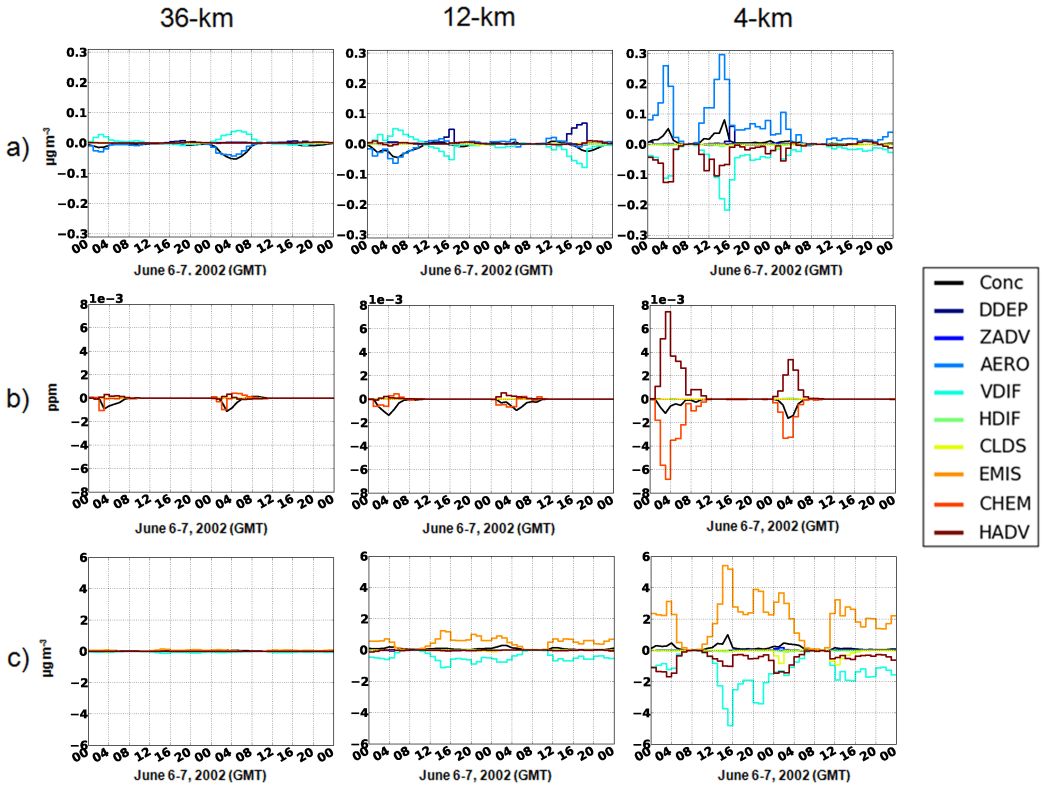

Figure 2.4: Modeled changes in Integrated Process Rates due to aircraft emissions for (a) SOA (surface layer), (b) NO_3^- radical (integrated over all layers above the PBL), and (c) POA (surface layer).

To determine the fate of nitrate radicals above the PBL, process rates in all layers above the PBL in the grid cell containing the airport (Figure A.13 of the Appendix A) were integrated using pyPA and examined using PERMM (Figure 2.4b). PyPA provides the ability to include (or exclude) results in layers above (or within) the PBL and accounts for the diurnal changes in PBL height. Figure 2.4b indicates that the CHEM process was the primary cause of the reduction of nitrate radical concentrations due to aircraft emissions during nighttime hours above the PBL. Integrated reaction

rates (not shown) indicate that this modeled reduction is attributed to increased NO_2 emissions from aircraft, both at the ground-level and aloft (up to 3,000 m in this particular instance), which reacted with nitrate radicals to form N_2O_5. The newly formed N_2O_5 was then both transported away from the grid cell containing the airport through advection as well as converted to HNO_3 by the N_2O_5 heterogeneous reaction to aerosol mechanism. Therefore, with the addition of aircraft emissions, fewer nitrate radicals were available to oxidize SOA precursors, thus lowering SOA production at the 36-km and 12-km grid resolutions

Using ambient measurements, (Rollins et al., 2012) indicated NO_x emissions can significantly increase nighttime SOA concentrations by forming of NO_3^- radicals (by way of reactions of NO_2 with O_3). Conversely, the modeled aircraft impacts here indicate aircraft NO_x emissions, the majority of which are NO (Wood et al., 2008), titrate O_3, and in the process convert NO to NO_2. The reduction in O_3 coupled with the increase in NO_2 concentrations (which reacts with NO_3^- to form N_2O_5) lower NO_3^- (and SOA) concentrations.

At the 4-km grid resolution, while nitrate radicals are similarly reduced with the addition of aircraft emissions, the CHEM process does not reduce modeled SOA production in the same manner as in the 36-km or 12-km resolutions. Instead, changes in modeled POA concentrations dominated changes to SOA concentrations, leading to higher SOA production due to aircraft emissions. As POA concentrations increased, additional organic matter promoted semi-volatile gas phase SOA species to partition to the particle phase, and modeled SOA yields determined by the Odum partitioning theory (Odum et al., 1996) increased (Hallquist et al., 2009; Schell et al., 2001). The modeled spike in POA concentrations at the 4-km grid resolution correlates with the highest SOA concentrations (Figure 2.4c). Figure 2.4c also indicates that the changes in modeled POA concentrations were attributed to direct emissions from aircraft. While the mass of POA emissions from aircraft was roughly equivalent at the three grid resolutions, larger grid volumes at the coarser resolutions led to dilution, lowering concentrations and reducing the impact of changes in POA on changes to SOA due to aircraft emissions (Figures 2.5a and 2.5b).

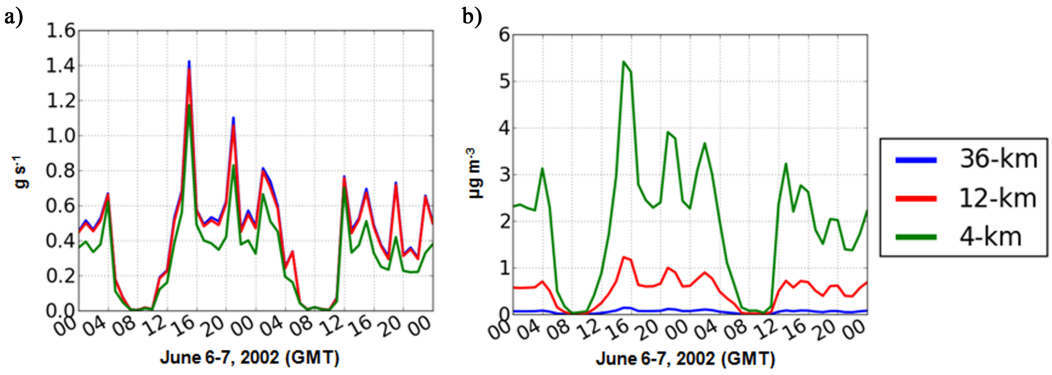

Figure 2.5: Modeled ground-level POA emissions from aircraft on (a) a mass (grams per second) basis and (b) a concentration (micrograms per cubic meter) basis at the grid cell containing the airport. Note in the 4-km grid resolution, a small portion of the airport extends into an adjacent grid cell, and therefore the mass-based emissions are slightly lower in the single grid cell containing the (majority of the) airport when compared against the 12-km and 36-km grid resolutions.

While changes in hourly biogenic SOA concentrations were more apparent compared to anthropogenic SOA (Figure 2.6a), reductions in anthropogenic SOA persisted throughout the day, accounting for 42% and 58% of the two-day average reduction in total SOA concentrations due to aircraft in the 36-km and 12-km grid resolutions, respectively (anthropogenic SOA accounts for 4% of the change in total SOA in the 4-km grid resolution). One would expect that anthropogenic SOA precursors contained in aircraft exhaust (toluene, xylene, and benzene) would increase SOA concentrations. Instead, NO emissions reduce OH and hydroperoxy (HOO) radicals through O_3 titration during the day and radical termination at night. Lower OH radical concentrations hinder the oxidation of anthropogenic SOA precursors (Reactions A.8, A.11, and A.14 of Appendix A). In CMAQ v4.7, anthropogenic SOA precursors only undergo oxidation with OH whereas biogenic SOA precursors undergo oxidation with OH, NO_3^-, O_3, and odd oxygen and therefore the change in OH radicals has a greater influence on anthropogenic SOA than biogenic. The reduction of HOO radicals lowers the amount of SOA formed through the low-NO_x pathway in CMAQ (Figure 2.6c; Reactions A.10, A.13, and A.16 of Appendix A). Note that CMAQ v4.7 only contains high and low-NO_x pathways for anthropogenic SOA, and therefore biogenic SOA is not impacted by changes in HOO. Given that more SOA is formed through the low-NO_x pathway at ATL in the base case (Figure 2.6d), reductions in HOO

concentrations prevent SOA from being formed via this pathway and therefore lead to more significant reductions in anthropogenic SOA concentrations compared to the high-NO_x pathway. In the 4-km resolution, O_3, OH, and HOO concentrations were similarly reduced but the increase in POA emissions counteracted any reduction in anthropogenic SOA.

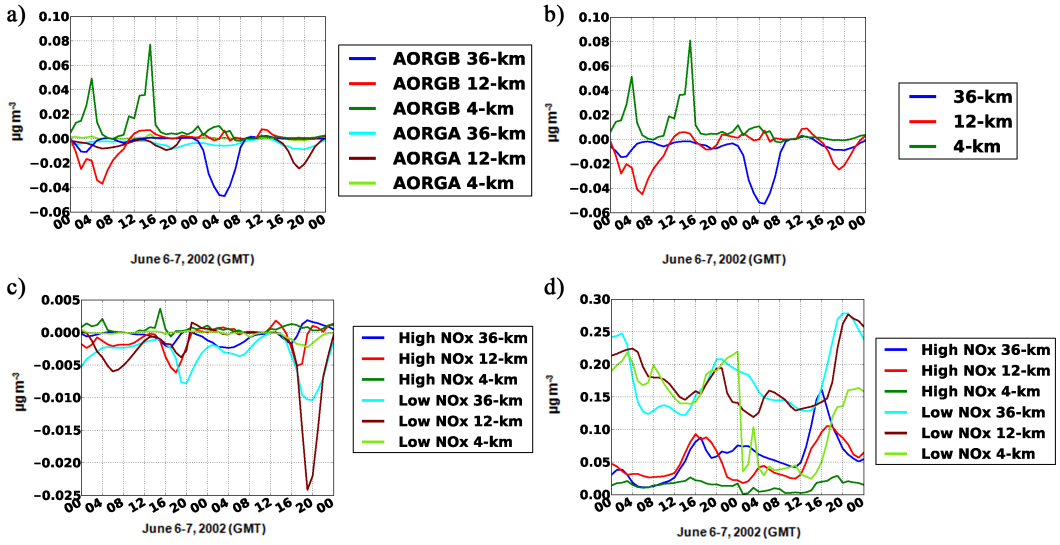

Figure 2.6: Changes in (a) anthropogenic (AORGA), biogenic (AORGB), and (b) total SOA concentrations due to aircraft emissions at ATL. Changes in anthropogenic SOA concentrations formed from low and high-NO_x pathways at ATL (c) due to aircraft emissions and (d) due to emissions from all sources.

2.5 Discussion

It is difficult to determine whether a particular grid resolution is a more accurate representation of the actual effects of aircraft emissions on SOA production, without further research. From a health impact perspective, Arunachalam et al. (2011) have shown that population exposure to $PM_{2.5}$ from aircraft activities varied little between 12-km and 36-km model resolutions and while the 4-km resolution had the highest overall contributions to $PM_{2.5}$ at the airport; total health impacts were lower compared to the 36-km resolution due to population distributions. Similarly from a policy perspective, though the results are not specific to aircraft, Arunachalam et al. (2006) have shown that a 12-km resolution is preferred when performing NAAQS-related modeling for O_3 and $PM_{2.5}$. For SOA from aircraft, recent smog chamber results have suggested that a significant fraction of $PM_{2.5}$ formed from aircraft emissions are comprised of SOA, which somewhat agrees with the 4-km results though likely

for the wrong reasons. The 4-km results were due to changes in biogenic SOA, and along with the 36-km and 12-km results suggest that none of the three modeled resolutions in this study accurately depict SOA formation from aircraft emissions. Therefore, current models appear to underpredict SOA production from aircraft emissions likely due to missing SOA precursor emissions in traditional emission inventories, and is an area where future enhancements are needed in modeling approaches (Miracolo et al., 2011). Complicating the problem is the lack of ambient SOA measurements from aircraft emissions, making comparisons against ambient data essentially impossible. Given the current modeling limitations for SOA from aircraft, care must be taken when interpreting aircraft contributions for other types of studies (e.g. health impacts) considering that the SOA component is likely underpredicted. However, this work provides insights into the model sensitivities of SOA formation as it pertains to aircraft emissions, as well as the need to continually evaluate how SOA is represented in AQMs.

Model results of aircraft contributions to TC concentrations at the ATL airport for June (0.019 μgC m^{-3}, 0.073 μgC m^{-3}, and 0.212 μgC m^{-3} for 36-km, 12-km, and 4-km, respectively) from this study were comparable to those of a modeling study (using organic markers) which estimated aircraft contributions to TC often exceeded 0.1 μgC m^{-3} in the Southeastern U.S. (Bhave et al., 2007). While one might suggest that these modeled contributions from aircraft are relatively small, because of the unique nature of aircraft emissions and the projected increase in demand for aviation, ongoing developments in our understanding of the formation of SOA and continued research to quantify their impacts at multiple modeling scales is imperative. This work is a prime example; although it is possible that other emission sources could produce similar modeled changes to SOA concentrations as those discussed here, factors unique to aircraft emissions, such as their 4-dimensional emissions profile, serve an important role in producing these results.

Future expansion of this work would include exploring alternative approaches to modeling SOA production for aircraft, such as the VBS. Jathar et al. (2012), building on the work of Miracolo et al. (2011), recently published SOA yields mapped to the VBS for unidentified non-traditional SOA (NTSOA) precursors from aircraft emissions and which are currently excluded in AQMs. These

yields, which were fit to sampling and smog chamber results, significantly enhanced SOA formation in a box model. They also provide the inputs necessary to predict NTSOA formed from aircraft emissions in an AQM using the VBS. Another consideration would include modeling aircraft individually using a sub-grid scale treatment, or other alternate approaches to include sub-grid variability, to track the formation of aerosols due to aircraft emissions near the aircraft engine and downstream to avoid sensitivities of results to model grid resolutions. Specifically, this would include obtaining additional information from previous and ongoing field campaigns that include measurement of volatile components of PM from aircraft engines (Kinsey et al., 2010) and newly developed techniques to estimate aircraft PM emissions such as the 1-D plume-scale Aerosol Dynamics Simulation Code (ADSC) model (Wong et al., 2008), as well as ongoing projects funded by the Transportation Research Board's Airport Cooperative Research Program (ACRP) and the U.S. Department of Defense Strategic Environmental Research and Development Program (SERDP) (Miracolo et al., 2011), and using this new information to enhance the modeling approaches discussed here.

It should be noted that the model emissions used in this study were originally generated for CMAQ v4.6 and therefore did not contain sesquiterpene from biogenic sources, one of the new SOA precursors implemented in v4.7. However, changes to SOA formed from sesquiterpene would likely exhibit similar results to the biogenic SOA results presented here, with aircraft reducing concentrations at the 36-km and 12-km grid resolutions and increasing concentrations at the 4-km grid resolution. And finally, given the relative importance of finer grid resolutions that are needed for characterizing maximum individual health risk versus coarser grid resolutions for characterizing general population health risk (Arunachalam et al., 2011), our findings from this investigation provide additional insights into the relevant atmospheric processes due to aircraft emissions occurring at different grid-scales, and that could further inform risk-based prioritization for air quality management.

2.6 Conclusions

CMAQ model results indicate that the modeled sensitivity of Atlanta aircraft emissions to forming SOA concentrations can vary depending on the modeled grid resolution. We used process analysis to successfully diagnose this varying sensitivity and explain the relevant atmospheric process causing

this. At the 36-km and 12-km grid cells containing the ATL airport, modeled NO_x emissions from aircraft react and reduce NO_3^-, OH, and HOO radicals. The reduction in NO_3^- prevented the oxidization of biogenic SOA precursors during the night. The reductions in OH radicals prevented the oxidation of anthropogenic SOA during the daytime while the reduction in HOO radicals prevented the formation of anthropogenic SOA through the low-NO_x pathway both during the day and at night. At the 4-km grid resolution however, modeled SOA formation is linked to concentrations of POA rather than to the chemistry of free radicals. Modeled POA concentrations reach significantly higher levels due to emissions from aircraft (max concentration of 1.00 μg m^{-3} at the 4-km grid resolution compared to 0.29 μg m^{-3} and 0.08 μg m^{-3} at the 12-km and 36-km grid resolutions respectively and average concentration of 0.16 μg m^{-3} at the 4-km resolution compared to 0.08 μg m^{-3} and 0.03 μg m^{-3} at the 12-km and 36-km resolutions respectively). This increase in organic mass also increased SOA as it promoted partitioning of semi-volatile gas phase species into the particle phase. Furthermore, the change in modeled SOA concentrations at the 4-km grid resolution was dominated by biogenic SOA, indicating this is a result of the interaction between aircraft emissions and biogenic SOA precursors.

Results from this study have demonstrated clearly the model sensitivities of SOA formation as it pertains to aircraft emissions and the identification of the relevant processes that cause them. However, they also indicate the need to continually evaluate how SOA is represented in AQMs, and to explore the role of other precursors for SOA formation and their representation in AQMs.

CHAPTER 3 ESTIMATES OF NON-TRADITIONAL SECONDARY ORGANIC AEROSOLS FROM AIRCRAFT SVOC AND IVOC EMISSIONS USING CMAQ

3.1 Abstract

Utilizing an aircraft-specific parameterization based on smog chamber data in the Community Multiscale Air Quality (CMAQ) model with the Volatility Basis Set (VBS), we estimated contributions of non-traditional secondary organic aerosols (NTSOA) for aircraft emissions during landing and takeoff (LTO) activities at the Hartsfield-Jackson Atlanta International Airport. NTSOA, formed from the oxidation of semi-volatile and intermediate volatility organic compounds (S/IVOCs), is a heretofore unaccounted component of fine particulate matter ($PM_{2.5}$) in most air quality models. We expanded a prerelease version of CMAQ with VBS implemented for the Carbon Bond 2005 (CB05) chemical mechanism to use the Statewide Air Pollution Research Center 2007 (SAPRC-07) chemical mechanism, and added species representing aircraft S/IVOCs and corresponding NTSOA oxidation products. Results indicated the maximum monthly average NTSOA contributions occurred at the airport, and ranged from 2.4 ng m^{-3} (34% from idle and 66% from non-idle aircraft activities) in January to 9.1 ng m^{-3} (33% and 67%) in July. This represents 1.7% (of 140 ng m^{-3}) in January and 7.4% in July (of 122 ng m^{-3}) of aircraft-attributable $PM_{2.5}$, compared to 41.0–42.0% from elemental carbon and 42.8–58.0% from inorganic aerosols. As a percentage of $PM_{2.5}$, impacts were higher downwind of the airport, where NTSOA averaged 4.6–17.9% of aircraft-attributable $PM_{2.5}$ and, considering alternative aging schemes, was high as 24.0% — thus indicating the increased contribution of aircraft-attributable SOA, as a component of $PM_{2.5}$. However, NTSOA contributions were generally low compared to smog chamber results, particularly at idle, due to the considerably lower ambient organic aerosol concentrations in CMAQ, versus those in the smog chamber experiments.

3.2 Introduction

Aircraft engines emit multiple pollutants during their various modes of activity from landing and takeoff (LTO) as well as from cruise which negatively impact air quality (Moussiopoulos et al., 1997;

Brasseur et al., 1998; Tarrasón et al., 2004; Unal et al., 2005; Schürmann et al., 2007; Yim et al., 2013). For example, emissions from commercial aircraft in the U.S. during the LTO phase have shown to contribute approximately 3.2 ng m^{-3} to annual average U.S. fine particulate matter ($PM_{2.5}$), or 0.05% of total $PM_{2.5}$ (Woody et al., 2011). Aircraft also represent the third largest producer of greenhouse gas emissions (11.6% of the total) within the U.S. transportation sector behind light duty vehicles (58.7%) and freight trucks (19.2%) (U.S. Department of Transportation, 2010) and account for 3.5% of global anthropogenic radiative forcing (Lee et al., 2009). However, uncertainty associated with the treatment of aircraft emissions in air quality models has led to a wide range of estimated aviation-attributable impacts. For example, air quality model estimates of aviation-attributable premature mortalities range from 620 per year (Jacobson et al., 2013) to as high as 12,600 (Barrett et al., 2010) for full-flight global aircraft emissions and from 75 (Levy et al., 2012) to 210 (Brunelle-Yeung et al., 2014) for LTO emissions in the U.S. Additionally, air quality model estimates of aircraft-attributable $PM_{2.5}$ range from less than 1% in winter and statistically insignificant impacts in summer from full flight emissions globally (Lee et al., 2013) to approximately 1.3% of annual average $PM_{2.5}$ from aircraft LTO activities at the Hartsfield-Jackson Atlanta International Airport (ATL) (Arunachalam et al., 2011) and as high as 9.4% of daily average $PM_{2.5}$ from LTO activities at ATL (Woody and Arunachalam, 2013). Similar uncertainty exists in organic aerosols from aircraft as well as other emission sources, due to the large number of organic compounds and multiple pathways involved, many of which are not fully understood and some are possibly yet to be discovered (Kroll and Seinfeld, 2008; Miracolo et al., 2011).

Organic aerosols (OA) as a whole represent a significant fraction of the total fine particulate matter ($PM_{2.5}$) mass in the atmosphere, comprising approximately 20–70% of $PM_{2.5}$ in the U.S., Europe, and East Asia (Zhang et al., 2007) and as high as 90% in the tropics (Kanakidou et al., 2005). However, air quality model predictions have shown that aircraft emissions produce little to no secondary organic aerosols (SOA) near airports (and in some instances decrease SOA concentrations) despite the presence of SOA precursors (e.g. xylene, toluene, benzene) (Woody et al., 2011; Arunachalam et al., 2011). Woody and Arunachalam (2013) indicated that these cases of reductions in modeled SOA in the presence of aircraft emissions are attributable to aircraft NO_x emissions reacting with

and thereby lowering radical concentrations near the airport, slowing the oxidation of SOA precursors from other emission sources, and that this effect is a function of grid resolution. This reduction in SOA due to aircraft emissions in air quality models contrasts recent sampling and experimental results from Miracolo et al. (2011). Aircraft emissions from a CFM56-2B engine formed significant amounts of secondary particulate matter (PM) after three hours of photo-oxidation in a smog chamber at typical summertime OH concentrations. SOA production was approximately 1200 mg/kg-fuel at 4% power and 15 mg/kg-fuel at 85% power compared to 150 mg/kg-fuel and 70 mg/kg-fuel for secondary sulfate and 35 mg/kg-fuel and 40 mg/kg-fuel for primary PM emissions (Miracolo et al., 2011). Box model predictions of SOA were unable to reproduce the total SOA formed in the chamber, suggesting that there are possible missing precursors from aircraft emission estimates being used in air quality models. Miracolo et al. (2011) proposed that semi-volatile and intermediate volatility organic compounds (S/IVOC) may be these missing precursors. S/IVOCs are species with volatilities between primary organic aerosols and VOC gas-phase species or C* values ranging from 10^0 to 10^7 μg m^{-3}. These species are generally considered to be missing from traditional emission inventories, and measurements have confirmed their existence in aircraft emissions (Miracolo et al., 2011; Cross et al., 2013).

Jathar et al. (2012), building on the work of Miracolo et al. (2011), published yields mapped to the volatility basis set (VBS) (Donahue et al., 2006) for unidentified non-traditional SOA (NTSOA) precursors (S/IVOCs) from a CFM56-2B aircraft engine and a T63 helicopter engine. NTSOA was assumed to be the difference in measured SOA and box model estimates of traditional SOA (TSOA, i.e., SOA formed from traditional SOA precursors such as xylene, toluene, benzene, etc.). Incorporating NTSOA yields into the box model significantly enhanced SOA predictions and provided better agreement with measurements. Jathar et al. (2012) also provide the inputs necessary to predict NTSOA formed from aircraft emissions in an air quality model using the VBS, which has previously been shown capable of representing particle formation from S/IVOC (Robinson et al., 2007; Presto et al., 2009).

In this work, we use the Community Multiscale Air Quality (CMAQ) model (Byun and Schere,

2006; Foley et al., 2010) with VBS to estimate NTSOA formed from S/IVOCs, representing unidentified SOA precursors previously considered missing in air quality models, from aircraft LTO emissions at ATL. VBS is the preferred model framework for OA here as the binning of species based on volatility (typically representing 4–9 orders of magnitude of volatilities) is better suited to represent the range of volatilities of S/IVOC emissions. Contrast this to the Odum 2-product model (Odum et al., 1996), traditionally used in CMAQ to represent semi-volatile oxidization products of SOA precursors, where SOA precursors (and emissions) are typically represented using more explicit species (e.g. toluene, xylene, benzene). NTSOA predictions were made by incorporating the aircraft-specific NTSOA parameterization developed by Jathar et al. (2012) into CMAQ with VBS and modeling two months, January and July, 2002, to capture seasonal variability. The end goal is to provide a more accurate representation of OA and PM formation from aircraft emissions in CMAQ.

3.3 Methodology

Organic aerosol concentrations were estimated in January and July, 2002 over a 12-km Eastern U.S. domain [which was selected to simultaneously test VBS in CMAQ (see Appendix B) and predict NTSOA formed from aircraft emissions] using CMAQ v5.0.1 with the VBS framework. VBS in CMAQ, implemented for the Carbon Bond 2005 (CB05) chemical mechanism (Yarwood et al., 2005) by Koo et al. (2014), provides for the treatment of four distinct organic aerosol groups: primary anthropogenic (representing hydrocarbon-like OA), secondary anthropogenic and biogenic (representing oxygenated OA), and primary biogenic (biomass burning). Each organic aerosol group is treated as semi-volatile, including primary organics (Robinson et al., 2007), using five volatility bins. The lowest bin is treated as non-volatile particles with the other four bins representing particles with C* values ranging from 10^0 to 10^3 μg m^{-3}. Primary organic aerosol (POA) emissions are replaced by SVOCs, which partition between the particle and gas phase. Additionally, gas-phase IVOC emissions are included which, when oxidized, form SVOCs and SOA.

In this study, we expanded the Koo et al. (2014) CMAQ VBS implementation for CB05 for use with the more explicit Statewide Air Pollution Research Center 2007 (SAPRC-07) chemical mechanism (Carter, 2010). In CMAQ, our VBS implementation for SAPRC-07 includes 150 gas phase species [13 representing SOA precursors — 9 anthropogenic (8 contained in aircraft emissions) and

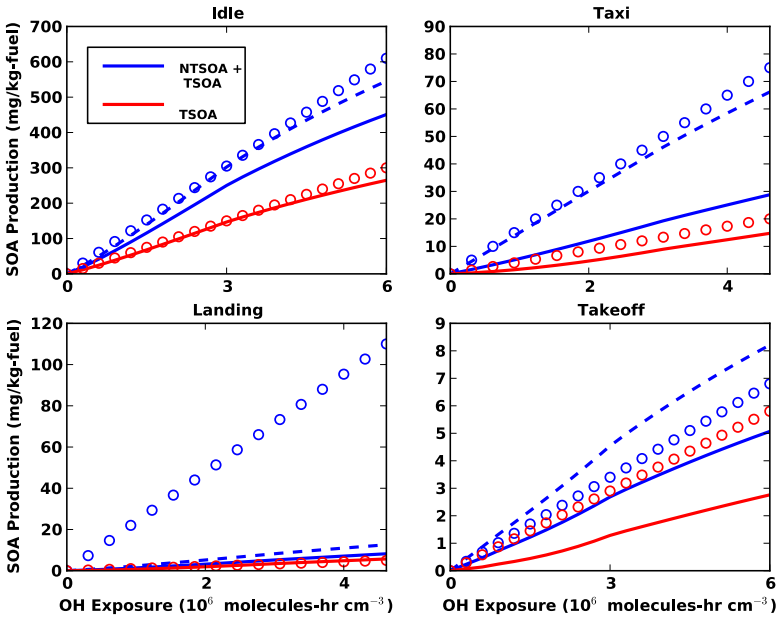

Figure 3.1: Comparison of traditional (TSOA) and non-traditional SOA (NTSOA) predictions in CMAQ (solid lines), box model results reported by Jathar et al. (2012) (circles) based on measurements from Miracolo et al. (2011), and NTSOA predictions in CMAQ with 1.5x increased yields (dashed lines) for a CFM56-2B engine at idle (4% power), taxi (7%), landing (30%), and takeoff (85%). OH exposure is the integration of OH concentrations over time to account for differences in OH concentrations between the two models.

4 biogenic] and 413 reactions compared to 80 gas phase species (6 representing SOA precursors — 3 anthropogenic and 3 biogenic) and 205 reactions in CB05. The SAPRC-07 chemical mechanism was selected due to the more explicit treatment of VOCs and specifically SOA precursors, as we theorized this would provide a better representation of TSOA formed from aircraft emissions. It also maintains consistency with the Jathar et al. (2012) study, which used SAPRC VBS yields for TSOA formed from aircraft emissions.

In our SAPRC-07 implementation of VBS in CMAQ, TSOA precursors with VBS are the same as with the CMAQ aerosol 6 module (AE6) (Carlton et al., 2010). However, we updated their semi-volatile oxidation products to map to VBS products with yields taken from Murphy and Pandis (2009) and Hildebrandt et al. (2009), similar to Koo et al. (2014). The aerosol module remained unchanged from Koo et al. (2014) except for the addition of NTSOA formed from aircraft S/IVOC emissions as described below. Additional details regarding our SAPRC-07 VBS implementation in CMAQ,

Table 3.1: Aircraft-specific mass yields for reactions of S/IVOC gas-phase species (NTSOA precursors) with OH. Values represent the mass transferred and the corresponding reduction in volatility ($\log_{10}$ C*) for each oxidation step and are 1.5x higher than the values reported by Jathar et al. (2012). For example, when reacted with OH, 1 g of NTSOA precursor from idle activities with a C* value of 10^7 would produce 0.15 g of SVOC with a C* of 10^2 (7 minus 5), 0.15 g of SVOC with a C* of 10^3, and 0.3 g of SVOC with a C* of 10^4.

Change in Volatility Bin ($\log_{10}$ C*)	-6	-5	-4	-3
Idle	0	0.15	0.15	0.3
Non-Idle	0.075	0.15	0	0

including comparisons of VBS results against the traditional AE6, can be found in Appendix B.

Specific for aircraft, we introduced aircraft S/IVOC species into CMAQ with a parameterization based on work by Jathar et al. (2012). The new species, in addition to using an aircraft-specific parameterization, allow for aircraft contributions to be tracked separately from other sources. Similar to the VBS representation of anthropogenic TSOA, five volatility bins were used to represent aircraft-specific NTSOA, with the lowest bin representing non-volatile organics and the other four bins spanning C* values from 10^0 to 10^3 μg m^{-3}. Emissions and chemistry of gas-phase IVOCs were included using 4 volatility bins with C* values ranging from 10^4 to 10^7 μg m^{-3}. At engine idle, aircraft emit considerably more organic PM and unburned hydrocarbons per unit fuel burned compared to other engine modes due to incomplete combustion (Herndon et al., 2008; Timko et al., 2010; Miracolo et al., 2011; Beyersdorf et al., 2014). For this reason, the production of NTSOA from idle and non-idle activities is tracked separately, with unique model species, precursors, and yields for both sets of activities. The parameterization also includes multi-generational aging reactions of NTSOA, using a rate constant of 1 x 10^{-11} cm^3 molecules^{-1} s^{-1} with each oxidation step lowering the volatility of the product by one order of magnitude (Murphy and Pandis, 2009; Farina et al., 2010; Jathar et al., 2011, 2012).

After implementation of the Jathar et al. (2012) aircraft parameterization in CMAQ, CMAQ predictions of NTSOA were evaluated using results from Jathar et al. (2012). secondary PM (Lobo et al., 2012), or organic carbon in the near field (1-50 m) of the aircraft engine (Agrawal et al., 2008; Kinsey et al., 2010; Timko et al., 2014). Only the Miracolo et al. (2011) study, which the Jathar et al.

(2012) NTSOA yields are based on, provide measurements of SOA formed from aircraft emissions (a CFM56-2B aircraft engine and T63 helicopter engine at various power settings) that the authors are aware of. Our evaluation compared NTSOA production (normalized for OH concentrations using OH exposure) for the CFM56-2B aircraft engine in a box model version of CMAQ (transport processes turned off) and the Jathar et al. (2012) box model using an identical NTSOA mechanism and similar inputs. CMAQ predictions of NTSOA from the CFM56-2B engine were lower at all power settings while TSOA results were generally in good agreement, with the exception of the 85% power setting (Figure 3.1). The NTSOA results suggest that the Jathar et al. (2012) yields in CMAQ would underpredict NTSOA from aircraft.

We conducted a series of sensitivity analyses in our CMAQ box model and found that increasing the Jathar et al. (2012) yields by 1.5x provided better agreement of the CFM56-2B experiments at 4% and 7% power (Figure 3.1), the two power settings with the highest emissions of S/IVOCs. At 30% power, the Miracolo et al. (2011) OA measurements exceeded the measured S/IVOCs emissions, and to reproduce the Jathar et al. (2012) results, S/IVOC emissions would have to be increased by 15x in addition to the 1.5x increase in yields. However, this increase in emissions is unrealistic, producing more S/IVOC emissions at 30% power than 7% power, which measurements do not support (Miracolo et al., 2011; Cross et al., 2013). Note, only one experiment was conducted at 30% power by Miracolo et al. (2011); therefore there is a higher level of uncertainty associated with results at this power setting compared to others. Given the better agreement at 4% and 7% power settings, our CMAQ simulations were conducted using the higher (1.5x) yields (Table 3.1).

The SAPRC-07 mechanism in CMAQ includes the formation of anthropogenic TSOA from eight model species contained in aircraft emissions: benzene (BENZ), toluene (TOL), xylene (MXYL, OXYL, PXYL), aromatics (ARO1 and ARO2), and alkanes (ALK5). Note, CMAQ also includes 1,2,4-trimethylbenzene (TRIMETH_BENZ124) as a TSOA precursor but it is not contained in aircraft emissions. In addition to the eight CMAQ model species contained in aircraft emissions, the box model used by Jathar et al. (2012) to develop the NTSOA parameterization included the formation of TSOA from aircraft emissions of model species representing alkenes (OLE1 and OLE2) and alkanes (ALK4). To be consistent with that study and because the Jathar et al. (2012) NTSOA yields were

Table 3.2: SPECIATE v4.3 speciation profile 5565B used to speciate aircraft TOG emissions to SAPRC-07 model species.

Common Name	Model Species	Mass Fraction	Molecular Weight (g/mol)
1,3-Butadiene	BDE13	0.0169	54.0904
Acetone	ACET	0.0036898	58.0791
Acrolein	ACRO	0.0245	56.0633
Acetylene	ACYE	0.0394	26.0373
Alkanes[a]	ALK1	0.0052098	30.069
Alkanes[a]	ALK2	7.8005E-4	44.0956
Alkanes[a]	ALK4	0.0066996	82.5378
Alkanes[a]	ALK5	0.1765	147.1058
Aromatics[a]	ARO1	0.0027295	111.0468
Aromatics[a]	ARO2	0.0246	133.8579
1,2,4-Trimethylbenzene	B124	0.0035	120.1916
Aromatic aldehydes	BALD	0.0103	113.2886
Benzene	BENZ	0.0168	78.1118
Acetaldehyde	CCHO	0.0427	44.0526
Phenols and Cresols	CRES	0.0072597	94.1112
Ethene	ETHE	0.1546	28.0532
Glyoxal	GLY	0.0182	58.0361
Formaldehyde	HCHO	0.1231	30.026
Isoprene products	IPRD	0.0103	70.0898
Methacrolein	MACR	0.0042902	70.0898
Methanol	MEOH	0.018	32.0419
Methylglyoxal	MGLY	0.015	72.0627
m-Xylene	MXYL	0.0014099	106.165
Alkenes[a]	OLE1	0.091	95.61
Alkenes[a]	OLE2	0.058	110.2306
o-Xylene	OXYL	0.0016604	106.165
Propene	PRPE	0.0453	42.0797
p-Xylene	PXYL	0.0014099	106.165
C3+ Aldehydes	RCHO	0.0697	127.1741
Toluene	TOLU	0.0064202	92.1384

[a] Lumping based on reaction rate with OH

based on the difference in measured SOA and predicted TSOA, we added the formation of TSOA from aircraft emissions of OLE1, OLE2, and ALK4 into CMAQ using yields based on Murphy and Pandis (2009) to provide for a more accurate prediction of total SOA formed from aircraft.

Meteorological inputs were generated using the Pennsylvania State University/NCAR mesoscale (MM5) model (Grell et al., 1994). Non-aviation emissions were generated using the Sparse Matrix Operator Kernel Emissions (SMOKE) model (Houyoux et al., 2000) and estimated using the U.S. EPAs 2002 National Emissions Inventory (NEI) (U.S. EPA, 2004). Non-aviation S/IVOC emissions were estimated using the high internal estimate option in CMAQ with VBS, where SVOC emissions are 3 times the traditional POA emissions and IVOC emissions are 4.5 times POA emissions. This

option was selected based on our comparisons of our SAPRC-07 implementation of CMAQ with VBS against OC ambient measurements, which indicated better agreement compared to CMAQ with VBS's conservative estimate of S/IVOC emissions (SVOC = traditional POA emissions and IVOC emissions = twice POA emissions). Additional details on CMAQ with VBS's internal S/IVOC emission estimates from non-aviation sources and comparisons of ambient measurements of OC and $PM_{2.5}$ against our SAPRC-07 CMAQ with VBS implementation can be found in Appendix B.

Our investigation focused on aircraft-attributable $PM_{2.5}$ contributions (calculated as difference between CMAQ predictions with and without aircraft emissions) from LTO activities below 1 km at ATL, which is the busiest airport in the world with approximately 2,400 flights daily (Federal Aviation Administration, 2013). Aircraft emissions estimates for NO_x, SO_2, CO, total organic gases (TOG), and primary PM (sulfate, organic aerosols, and elemental carbon) at ATL were based on the Aircraft Environmental Design Tool (AEDT) global aircraft emission inventory for 2006 (Wilkerson et al., 2010). The inventory provides high resolution emissions data both in space and time for individual flights globally. Gas-phase emissions in AEDT were based on International Civil Aviation Organization (ICAO) reported mode-specific emission factors (EFs) while primary PM emissions were based on the First Order Approximation v3 (FOA3) (Wayson et al., 2009). Primary organic emissions were treated as non-volatile, consistent with the assumption used by FOA3. Also, this prevents any possible double counting of NTSOA, as VBS in CMAQ converts a portion of volatile POA (SVOCs) to SOA. However, measurements collected by Presto et al. (2011) indicate the majority of aircraft POA emissions are semi-volatile, suggesting that a semi-volatile treatment of aircraft POA emissions should be considered in future studies. CMAQ-ready emission files for aircraft sources were generated using the AEDTproc tool (Baek et al., 2012), which allocates aircraft emissions in four dimensions (column, row, layer, and time) using aircraft trajectories taken from the AEDT database, and performs appropriate conversions of inventory pollutants into model species. These aircraft emissions were then merged with the non-aviation emissions files from the NEI to create the final files used in the CMAQ simulations. TOG was speciated into SAPRC-07 model species using the most recent EPA speciation profile (SPECIATE profile 5565B, Table 3.2) which is based on results of a joint Federal Aviation Administration (FAA) and EPA effort (U.S. EPA, 2009a,b). Aircraft S/IVOC emissions were

estimated using the mode-specific EFs for a CFM56-2B engine reported by Jathar et al. (2012) and normalized by ICAO hydrocarbon (HC) EFs calculated as

$$EF_{S/IVOC,engine\ i} = \frac{EF_{S/IVOC,CFM56-2B} \times EF_{HC,engine\ i}}{EF_{HC,CFM56-2B}} . \quad (3.1)$$

Table 3.5 provides monthly total aircraft emissions estimates of S/IVOCs during the modeling period. These emissions, when oxidized, form NTSOA, and modeled NTSOA is discussed in Section 3.4.1. IVOC emissions are similar in magnitude to aircraft emissions of long-chain alkanes (ALK5) (Table 3.3). Also note, the majority of idle S/IVOC emissions are primarily at higher volatilities (C* values of 10^6–10^7 μg m^{-3}) while non-idle emissions are at slightly lower volatilities (10^3–10^4 μg m^{-3}). Therefore, while the total S/IVOC mass from idle emissions is higher than for non-idle emissions, additional oxidation steps are required to lower the volatility enough for significant partitioning to the particle phase.

Table 3.3 provides similar aircraft emissions estimates for TOG and TSOA precursors in CMAQ (ALK4, ALK5, ARO1, ARO2, BENZ, OLE1, OLE2, TOL, and XYL). The non-idle SOA precursor emissions in Table 3.3 represent those traditionally considered when assessing aircraft contributions to TSOA. The TSOA idle emissions are those estimated using the Fuel Flow Method2 as described below and are not included in AEDT by default. They represent approximately a 50% increase in TOG and TSOA precursor emissions from aircraft. Results of TSOA formed from the precursors in Table 3.3 are presented in Section 3.4.2. Finally, Table 3.4 provides aircraft emissions estimates of primary PM species (sulfate, organic aerosols, and elemental carbon) and inorganic PM precursors (NO_x and SO_2) for the modeling period.

One limitation to our approach for estimating S/IVOC aircraft emissions is that the ICAO database assumes a 7% power setting for idle activities while most modern aircraft engines generally idle below this setting (Herndon et al., 2009). Here a value of 4% was assumed for aircraft idle. To estimate S/IVOC idle emissions at 4% power, the Boeing Fuel Flow Method2 (FF2) (DuBois and Paynter, 2007) was used to extrapolate idle hydrocarbon EFs for each flight at Atlanta during the modeling episode. The FF2 method assumes a bilinear fit of ICAO-reported hydrocarbon EFs (one

Table 3.3: Monthly total aircraft emissions (short tons) in January (Jan) and July (Jul) of total organic gases (TOG, the speciation of which is listed in Table 3.2) and CMAQ SOA precursors [alkanes (ALK4 and ALK5), aromatics (ARO1 and ARO2), benzene (BENZ), alkenes (OLE1 and OLE2), toluene (TOL), and xylene (XYL, which includes MXYL, OXYL, and PXYL)]. Note that SOA production from ALK4, ARO1, and ARO2 was only considered from aircraft and that idle emissions, which are not included in AEDT emissions by default, were only considered in sensitivity simulations described in Sections 3.4.2 and 3.4.4.

		TOG	ALK4	ALK5	ARO1	ARO2	BENZ	OLE1	OLE2	TOL	XYL
Non-Idle	Jan	64.3	0.41	9.2	0.15	1.4	1.1	4.4	2.6	0.41	0.29
	Jul	78.1	0.49	11.1	0.18	1.7	1.3	5.4	3.1	0.50	0.35
Idle	Jan	39.8	0.25	5.7	0.09	0.9	0.7	2.7	1.6	0.30	0.18
	Jul	64.9	0.41	9.3	0.15	1.4	1.1	4.5	2.6	0.42	0.29

linear fit for 85% to 30% power settings and a separate linear fit for 4% to 30% power settings) and a linear fit of ICAO-reported fuel flows. For each flight, time-in-mode for idle activities was calculated as the difference between total time spent in taxi/idle modes (reported as one value in AEDT) and the average unimpeded taxi time at the Atlanta airport reported by the FAA's Aviation Performance Metrics (Federal Aviation Administration, 2013). Hydrocarbon (and S/IVOC) emissions from idle activities were then estimated by flight as the product of idle time, fuel flow, and S/IVOC EF. Using this methodology, we estimated that, due to long idle times and despite low fuel flows at idle, approximately 23–33% of LTO fuel burn occurs during aircraft idling. For comparison, taxi accounted for 31–36% of fuel burn, approach 22–26%, and takeoff 12–15%. It should be noted that while applying a normalized EF for SVOC and IVOC emissions from all aircraft based on a single engine type introduces some uncertainty (the CFM56-2B engine is primarily used for military aircraft, but the CFM56 series is used on approximately 20% of US commercial flights in 2006), limited data currently exists on these emissions from other engine types and is therefore considered an acceptable approximation for this work.

Another limitation is that 29.1% of measured TOG mass was unidentified during the derivation of EPA's aircraft TOG speciation profile (U.S. EPA, 2009a). Using a "best fit" approach, this unidentified mass was assigned to model species to ensure 100% of TOG mass was represented. Our newly added S/IVOC emissions likely represent a portion of this unidentified mass since S/IVOCs are generally unidentifiable by gas chromatograph. Therefore, there is the potential for double counting emissions

Table 3.4: Monthly total aircraft emissions (short tons) in January (Jan) and July (Jul) of NO_x and SO_2 (inorganic PM precursors) and primary elemental carbon (PEC), organic carbon (POA), and sulfate (PSO4).

	NO_x	SO_2	PEC	POA	PSO4
Jan	466.6	37.2	1.6	1.3	1.1
Jul	511.9	42.7	1.7	1.4	1.3

and SOA formed from those emissions. However, the newly added S/IVOC emissions do not impact gas phase chemistry in the model, only participating in SOA formation. This is consistent with the VBS treatment in CMAQ of IVOCs from all other sources as implemented by Koo et al. (2014). Furthermore, the SOA formed from traditional SOA precursors is insignificant compared to NTSOA and any potential overlap of SOA mass would be small compared to the magnitude of NTSOA.

3.4 Results and Discussion

3.4.1 CMAQ Predictions of NTSOA from Aircraft

Monthly average $PM_{2.5}$ contributions from aircraft operations in the grid cell containing the airport (the grid cell with the highest absolute aircraft contribution in the domain) ranged from 140 ng m^{-3} in January (daily averages ranging from 32 to 311 ng m^{-3}) to 122 ng m^{-3} in July (daily averages of 58–312 ng m^{-3}) (Figures 3.3 and 3.2). This is lower than aircraft impacts at ATL reported by Arunachalam et al. (2011) (annual average impacts of approximately 200 ng m^{-3}), which used a different (higher) emission inventory that was based upon the Emissions Dispersion Modeling System (EDMS) (Federal Register Notice, 1998). Similar to previous 12-km CMAQ modeling studies at ATL (Arunachalam et al., 2011; Woody and Arunachalam, 2013), aircraft emissions reduced biogenic TSOA concentrations in July, which is further discussed in Section 3.4.2. Newly added NTSOA formed from aircraft S/IVOC emissions accounted for 2.4 ng m^{-3} in January (1.7% of total $PM_{2.5}$ from aircraft; daily averages of 0.2–9 ng m^{-3}) and 9.1 ng m^{-3} in July (7.4%, daily averages of 1–38 ng m^{-3}), which is approximately 4–6 times higher than TSOA formed from idle and non-idle aircraft TSOA precursor emissions (Section 3.4.2). Idle activities accounted for 34% in January and 33% in July of the total NTSOA formed. Additional photochemistry in July compared to January produced higher average OH concentrations at ATL (2.4 x 10^6 molecules cm^{-3} compared to 2.4 x 10^5 molecules cm^{-3}). This allowed for more aircraft S/IVOCs to be oxidized in July and, despite similar

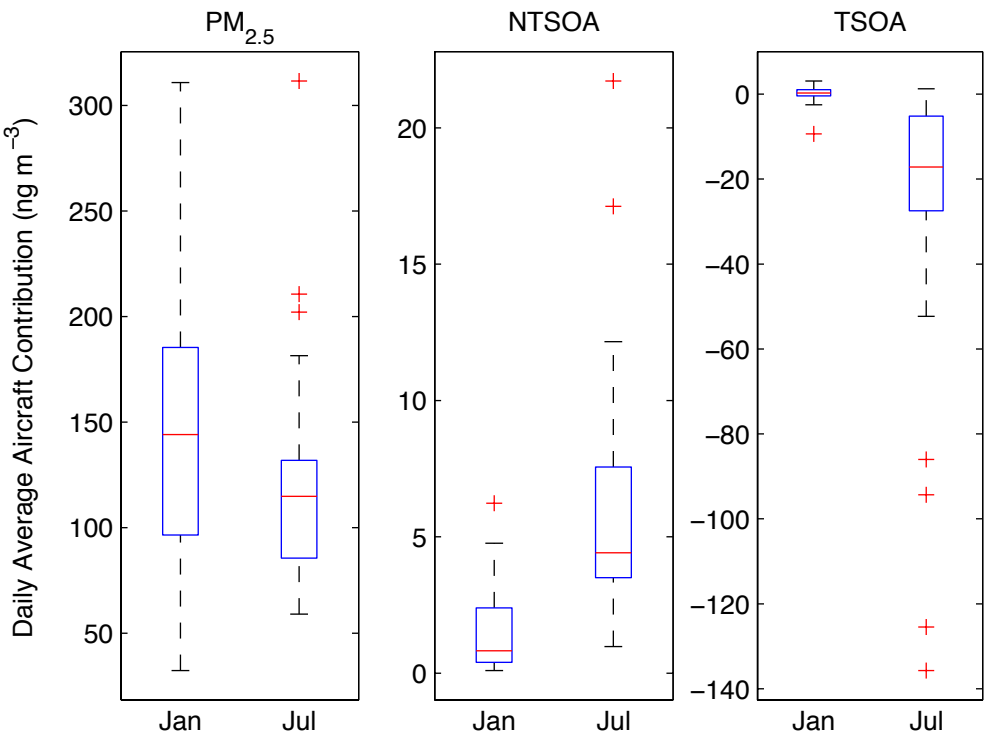

Figure 3.2: Box-and-whisker plots showing the 25th, 50th (red line), and 75th percentiles, and minimum and maximum values of daily average aircraft-attributable $PM_{2.5}$, non-typical SOA (NTSOA), and traditional SOA (TSOA) in the grid cell containing ATL. Outliers are defined as values more than 1.5 times the inter-quartile range above the 75th percentile and below the 25th percentile.

non-idle emissions in January and July (Table 3.5), produce approximately four times more NTSOA from non-idle activities. Furthermore, while idle emissions were approximately 50% higher in July due to longer idle times, the ratio of idle to non-idle NTSOA was similar in July and January.

Impacts on $PM_{2.5}$ in January and July were highest near the airport, although impacts as high as 10 ng m^{-3} extended up to 100 km away from the airport in July (Figure 3.4a,b). NTSOA contributions were generally confined to grid cells surrounding the airport, similar to primary PM species, though impacts of 1 ng m^{-3} or higher were located 50 km away from the airport (Figure 3.4c,d). Additionally, the percentage of aircraft-attributable $PM_{2.5}$ comprised of NTSOA increased moving away from the airport as aircraft S/IVOC were oxidized (Figures 3.4e,f and 3.5). At distances 6–30 km away from the airport, NTSOA averaged 4.6% in January and 11.8% in July of aircraft-attributable $PM_{2.5}$; 14.0%

Table 3.5: Monthly total aircraft emissions (short tons) in January (Jan) and July (Jul) from LTO activities at ATL of SVOCs and IVOCs (non-traditional SOA precursors).

		SVOCs				IVOCs			
	C*	10^0	10^1	10^2	10^3	10^4	10^5	10^6	10^7
Non-Idle	Jan	0.52	0.88	1.03	4.14	5.6	1.0	2.4	2.4
	Jul	0.54	0.92	1.09	4.43	6.0	1.1	2.5	2.5
Idle	Jan	0.05	0.03	0.03	0.08	0.2	0.6	10.6	10.6
	Jul	0.07	0.06	0.06	0.13	0.3	0.9	16.9	16.9

in January and 7.7% in July at distances 31–54 km away from the airport; and 17.9% in January and 4.0% in July at distances 55–102 km away from the airport. Note that while percentages were higher in January, $PM_{2.5}$ (and NTSOA) concentrations dropped off more rapidly moving away from the airport in January as absolute aircraft-attributable $PM_{2.5}$ concentrations were approximately 15 (6–30 km), 94 (31–54 km), and 196 (55–102 km) times lower than the grid cell containing ATL in January and 8, 13, and 16 times lower in July. NTSOA was important away from the airport, but aircraft-attributable $PM_{2.5}$ was dominated by inorganic species (secondary ammonium, nitrate, and sulfate) formed from aircraft emissions of NO_x and SO_2 (Figure 3.5), similar to previous modeling studies in CMAQ (Arunachalam et al., 2011; Woody et al., 2011; Rissman et al., 2013).

Absolute NTSOA contributions were generally low compared to elemental carbon and inorganic aerosols, which contributed 59 ng m^{-3} (38.9% of $PM_{2.5}$) and 63 ng m^{-3} (41.6%) in January and 50 ng m^{-3} (41.1%) and 70 ng m^{-3} (57.9%) in July in the grid cell containing ATL, respectively. This is somewhat contradictory to the smog chamber results of Miracolo et al. (2011, 2012), where reported aircraft SOA production were comparable to secondary sulfate and higher than primary PM except at the highest power setting. OA concentrations and the volume into which aircraft emissions mix can significantly influence aircraft-attributable SOA (Woody and Arunachalam, 2013). OA concentrations serve a key role in gas-particle partitioning, with higher values promoting partitioning to the particle phase. In the smaller volume of the smog chamber, where aircraft emissions were concentrated, total OA concentrations (POA + SOA + NTSOA) ranged between 6 μg m^{-3} at 85% power to 250 μg m^{-3} at 4% power (Jathar et al., 2012). Contrast this with the larger volume of the grid cell (12 km x 12 km x 38 m) containing ATL, where average OA concentrations ranged from 3–4 μg m^{-3} and were largely determined by emissions from sources other than aircraft. The differences in partitioning due to OA

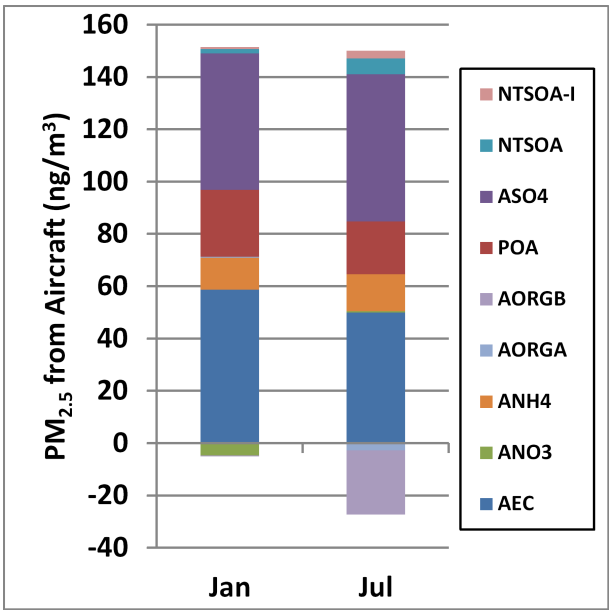

Figure 3.3: Speciated monthly average $PM_{2.5}$ contributions from aircraft in the grid cell containing the Atlanta airport in January and July. Species include non-traditional SOA from engine idle activities (NTSOA-I), non-traditional SOA from all other engine modes (NTSOA), sulfate (ASO4), primary organics (POA), biogenic TSOA (AORGB), anthropogenic TSOA (AORGA), ammonium (ANH4), nitrate (ANO3), and elemental carbon (AEC) aerosols.

were highest at idle, where smog chamber OA concentrations were highest, emissions of IVOCs were highest (highest potential for NTSOA formation), and NTSOA products were of relatively higher volatilities (C* values of 10^2 to 10^4).

To test the impact of OA concentrations on NTSOA concentrations, we conducted a sensitivity analysis again using our CMAQ box model. Two test cases were simulated, one using typical ambient OA concentrations (5 µg m^{-3}) and the other using mode-specific OA concentrations measured in the smog chamber (6–250 µg m^{-3}) during the Miracolo et al. (2011) experiments. Results indicated that when ambient OA concentrations were used, NTSOA and SOA production at the 4% power setting were approximately a factor of six lower compared to the same simulation using smog chamber OA concentrations. This also provides one indication of why the majority of NTSOA contributions were from non-idle aircraft activities, despite the higher potential from idle emissions. NTSOA model results at a finer scale, such as plume scales where aircraft emissions would be more concentrated (Rissman et al., 2013), would likely be higher, particularly for idle emissions.

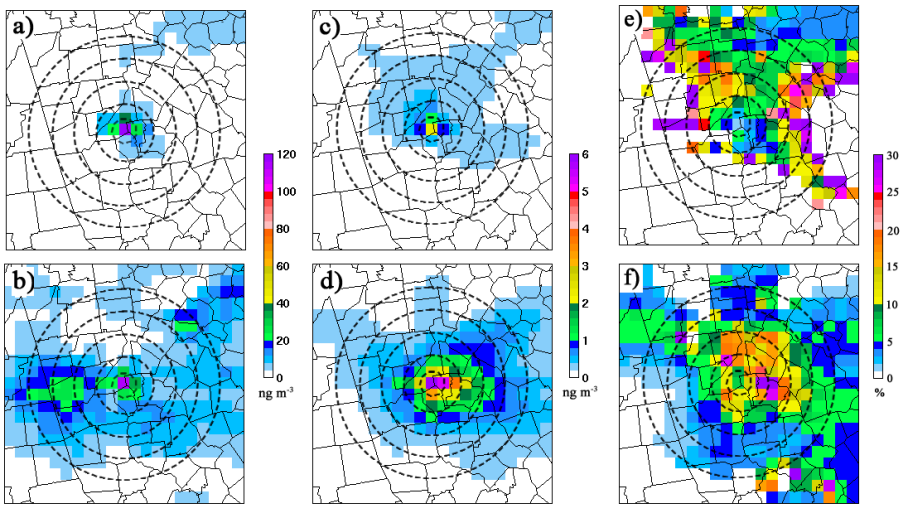

Figure 3.4: Monthly average contributions from aircraft to $PM_{2.5}$ in a) January and b) July, to non-traditional SOA (NTSOA) in c) January and d) July, and NTSOA (> 0.1 ng m^{-3}) as a percentage of aircraft-attributable $PM_{2.5}$ in e) January and f) July. Note the differences in scales, that the absolute maximum impacts occur in the grid cell containing ATL but the percentage of aircraft-attributable $PM_{2.5}$ comprised of NTSOA is higher away from the airport, and that the map covers an area of 720 km x 720 km. Circles indicate the location of ATL and 30 km, 54 km, 78 km, and 102 km away from ATL.

3.4.2 CMAQ Predictions of TSOA from Aircraft

Aircraft contributions to TSOA in the grid containing the airport were generally lower than NTSOA contributions. Aircraft increased anthropogenic TSOA in January by 1.3 ng m^{-3} (0.9% of $PM_{2.5}$; daily average ranging from -9 to 3 ng m^{-3}) and lowered it by 1.7 ng m^{-3} (-1.4%; daily averages ranging from -136 to 1 ng m^{-3}) in July (Figure 3.2). TSOA formed directly from aircraft emissions of SOA precursors contributed 0.1 ng m^{-3} (0.1%) in January and 0.7 ng m^{-3} (0.6%) in July with the remainder (1.2 ng m^{-3} and -2.4 ng m^{-3}) attributable to the interaction of aircraft emissions and TSOA precursors emitted from other anthropogenic sources. With the inclusion of idle emissions listed in Table 3.3, TSOA formed directly from aircraft TSOA precursors increased to 0.4 ng m^{-3} (0.4%) in January and 2.4 ng m^{-3} (2.0%) in July. Finally, the interaction of aircraft emissions with biogenic TSOA precursors lowered biogenic TSOA by 0.1 ng m^{-3} (-0.1%) in January and 23.6 ng m^{-3} (-19.4%) in July (Figure 3.3).

The reduction in TSOA near the airport is similar to previous studies (Arunachalam et al., 2011;

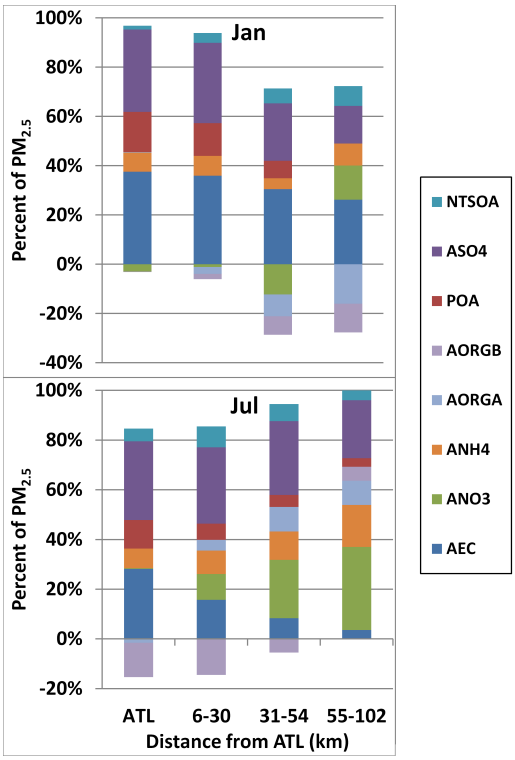

Figure 3.5: Monthly average composition of aircraft-attributable $PM_{2.5}$ at the grid cell containing ATL and at various distances away from ATL. Note that absolute aircraft-attributable $PM_{2.5}$ concentrations are approximately 15 (6–30 km), 94 (31–54 km), and 196 (55–102 km) times lower moving away from ATL in January and 8, 13, and 16 times lower in July.

Woody et al., 2011; Woody and Arunachalam, 2013) and attributable to the NO_x-dependent TSOA pathways in CMAQ with VBS. Aircraft NO_x has been shown to lower free radicals in the grid cell containing the airport, slowing oxidation of precursors (particularly the low NO_x pathway), and thereby reduce TSOA formation from all sources (Woody and Arunachalam, 2013). With the traditional treatment of aircraft in grid-based models, aircraft emissions are instantaneously diluted into a grid cell and interact with non-aviation emissions which may or may not occur near the airport (e.g. biogenic TSOA precursors). Plume-in-grid modeling techniques would provide an alternative modeling approach to possibly prevent this result, where aircraft emissions would evolve in plumes prior to interacting with non-aviation emissions when the plumes are merged back into the underlying grid (Rissman et al., 2013).

To evaluate TSOA CMAQ results, we compared CMAQ box model results to the Jathar et al. (2012) box model predictions. The two models use similar mechanisms, utilizing SAPRC VBS SOA

yields taken from Murphy and Pandis (2009). However, CMAQ used 11 lumped SOA precursors compared to 91 explicit SOA precursors used by the Jathar et al. (2012) box model. The comparison, normalized for OH concentrations by using OH exposure, indicated that the two models generally agreed (Figure 3.1). The underprediction of the CMAQ box model at taxi and takeoff is likely due to the lumping of SOA precursors. However, grid-based SOA contributions from aircraft again appear low compared to the chamber experiments, providing further evidence to support the influence that model grid resolution and OA concentrations have on SOA contributions from aircraft emissions as detailed in Woody and Arunachalam (2013).

3.4.3 CMAQ Predictions of POA from Aircraft

At ATL, aircraft POA contributed 26 ng m^{-3} (16.9% of $PM_{2.5}$) in January and 20 ng m^{-3} (16.6% of $PM_{2.5}$) in July. However, these values may be biased high due to our non-volatile treatment of aircraft POA. Also, while FOA3 is widely used for aircraft PM emission estimates in air quality models (including this work), it has known limitations. For example, two versions of FOA3 are currently in use, FOA3 (Wayson et al., 2009) and FOA3a (Ratliff et al., 2009), where FOA3a accounts for uncertainties in PM emissions science and characterization at the time it was developed and estimates five times more PM emissions than FOA3. Also, comparisons against measurements have shown FOA3 estimates vary by an order of magnitude for 40% of aircraft engines (Stettler et al., 2011). FOA3 assumes POA emissions are non-volatile and does not account for variations in primary organic emissions due to changes in ambient temperature. However, measurements have shown that organic aerosol formation 30 meters downwind of the engine is highly dependent on ambient temperature due to their volatility (Beyersdorf et al., 2014). These limitations highlight the uncertainties associated with aircraft POA emissions estimates, and the need to improve methods of estimating POA emissions from aircraft and their representation in air quality models.

3.4.4 Alternative Modeling Techniques to Predict NTSOA

We conducted three sensitivity simulations to determine if alternative modeling techniques could capture NTSOA formation from aircraft without an aircraft-specific parameterization. In the first sensitivity simulation (sensitivity A), aircraft IVOC emissions were remapped to traditional CMAQ SOA precursors using AE6 yields (Carlton et al., 2010) to determine if altering emission estimates could

provide similar results to the updated NTSOA parameterization. While contributions from aircraft to anthropogenic TSOA contributions increased in the sensitivity case using AE6 (e.g. from approximately 0.1 ng m^{-3} to 0.3 ng m^{-3} in January, leading to a 200% increase), total aircraft contributions to anthropogenic TSOA were below 0.3% of the total $PM_{2.5}$ formed from aircraft emissions in January and below 0.8% in July. In the second sensitivity simulation (sensitivity B), TOG emissions (and thus traditional SOA precursors) were updated to include estimates of idle emissions at 4% engine thrust levels. This sensitivity case increased TOG emissions by approximately 50% (Table 3.3). However, the overall impact of anthropogenic TSOA was small, comprising less than 0.3% of $PM_{2.5}$ in January and 0.4% in July. The third sensitivity simulation used the default configuration of CMAQ with VBS to estimate SOA formed from S/IVOC emissions, where S/IVOCs estimates for aircraft were keyed to POA emissions (sensitivity C where SVOC = 3 x POA and IVOC = 4.5 x POA). While this case predicted the highest SOA from aircraft in January of the three sensitivity cases (0.5% of total $PM_{2.5}$), July predictions of SOA lowered total $PM_{2.5}$ from aircraft by 2%.

None of these three sensitivity cases were able to reproduce the NTSOA estimates in CMAQ as represented in Section 3.4.1. Ratios of SOA to POA in the sensitivity cases ranged from -0.14 (sensitivity C in July) to 0.04 (sensitivity A in July) compared to values ranging from 0.16 to 0.48 in the explicit NTSOA case, which was still below the SOA to primary PM ratios (ranging from 0.4 at 85% engine load to 30 at 4% engine load) reported by Miracolo et al. (2011). While aircraft impacts to $PM_{2.5}$ are, in general, low compared to other anthropogenic emission sources (Arunachalam et al., 2011; Woody et al., 2011), without this parameterization, predictions of aircraft impacts to PM near airports would likely be underpredicted by up to 10% in air quality models, particularly in summer months.

3.4.5 NTSOA Sensitivity to Aging

One limitation to the Jathar et al. (2012) parameterization is the uncertainty associated with aging of NTSOA. The Miracolo et al. (2011) chamber experiments were conducted over a relatively short time period (hours) and did not capture aged SOA formed over longer time scales (days). Therefore, to test how sensitive aged NTSOA formation from aircraft was to the aging scheme used, two sensitivity simulations were conducted. The first doubled the aging rate constant from 1 x 10^{-11} cm^3 $molecules^{-1}$

s^{-1} to 2 x 10^{-11} cm^3 $molecules^{-1}$ s^{-1}. This rate constant is consistent with CMAQ VBS TSOA aging reactions. The second sensitivity test used the aging scheme used by Pye and Seinfeld (2010), and is based on wood smoke experiments. The Pye and Seinfeld (2010) aging scheme uses a rate constant of 2 x 10^{-11} cm^3 $molecules^{-1}$ s^{-1}, lowers the volatility of products by two orders of magnitude, only allows for one oxidation step per parent hydrocarbon (vs. multi-generational aging), and assumes that oxidation produces a product 50% heavier than the parent hydrocarbon.

By doubling the aging rate constant, total NTSOA concentrations in the grid cell containing ATL increased by 1% (from 2.38 ng m^{-3} to 2.40 ng m^{-3}) in January (0.2% increase in non-idle NTSOA and 2.2% increase in idle NTSOA) and 10.5% in July (2.8% increase in non-idle NTSOA and 28.6% increase in idle NTSOA). Alternatively, using the Pye and Seinfeld (2010) aging scheme, NTSOA concentrations increased by 13.3% in January (18.4% increase in non-idle NTSOA and 2.9% increase in idle NTSOA) and 38.6% in July (16.7% increase in non-idle NTSOA and 76.2% increase in idle NTSOA). These aging schemes, could produce NTSOA concentrations as high as 10.1 ng m^{-3} (2x aging) or 12.6 ng m^{-3} [Pye and Seinfeld (2010) aging] in July, which corresponds to 7.2% and 10.3% of aircraft-attributable $PM_{2.5}$, respectively.

Further away from the airport, the percent increase of NTSOA was higher as the increased distance provided additional time for aging reactions to occur. At distances of 6–30 km, 31–54 km, and 55–102 km away from ATL, the 2x aging scheme increased NTSOA by 2.9%, 3.9%, and 6.4% in January and 24.0%, 37.8%, and 48.5% in July, respectively. The Pye and Seinfeld (2010) aging scheme increased NTSOA by 22.1%, 26.0%, and 33.9% in January and 65.5%, 84.9%, and 91.0% in July at the same set of distances. As a percentage of aircraft-attributable $PM_{2.5}$, the Pye and Seinfeld (2010) NTSOA aging results correspond to contributions of 5.6% in January and 19.5% in July 6–30 km away from ATL, 17.7% and 14.3% 31–54 km away, and 24.0% and 7.5% 55–102 km away, suggesting aircraft-attributable $PM_{2.5}$ could be underpredicted by as much as 20–24% downwind of the airport.

3.5 Conclusions

An aircraft-specific parameterization of NTSOA formed from aircraft engine emissions of S/IVOC and based on smog chamber data was successfully incorporated into CMAQ with VBS using SAPRC-07 chemical mechanism. The newly represented NTSOA, a heretofore unaccounted for $PM_{2.5}$ component in most air quality models, was generally confined to near the airport and increased monthly average $PM_{2.5}$ contributions by 2.4 ng m^{-3} (34% from idle and 66% from non-idle) in January and 9.1 ng m^{-3} (33% and 67%) in July. This represents a 1.7% (of 140 ng m^{-3}) and 7.4% (of 122 ng m^{-3}) increase in aircraft-attributable $PM_{2.5}$ and are approximately 6 times higher than TSOA contributions from aircraft emissions. Downwind of the airport, NTSOA as a percentage of aircraft-attributable $PM_{2.5}$ was higher, where NTSOA averaged 4.6% in January and 11.8% in July 6–30 km downwind, 14.0% and 7.7% 31–54 km downwind, and 17.9% and 4.0% 55–102 km downwind. These results suggest that grid-based air quality models may underestimate the impacts of aircraft emissions on $PM_{2.5}$ by 2–7% near airports and 4–18% downwind due to missing contributions from NTSOA, and could be as high as 10% near the airport and 20–24% downwind when considering uncertainty associated with NTSOA aging.

However, as a percentage of aircraft-attributable $PM_{2.5}$, SOA results were generally low compared to other PM components, such as inorganic aerosols and elemental carbon, particularly near the airport. We, at least partially, attribute this to the spatial scales (modeled grid resolution) at which SOA was considered. SOA gas-particle partitioning is dependent on the total OA concentration. At smaller volumes, such as inside aircraft plumes or smog chambers, OA concentrations can potentially reach much higher levels due to concentrated POA emissions, partitioning a large fraction of semi-volatile organics to the particle phase.

Additional research to assess aircraft impacts on PM could include the treatment of POA emissions as semi-volatile as well as use a sub-grid scale treatment, or other alternate approaches to include sub-grid variability, to track the formation of aerosols due to aircraft emissions near the aircraft engine and downstream. Specifically, this would include obtaining additional information from previous and ongoing field campaigns that include measurements of volatile components of PM from aircraft engines (Kinsey et al., 2010) and newly developed techniques to estimate aircraft PM emissions in place

of FOA3, such as the 1-D plume-scale Aerosol Dynamics Simulation Code (ADSC) model (Wong et al., 2008) which has recently been expanded to provide aircraft emission estimates of S/IVOCs. With the sub-grid scale treatment, the impacts of aircraft NO_x emissions on reductions in biogenic TSOA concentrations seen in previous studies (Arunachalam et al., 2011; Woody et al., 2011; Woody and Arunachalam, 2013) would likely be mitigated and the ratio of SOA to POA may increase.

This study is a part of a larger effort to create an integrated modeling system to model aircraft emissions at airports — using an enhanced VBS framework in CMAQ (to improve OC contributions), to incorporate plume-scale models such as CMAQ-APT (Karamchandani et al., 2014) (to improve sub-grid scale characterization), and ADSC (to improve near-field estimates) with an end goal of improved characterization of $PM_{2.5}$ contributions from aircraft emissions at multiple spatial scales.

CHAPTER 4 MULTISCALE PREDICTIONS OF AIRCRAFT-ATTRIBUTABLE $PM_{2.5}$ MODELED USING CMAQ-APT FOR U.S. AIRPORTS

4.1 Abstract

Aviation activities represent an important and unique mode of transportation, but also impact air quality due to gaseous and particulate emissions. In this study, we aim to quantify the impact of aircraft on air quality, focusing on aviation-attributable $PM_{2.5}$ at scales ranging from local (a few kilometers) to continental (spanning hundreds of kilometers) using the Community Multicale Air Quality-Advanced Plume Treatment (CMAQ-APT) model. In our CMAQ-APT simulations, a plume-scale treatment is applied to aircraft emissions from 99 major U.S. airports over the contiguous U.S. in January and July. In addition to the plume-scale treatment, we account for the formation of non-traditional secondary organic aerosols (NTSOA) from the oxidation of aircraft S/IVOC emissions, and utilize alternative emission estimates from the Aerosol Dynamics Simulation Code (ADSC), a 1-D plume scale model that estimates engine specific PM and S/IVOC emissions at ambient conditions (accounting for relative humidity and temperature). We estimated monthly and contiguous U.S. average aviation-attributable $PM_{2.5}$ to be 2.7 ng m^{-3} in January and 2.6 ng m^{-3} in July using CMAQ-APT with ADSC emissions. This represents an increase of 40% and 12% in January and July, respectively, over impacts using traditional modeling approaches (traditional emissions and without APT). Furthermore, the maximum fine-scale (subgrid scale) impacts near a major airport were 23.7 μg m^{-3} in January (5-km downwind of the airport) and 59.3 μg m^{-3} in July (1-km downwind of the airport), considerably higher than the maximum grid-based impacts near the airport of 4.3 μg m^{-3} in January and 0.5 μg m^{-3} in July.

4.2 Introduction

Fine particulate matter ($PM_{2.5}$) has known adverse health effects (Dockery and Pope, 1994), negatively impacts visibility (Sisler and Malm, 2000), and influences climate change (Bauer and Menon, 2012). Additionally, $PM_{2.5}$ is one of six criteria air pollutants regulated by the U.S. Environmental

Protection Agency (EPA) under the Clean Air Act. Emission mitigation and control strategies have led to a decline in national average $PM_{2.5}$ concentrations by 33% from 2000 to 2012 (U.S. Environmental Protection Agency, 2013). However, the number of total passengers traveling by aircraft (which both directly emit $PM_{2.5}$ as well as precursors of $PM_{2.5}$) grew 10% over this same 12 year span (Federal Aviation Administration, 2014a). Furthermore, the number of passengers traveling via aircraft in the U.S. is expected to grow 2.3% per year over the next 20 years (Federal Aviation Administration, 2014a). Given the opposing trends in U.S. $PM_{2.5}$ concentrations and aviation activity, it is important to accurately quantify aviation-attributable $PM_{2.5}$ to both estimate current aviation related impacts and provide guidance for future policies and regulations.

Source specific air quality impacts are commonly estimated using air quality models (AQMs) (e.g. Unal et al., 2005; Nam et al., 2006; Hodzic et al., 2007; Bergin et al., 2008; Pacsi et al., 2013). However, uncertainty in aircraft emissions and their treatment in AQMs, have led to varying results. For example, aviation-attributable premature mortalities based on AQM estimates range from 620 per year (Jacobson et al., 2013) to as high as 12,600 (Barrett et al., 2010) for full-flight global aircraft emissions and from 75 (Levy et al., 2012) to 210 (Brunelle-Yeung et al., 2014) for landing and takeoff (LTO) emissions in the U.S.

A portion of the uncertainty originates from the treatment of aircraft emissions in AQMs. Traditionally, aircraft LTO emissions are instantaneously diluted into the grid cell containing the airport. However, when assessing aviation impacts, this may not be a good assumption. Unal et al. (2005) sought to improve this approach in an AQM by allocating aircraft emissions vertically and found that the improved treatment lowered ozone and $PM_{2.5}$ impacts from aircraft by 75–80% at the Hartsfield-Jackson Atlanta International Airport (ATL). Additionally, the instantaneous dilution of aircraft emissions can produce non-linearities in aviation-attributable $PM_{2.5}$ at varying modeled grid resolutions. For example, Arunachalam et al. (2011) indicated that at a finer grid resolution (4-km), aviation emissions from ATL increased the secondary organic aerosol (SOA) component of $PM_{2.5}$ but when modeled at a coarser grid resolutions (12-km and 36-km), the same emissions reduced SOA concentrations. Woody and Arunachalam (2013) found that at the finer resolution aircraft emissions

of primary organic aerosol (POA) influenced the gas to particle phase partitioning of semi-volatile organics, promoting partitioning to the particle phase to form additional SOA. However, at the coarser resolution, NO_x (emitted from aircraft) chemistry had a greater influence on SOA concentrations by lowering free radical concentrations and thus lowering SOA precursor (from all sources) oxidation.

Furthermore, air quality estimates in grid-based AQMs, such as the Community Multiscale Air Quality (CMAQ) model (Byun and Schere, 2006), are only available at scales equivalent to the modeled grid resolution. If results at scales finer than the AQM grid are desired, other models or modeling techniques are required (e.g. dispersion models). Additionally, finer AQM grid resolutions (e.g. 4-km) are generally used to obtain fine scale air quality estimates, but due to increased computational costs, the domains cover a smaller area (e.g. hundreds of km). Alternatively, coarser grid resolutions (e.g. 36-km) can provide more widespread impacts (e.g. contiguous U.S.), but at the cost of coarser impacts.

An alternative modeling approach, the plume-in-grid (PinG) treatment, could potentially alleviate some of these limitations. PinG treats emissions from a particular source at the subgrid scale level, allowing those emissions to evolve chemically prior to being diluted into the grid. Therefore, this treatment could prevent non-linearities in chemistry at varying model resolutions as emissions would no longer be immediately diluted into the grid, but instead are chemically aged in the plume before interacting with background concentrations. PinG also has the added advantage of simultaneously providing subgrid scale (fine scale) impacts and grid-based (larger scale) impacts using a consistent modeling framework (i.e. same chemical mechanism, aerosol treatment, emissions, meteorology, etc.). Because the model tracks individual plumes, the locations and concentrations within plumes can be used to provide air quality impacts at any given point in the model (plume concentration plus grid cell concentrations), as opposed to just a grid-based concentration.

The PinG modeling approach is generally used for large emission sources, such as electric generating units (EGUs) though a number of recent studies have examined using PinG modeling techniques to represent aircraft emissions (Jacobson et al., 2013; Cameron et al., 2013; Rissman et al., 2013). Cameron et al. (2013) indicated that when aircraft emissions are treated using PinG, ozone production is reduced by 33% for a single flight and up to 77% for multiple overlapping flights compared

Figure 4.1: Locations and tier classifications of the 99 airports.

to a grid-based treatment. At the ATL airport, Rissman et al. (2013) using the CMAQ - Advanced Modeling System for Transport, Emissions, Reactions, and Deposition of Atmospheric Matter (AMSTERDAM) model (an earlier version of the PinG model used in this study) found that treating LTO aircraft emissions using PinG tended to increase secondary aircraft-attributable $PM_{2.5}$ by up to 10% while also lowering primary aircraft-attributable $PM_{2.5}$ by approximately 5%.

Additional uncertainty in AQM predictions of aviation-attributable $PM_{2.5}$ is introduced by the methodology used to estimate aircraft PM emissions, typically the First Order Approximation (FOA3) (Wayson et al., 2009). Comparisons against measurements have shown FOA3 estimates of POA and elemental carbon (EC) vary by an order of magnitude for 40% of aircraft engines (Stettler et al., 2011). Also, FOA3 assumes POA emissions are non-volatile and does not account for variations in POA emissions due to changes in ambient temperature. However, measurements have shown that organic aerosol formation 30 meters downwind of the engine is highly dependent on ambient temperature due to their volatility (Beyersdorf et al., 2014).

Finally, uncertainty is introduced from missing formation pathways for the SOA component of aircraft-attributable $PM_{2.5}$ in AQMs, which is believed to be the case for other emission sources as

well (Jathar et al., 2014). Miracolo et al. (2012) measured a significant amount of SOA formed from aircraft emissions in a smog chamber and were unable to reproduce the results using traditional modeling approaches. They concluded that the gap between measurements and the model was attributable to SOA formed from semi-volatile and intermediate volatility organic compounds (S/IVOCs) emitted by aircraft. Jathar et al. (2012), utilizing the smog chamber measurements of Miracolo et al. (2012), developed a parameterization to estimate non-typical SOA (NTSOA) formed from aircraft emissions of S/IVOCs in an AQM. When implemented, this parameterization estimated NTSOA comprised an additional (and previously unaccounted for) 2–24% of aircraft-attributable PM (Woody et al., 2014).

The goal of this study is to reduce uncertainty in aircraft-attributable PM estimates in an AQM introduced by 1) varying results produced at different model grid resolutions, 2) emission estimates, and 3) missing PM formation pathways. We aim to accomplish this goal in three ways. First, we use a plume-in-grid treatment for aircraft emissions, allowing aircraft emissions to chemically evolve in a plume before adding them back into the grid and which simultaneously provide fine scale and larger scale aviation related impacts. Second, we employ alternative PM emission estimates (which include S/IVOCs) derived from the 1-D plume model Aerosol Dynamics Simulation Code (ADSC) (Wong et al., 2008). Finally, we include the formation of NTSOA from aircraft emissions of S/IVOCs, using the volatility basis set (VBS) framework (Donahue et al., 2006), to reflect the findings of recent sampling and smog chamber data (Miracolo et al., 2012). This modeling framework is applied to a 36-km continental U.S. modeling domain in January and July, 2005 in an effort to quantify $PM_{2.5}$ produced from aircraft LTO emissions at 99 major contiguous U.S. airports.

4.3 Methodology

Aircraft-attributable $PM_{2.5}$ was estimated in January and July, 2005 using CMAQ - Advanced Plume Treatment (APT) (Byun and Schere, 2006; Karamchandani et al., 2014), which incorporates a plume scale treatment into CMAQ v5.0.1 using the Second-order Closure Integrated puff model with CHEMistry (SCICHEM) (Electric Power Research Institute, 2003). SCICHEM uses overlapping 3-D puffs to represent plumes and includes plume dynamics, such as plume rise, dispersion, puff merging/splitting, and an identical chemical mechanism and aerosol module as the parent model. We utilized the Carbon Bond 2005 (CB05) (Yarwood et al., 2005) chemical mechanism and the aerosol 6

Table 4.1: Monthly total aircraft emissions (short tons) in January (Jan) and July (Jul) of CO, NO_x (as NO_2-equivalent), SO_2, and VOCs.

	CO	NO_x	SO_2	VOCs
Jan	3,787	7,934	481	1,681
Jul	4,097	8,562	521	1,835

Table 4.2: Monthly total aircraft emissions (short tons) in January (Jan) and July (Jul) of primary elemental carbon (PEC), primary organic aerosol (POA) plus primary semi-volatile organic carbon (pSVOC), and primary sulfate (PSO4) for AEDT (based on FOA3) and ADSC.

		PEC	POA + pSVOC	PSO4
Jan	AEDT	15.3	39.0	14.9
	ADSC	89.8	82.5	10.6
Jul	AEDT	16.3	42.3	16.1
	ADSC	95.0	91.2	11.6

(AE6) module with the VBS approach to model organic aerosols recently incorporated in CMAQ by Koo et al. (2014). VBS for organics is preferred in this study because of its ability to include a non-traditional secondary organic aerosols (NTSOA) parameterization for aircraft emissions as described in Jathar et al. (2012) and implemented in CMAQ in Woody et al. (2014). Additionally, it provides a framework for us to treat POA as semi-volatile, which we apply to aircraft POA emissions and marks the first time (we are aware of) that this treatment has been applied to aircraft emissions in a regional air quality model.

The modeling domain consisted of a 36-km horizontal grid resolution over the contiguous U.S. and 34 variable width vertical layers from the surface to 50 millibars. Meteorological inputs were based on NASA's Modern-Era Retrospective Analysis for Research and Applications (MERRA) (Rienecker et al., 2011) and downscaled using the Weather Research and Forecasting (WRF) model (Skamarock and Klemp, 2008). Dynamically varying boundary conditions were derived from global Community Atmosphere Model with Chemistry (CAM-chem) (Lamarque et al., 2012) output (Olsen et al., 2013). Spatio-temporally resolved lightning NO_x emissions were included and estimated using National Lightning Detection Network (NLDN) (Orville et al., 2002) flash density data (Allen et al., 2012). Non-aviation emissions were generated using the Sparse Matrix Operator Kernel Emissions (SMOKE) model (Houyoux et al., 2000) and estimated using the U.S. EPA's 2005 National Emissions Inventory (NEI) (U.S. EPA, 2007).

Table 4.3: Monthly total aircraft emissions (short tons) in January (Jan) and July (Jul) of SVOCs and IVOCs for AEDT and ADSC.

		SVOCs						IVOCs				
C*		Non-Vol	10^0	10^1	10^2	10^3	Total	10^4	10^5	10^6	10^7	Total
Jan	AEDT	12.6	3.8	4.5	4.8	13.3	39.0	11.9	13.2	171.1	184.5	380.7
	ADSC	3.6	4.2	16.7	0.8	57.2	82.5	22.0	204.4	48.3	181.9	456.6
Jul	AEDT	13.6	4.2	4.9	5.3	14.4	42.3	13.2	15.9	216.1	233.1	478.4
	ADSC	3.9	4.5	17.8	0.9	64.1	91.2	26.8	222.2	52.5	197.6	499.0

Aircraft emissions from landing and takeoff (LTO) activities up to 1 km at 99 major U.S. airports (Figure 4.1 and Table C.1) for NO_x [speciated to NO, NO_2, and HONO using Wood et al. (2008)], SO_2, CO, total organic gases (TOG) (Table 4.1), and primary PM (sulfate, organic aerosols, and elemental carbon) (Table 4.2) were incorporated into CMAQ. Emission estimates were based on the Aircraft Environmental Design Tool (AEDT) global aircraft emission inventory for 2005 (Olsen et al., 2013). The inventory provides high resolution emissions data both in space and time for individual flights globally. Gas-phase emissions in AEDT were based on International Civil Aviation Organization (ICAO) reported mode-specific emission factors (EFs) while primary PM emissions were based on the First Order Approximation v3 (FOA3) (Wayson et al., 2009). The 99 airports represent approximately 85% of total flight activity in the U.S. and are identical to those used in Woody et al. (2011).

Aircraft POA/SVOC emissions were estimated using AEDT POA emissions and split into VBS volatility bins (spanning volatilities from non-volatile up to a C* of 10^3 μg m^{-3}) using engine power setting specific fractions reported by Jathar et al. (2012). This maintains the mass of POA emissions from AEDT. However, higher volatility SVOC emissions will evaporate to the gas phase and therefore lower total particle emissions. This treatment operates on the assumption that POA emission factors were made at low dilution and therefore most semi-volatiles are measured in the particle phase whereas at ambient conditions portions of SVOC/POA would evaporate to the gas phase. Similarly, IVOC emissions (C* of 10^4 – 10^7 μg m^{-3}) were scaled from AEDT POA emissions using Jathar et al. (2012) fractions for IVOCs. S/IVOC emission estimates are provided in Table 4.3.

Alternative aircraft PM emissions (primary sulfate, elemental carbon, and POA) and S/IVOCs were estimated using ADSC, which has previously shown to provide accurate PM emission estimates

of primary sulfate from aircraft (Wong et al., 2008). ADSC currently provides aircraft emissions for 6 engines (BR-715, CF34-3B, CFM56-2C5, CFM56-7B26, JT8D-219, and PW2037) across a range of engine power settings and ambient conditions. The 6 ADSC engines (out of 500 ICAO certified engines) accounted for approximately 25% of U.S. flights in 2005.

To generate an emission inventory using ADSC, a total of 2,304 ADSC simulations were performed for the 6 aircraft engines, at 6 power settings (4%, 7%, 30%, 65%, 85%, and 100%), 8 relative humidities (10–80%), and 8 temperatures (275–310 K). Considerations were made to incorporate ADSC into CMAQ to run inline. However, ADSC run times made this impractical (typically 1-2 hours for a single simulation and up to 1-2 days in some instances). Therefore, the ADSC simulations were performed offline and lookup tables containing emission factors for each engine/power setting/humidity/temperature combination were generated (Figure C.3). The lookup tables were interfaced with AEDT aircraft information (locations, engine types, time-in-mode) and ambient conditions (temperature and relative humidity) from WRF data to generate emission estimates (Figure C.4). Non-ADSC engines were mapped to ADSC engines using ICAO reported smoke number, a proxy for aircraft EC emissions.

Table 4.2 provides a comparison of AEDT and ADSC emissions. In general, EC emissions are approximately six times higher with ADSC while POA emissions are approximately twice as high. However, the volatility split of SVOC (and IVOC) emissions is different in ADSC (Table 4.3). More ADSC emissions are in the higher volatility bins compared to AEDT, suggesting that while ADSC may have higher POA emissions, much of that additional mass will likely be found in the gas phase. The ADSC model assumes a different speciation of SO_2 and sulfate emissions and, while the total amount of sulfur is consistent between the two models, ADSC estimates slightly lower sulfate emissions and slightly higher SO_2 emissions compared to AEDT.

CMAQ-ready point source inline emission files for aircraft were generated using the AEDT2inline tool, which, using aircraft trajectories taken from the AEDT database, allocates aircraft emissions in four dimensions (x, y, z, and time) and performs appropriate conversions of inventory pollutants into model species. TOG was speciated into CB05 model species using the most recent EPA speciation profile (SPECIATE profile 5565B, Table 3.2) which is based on results of a joint Federal Aviation

Table 4.4: SPECIATE v4.3 speciation profile 5565B used to speciate aircraft non-hazardous air pollutant (non-HAP) total organic gas (TOG) emissions to CB05 model species. Note that the total mass fraction is >100% as benzene is classified as a HAP species but is included due to its role as an SOA precursor.

Common Name	Model Species	Mass Fraction	Molecular Weight (g/mol)
Paraffin	PAR	0.3759	14.3326
Terminal Olefin	OLE	0.0876	28.5737
Methanol	MEOH	0.0181	32.0419
Internal Olefin	IOLE	0.0246	56.1063
Formaldehyde	FORM	0.1389	29.3904
Ethane	ETHA	0.0052146	30.069
Ethene	ETH	0.1546	28.0532
Benzene	BENZENE	0.0168	78.1118
Aldehydes	ALDX	0.0585	35.2256
Acetaldehyde	ALD2	0.0435	43.6298
Toluene	TOL	0.0223	98.148
Unreactive	UNR	0.043	13.4366
Xylene	XYL	0.0278	105.7999

Administration (FAA) and EPA effort (U.S. EPA, 2009a,b).

Airports were divided into three tiers based on size/flight activity, where Tier I represents large airports, Tier II represents medium sized airports, and Tier III represents smaller airports (Figure 4.1 and Table C.1). The tier grouping loosely maps to FAA's large, medium, and small hub designation. The 12 airports in Tier I represent approximately 33% of total flight activity across the 99 airports, the 17 Tier II airports represent approximately 30% of flight activity, and the other 47 Tier III airports comprise the remaining 37% of activity. This grouping was used to determine the number of points used to represent aircraft PinG emitter locations at each airport. A total of 1,923 point sources were utilized across the 99 airports, with 49 points at each Tier I airport, 25 at each Tier II airport, and 13 at each Tier III airport. This approach provides a more explicit treatment at larger airports compared to smaller airports and reduces the total number of emitters used in CMAQ-APT to produce reasonable model run times.

Three dimensional aircraft emitter locations were determined using AEDT aircraft locations, as AEDT has the ability to provide highly resolved flight trajectories based on radar data. However, this type of accuracy is generally reserved to AEDT simulations at a single airport or a handful of airports. For large applications with hundreds of airports, such as the global inventory used in this study, the trajectories in the near field of the airport are not as highly resolved. Therefore, aircraft emitter points

Table 4.5: Summary of CMAQ model scenarios.

Case	Aircraft Emissions	PinG?
base	N/A	No
AEDT	AEDT	No
AEDT_APT	AEDT	Yes
ADSC_APT	ADSC	Yes

begin at the airport and radiate out in straight lines, similar to the locations provided by AEDT (Figure C.1).

A total of four CMAQ cases were simulated in January and July 2005. Table 4.5 summarizes each of the CMAQ cases. Aircraft contributions (and contributions from the PinG treatment and ADSC emissions) were calculated as the difference in scenarios with aircraft emissions (or PinG/ADSC) versus those without.

Fine scale (subgrid scale) CMAQ-APT impacts were determined as a post-processing step using on-demand receptors. These receptors were located in concentric circles surrounding each airport at distances of 1, 5, 10, 25, and 50 km. Concentrations at receptors were meant to represent exposures and were estimated as grid-based concentrations plus the concentration of plumes located at that receptor. Therefore, in the absence of a plume at a given receptor, the concentration reported at that receptor would be the equivalent to the grid-based concentration.

4.4 Results and Discussion

4.4.1 Contiguous U.S. Results

Within the contiguous U.S., model predictions using ADSC emissions with plume-in-grid (ADSC_APT) indicated aircraft emissions increased monthly average $PM_{2.5}$ by 2.7 ng m^{-3} in January and 2.6 ng m^{-3} in July (Figure 4.2). These impacts represent an increase of 40% and 12% in January and July, respectively, over impacts estimated using traditional modeling approaches [AEDT emissions and without PinG (AEDT) scenario].

In January, the major component of aircraft-attributable $PM_{2.5}$ was ammonium nitrate aerosol (AHN4 + ANO3), comprising approximately 58% of $PM_{2.5}$ (Figure 4.2), formed from the interaction of aircraft NO_x emissions with ammonium emissions from agricultural activities. This is predominately seen in agricultural areas rich in ammonia, such as Eastern North Carolina and Iowa, Michigan,

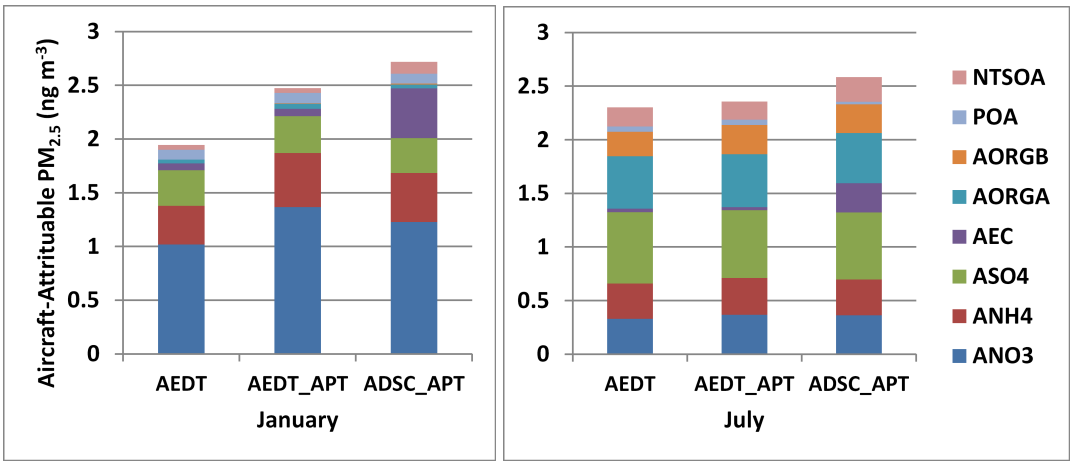

Figure 4.2: Speciated monthly average aircraft-attributable $PM_{2.5}$ in January and July 2005 for AEDT, AEDT_APT, and ADSC_APT, relative to the base simulation. $PM_{2.5}$ species include non-traditional secondary organic aerosol (NTSOA), primary organic aerosol (POA), biogenic SOA (AORGB), traditional anthropogenic SOA (AORGA), elemental carbon (AEC), sulfate aerosol (ASO4), ammonium aerosol (ANH4), and nitrate aerosol (ANO3).

Minnesota, and Illinois.

In July, higher temperatures meant the formation of ammonium nitrate was thermodynamically less favorable, allowing the formation of more ammonium sulfate (ANH4 + ASO4) relative to ammonium nitrate and which comprised 33% of aircraft-attributable $PM_{2.5}$ in July. The increase in temperatures (and photooxidation) also increased SOA species [traditional anthropogenic SOA (AORGA), NTSOA, and biogenic SOA (AORGB)] concentrations (37% of $PM_{2.5}$) due to an increase in radical concentrations and therefore additional SOA precursor oxidation (Figure 4.2). This is in contrast to Woody et al. (2011), who found that approximately 95% of aircraft-attributable $PM_{2.5}$ consisted of inorganic species (ammonium nitrate and ammonium sulfate) and is likely due to the use of a different aerosol module in CMAQ [AE4 in Woody et al. (2011) versus AE6 + VBS in this study] and the addition of NTSOA. The shift in $PM_{2.5}$ composition from January to July also corresponded with a shift in spatial impacts, with higher impacts seen around airports in July (e.g. Atlanta, GA; New York, NY; Los Angles, CA; etc.) (Figure 4.3).

The increase in aviation-attributable $PM_{2.5}$ in ADSC_APT over AEDT was largely due to ammonium nitrate and EC in January and EC in July. However, ammonium nitrate impacts with ADSC_APT were approximately 10% lower compared to the AEDT emissions with plume-in-grid (AEDT_APT

scenario) due to changes in primary sulfate emissions between the two cases. In ADSC_APT, the speciatation of sulfate and SO_2 emissions led to lower sulfate emissions (instead emitted as SO_2) and thereby lowered both ammonium sulfate and ammonium nitrate impacts. However, given the relatively higher impacts of ammonium nitrate, the changes in nitrate were more pronounced. Spatially, ADSC_APT inputs were similar to AEDT_APT (discussed below) with the exception of increased contributions at and near airports from additional EC emissions (Figure 4.3).

Aircraft do not directly emit biogenic SOA precursors. Therefore increased biogenic SOA concentrations were the result of interactions between aircraft emissions and biogenic SOA precursors. This may be true for anthropogenic SOA as well. Results from Woody et al. (2014) indicated anthropogenic SOA formed from aircraft emissions in summer was minimal ($< 1\%$) at ATL. This, coupled with the increase in biogenic SOA concentrations suggest aircraft increase radical concentrations and therefore the oxidation of SOA precursors emitted by non-aviation sources. Finally, NTSOA comprised 9% of aircraft-attributable $PM_{2.5}$ in July but only 4% in winter, consistent with the results presented in Chapter 3.

AEDT_APT estimates indicated aircraft-attributable monthly average $PM_{2.5}$ concentrations increased in the U.S. in January compared to AEDT estimates (from 1.9 ng m^{-3} to 2.5 ng m^{-3}, 27% increase) and produced similar concentrations in July (from 2.3 to 2.4 ng m^{-3}, 2% increase) (Figure 4.2). The increase in winter was attributable to an increase in ammonium nitrate aerosol, as aircraft NO_x emissions in puffs were converted to nitric acid which, when neutralized, formed ammonium nitrate. Spatially, this effect generally occurred throughout the U.S., with the use of PinG increasing aircraft-attributable $PM_{2.5}$ at and around airports (Figure 4.3). In July, the formation of ammonium nitrate was thermodynamically less favorable and therefore this formation pathway for $PM_{2.5}$ was less pronounced. PinG did not significantly alter any of the other $PM_{2.5}$ species and therefore resulted in a minimal change in July. This is also true spatially, as impacts were similar with and without PinG with slight increases and decreases throughout the U.S. in July (Figure 4.3).

Predictions from the AEDT scenario represent a more traditional modeling approach and provide a baseline we can use to compare our results to other traditional modeling studies. The AEDT scenario estimated aircraft increased $PM_{2.5}$ by 1.9 ng m^{-3} in January and 2.4 ng m^{-3} in July, which is

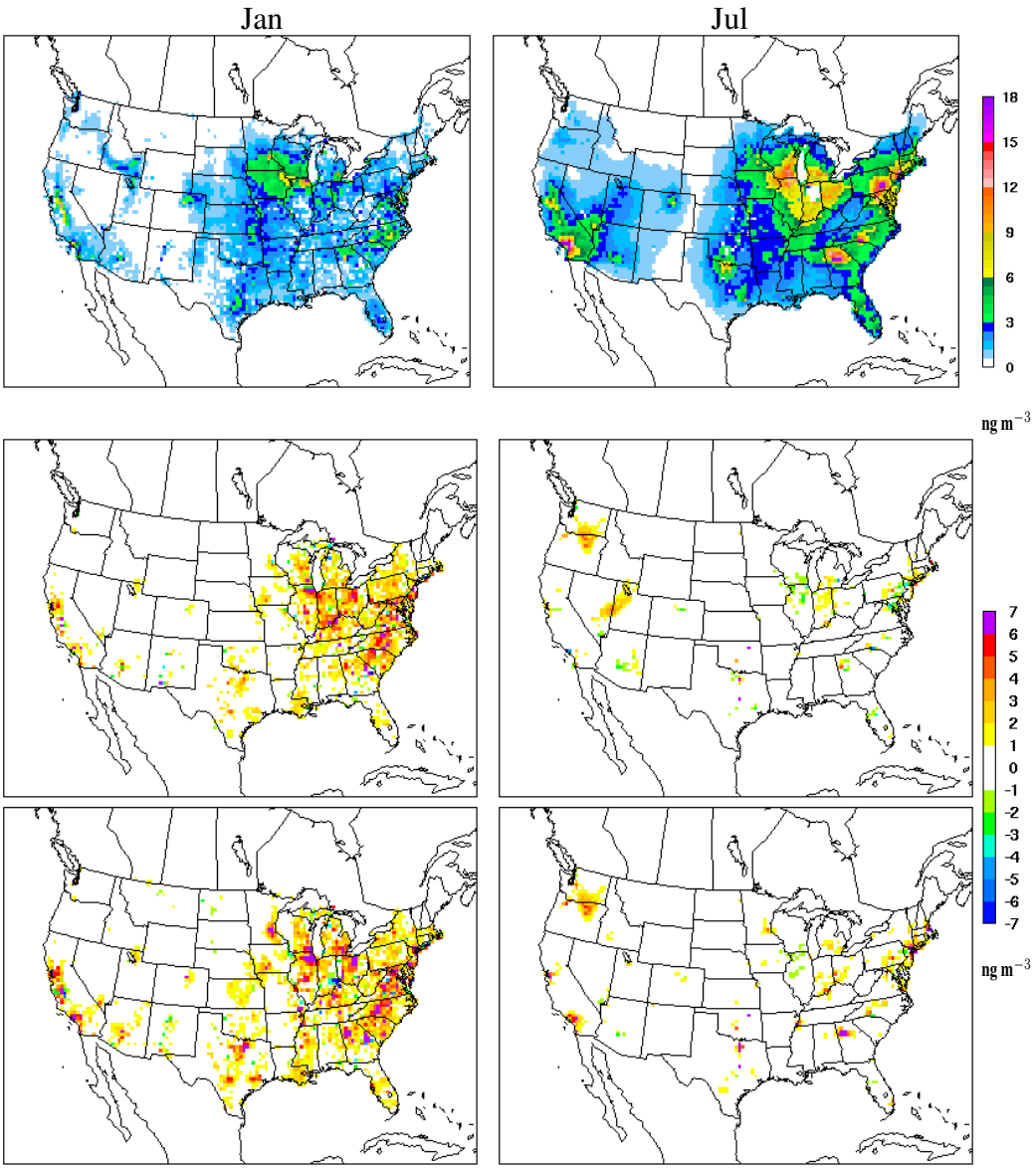

Figure 4.3: Monthly average aircraft-attributable $PM_{2.5}$ in January and July 2005 for AEDT (top), AEDT_APT minus AEDT (middle), and ADSC_APT minus AEDT (bottom).

slightly lower than the 3.2 ng m^{-3} reported by Woody et al. (2011) for aircraft impacts from the same 99 airports on an annual average basis. Note that Woody et al. (2011) used a different emission inventory based on the predecessor to AEDT [Emission Dispersion Modeling System (EDMS), (Federal Register Notice, 1998)], included LTO emissions up to 3 km (opposed to 1 km used in this study), and used an earlier version of CMAQ (v4.6).

4.4.2 Fine Scale Impacts

Impacts at and around three airports [Atlanta (ATL) (Tier I; 2,650 flights per day), Salt Lake City (SLC) (Tier II; 1,150 flights per day), and Cleveland (CLE) (Tier III; 800 flights per day)] were further analyzed to assess local impacts. These airports were selected due to being located in areas of $PM_{2.5}$ non-attainment and therefore eligible to participate in the FAA's Voluntary Airport Low Emissions (VALE) program (Federal Aviation Administration, 2014b). They are also spatially isolated from other airports, minimizing the influence of emissions from other airports on model results at and around these 3 airports.

ADSC_APT model results indicated that aircraft emissions increased $PM_{2.5}$ in the grid cell containing ATL, SLC, and CLE by 30.0, 10.9, and 8.1 ng m^{-3} in January and 52.9, 5.7, and 10.5 ng m^{-3} in July, respectively (Figure 4.4). $PM_{2.5}$ impacts at ATL and SLC were dominated by primary species directly emitted by aircraft (ASO4, PEC, POA), comprising 71–85% of aircraft-attributable $PM_{2.5}$ (Figure 4.4). However, at CLE primary species only comprised 53% in January and 25% in July of aircraft-attributable $PM_{2.5}$, with higher relative contributions from ammonia nitrate compared to ATL and SLC. Note that biogenic SOA concentrations were lowered at ATL by aircraft emissions in the AEDT scenario, consistent with previous studies (Arunachalam et al., 2011; Woody et al., 2011; Woody and Arunachalam, 2013) but not in the APT scenarios. Moving 18–90 km downwind of the airports, secondary components such as ammonium nitrate in January and SOA in July became more important (Figure 4.4).

As previously discussed, the PinG results also provide the opportunity to examine subgrid scale impacts, defined as puff plus grid scale aircraft impacts, or concentrations representing exposure at a given receptor location attributable to aircraft (Figure 4.5). AEDT_APT concentrations at receptors led to aircraft-attributable $PM_{2.5}$ estimates approximately an order of magnitude higher than

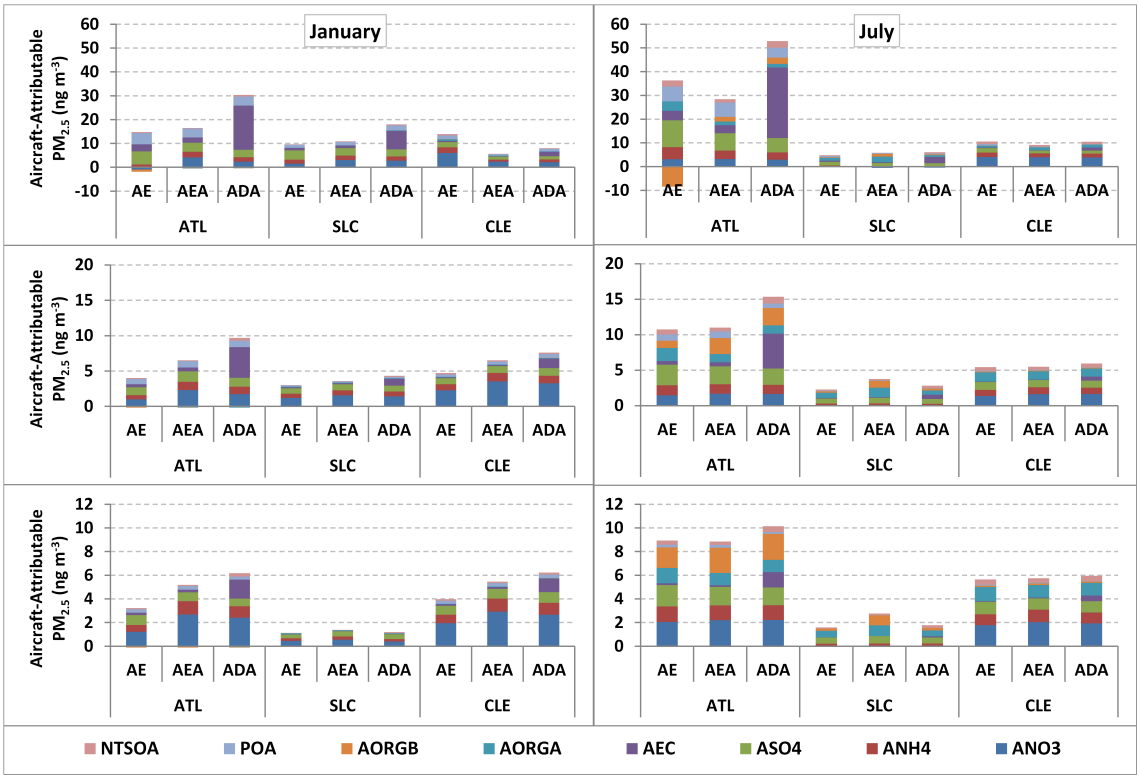

Figure 4.4: Speciated monthly average aircraft-attributable $PM_{2.5}$ in January and July 2005 for AEDT (AE), AEDT_APT (AEA), and ADSC_APT (ADA) in the grid cells containing the Atlanta (ATL), Salt Lake City (SLC), and Cleveland (CLE) airports (top), 19-54 km away from the airports (middle), and 55-90 away from the airports (bottom). Note the change in scale with distance from the airports.

grid-based concentrations alone (Figures C.6 and C.7). Additionally, maximum $PM_{2.5}$ concentrations were as high as 8.4 μg m^{-3} in January (5-km downwind of the airport) and 25.4 μg m^{-3} in July (1-km downwind of the airport), which is approximately two times the maximum grid-based impact in the area surrounding ATL in January (4.3 μg m^{-3}) and approximately 50 times higher the maximum aircraft impact in July (0.5 μg m^{-3}). However, not all puffs, (including those aloft) pass by the receptors and therefore would be detected. It is possible that puffs with higher overall $PM_{2.5}$ concentrations exist but were not included. Furthermore, receptor-based impacts were generally highest 1–5 km downwind of the airport, when puffs were dominated by primary PM species, of relatively small volume, and prior to dilution.

Subgrid scale impacts increased considerably in the ADSC_APT case as receptor-based aircraft impacts reached as high as 23.7 μg m^{-3} in January (5-km downwind of the airport) and 59.3 μg m^{-3} in July (1-km downwind of the airport) (Figure 4.5). This corresponds to increased aircraft impacts of 15.5 μg m^{-3} in January and 33.9 μg m^{-3} in July over AEDT_APT impacts (and 19.4 μg m^{-3} in January and 58.8 μg m^{-3} in July over the maximum grid-based concentrations near ATL). The ADSC_APT impacts were attributable to an increase in both EC and POA concentrations, which is slightly different than grid-based ADSC_APT results where increased aircraft contributions were primarily attributable to EC only. ADSC emission estimates included both higher emissions of EC and POA (Table 4.2). However, much of those emissions occurred at a higher volatility (C* of 10^3 μg m^{-3}) relative to AEDT POA emissions (Table 4.3), and the majority of which would be located in the gas-phase at ambient conditions. However, in puffs where volumes were smaller relative to the grids and organic aerosol concentrations were higher, higher volatile organics partitioned to the particle phase and increased POA concentrations. Once puff volumes increased or the contents of the puffs were merged into the grid and the organic aerosol concentrations returned to values closer to ambient conditions, these higher volatility POA species partitioned back from the particle phase to gas phase.

4.5 Conclusions

We have successfully used CMAQ-APT to model a large number of aircraft sources (∼2,000) as PinG emissions sources on a large scale, simultaneously estimating impacts at fine (subgrid) scales

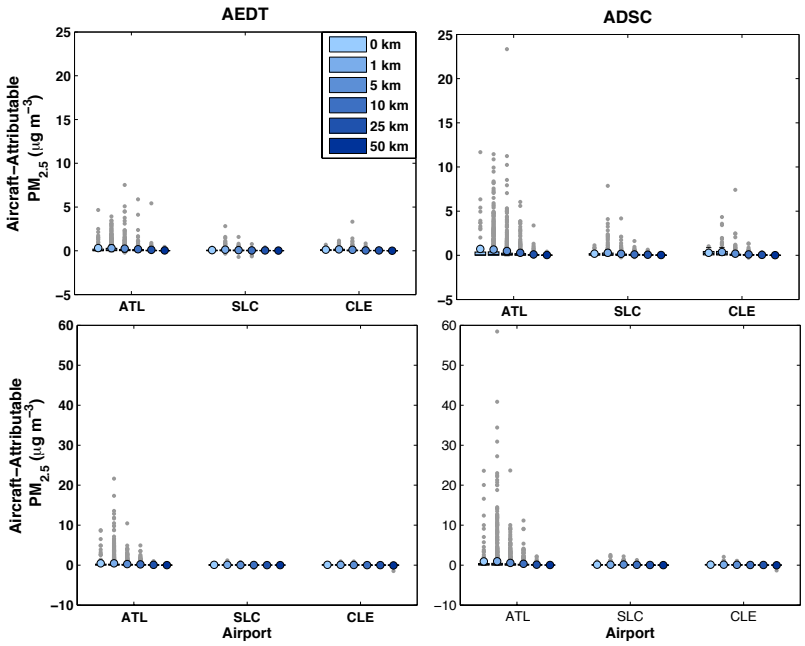

Figure 4.5: Box-and-whisker plots of aircraft-attributable $PM_{2.5}$ (grid plus puff concentrations) at receptors located at the Atlanta (ATL), Salt Lake City (SLC), and Cleveland (CLE) airports and at distances of 1 km, 5 km, 10 km, 25 km and 50 km away in January (top) and July (bottom). Grey dots represent outliers which are defined as values more than 1.5 times the inter-quartile range above the 75th percentile and below the 25th percentile. Figure C.7 in Appendix C replicates this figure but with outliers removed.

and regional scales. Additionally, we have successfully incorporated 1-D plume scale emission estimates into the modeling framework to provide updated emission estimates that include variations based on ambient conditions and volatility based S/IVOC emissions.

Within the contiguous U.S., monthly average aviation-attributable impacts estimated using ADSC emissions and PinG were 2.7 ng m^{-3} in January and 2.6 ng m^{-3} in July. This represents an increase of 40% in January and 12% in July over AEDT emissions without the use of PinG, primarily due to increased contributions from ammonium nitrate in January and EC in both January and July. Subgrid scale impacts were also much higher in ADSC, with a maximum impact of 23.7 μg m^{-3} in January (5-km from the airport) and 59.3 μg m^{-3} in July (1-km from the airport) which was 5.5 μg m^{-3} higher in January and 33.9 μg m^{-3} higher in July over AEDT_APT impacts (and 19.4 μg m^{-3} in January and 58.8 μg m^{-3} in July over the maximum grid-based concentrations near the airport). The higher subgrid impacts in ADSC were largely attributable to the higher primary emissions of EC and POA.

The use of PinG with AEDT emissions generally increased aircraft-attributable $PM_{2.5}$ concentrations in January both locally and regionally due to an increase in ammonium nitrate concentrations compared to scenario with AEDT emissions and without PinG. In July, however, the use of PinG only slightly altered aircraft-attributable $PM_{2.5}$ (increase of 2%). Subgrid scale impacts at and around the airport were approximately an order of magnitude higher than grid-based impacts, with concentrations reaching as high as 8.4 μg m^{-3} in January and 25.4 μg m^{-3} in July, or approximately 2 and 50 times higher than grid-based impacts. Furthermore, the use of PinG prevented the interaction of aircraft NO_x emissions and biogenic SOA precursors. Where previous model results indicated aircraft NO_x emissions lowered biogenic SOA concentrations (Chapter 2), this was no longer the case with PinG.

Future considerations of this work could explore how sensitive model estimates are to the number and location of emitters used to represent aircraft. Specifically, this would include incorporating higher resolution AEDT aircraft locations from single airport AEDT simulations into CMAQ-APT, providing radar based aircraft locations near the airport. Additional considerations include developing ADSC look-up tables for additional aircraft engines to provide a broader base of engines to pull from when developing an ADSC based emission inventory. And finally, considerations should be made

to compare grid-based and subgrid-based aircraft impacts to measurements from field campaigns, though currently a limited number of measurement studies appropriate for comparison to these model results currently exist.

CHAPTER 5 CONCLUSIONS

The primary goal of this work was to reduce uncertainty in predictions of aviation-attributable $PM_{2.5}$ in an air quality model, which was accomplished in three ways:

1. by investigating the non-linearity of SOA produced from aircraft emissions at the Atlanta airport from Arunachalam et al. (2011), examining the CMAQ model processes responsible for the changes in SOA concentrations using process analysis (Chapter 2);

2. by updating CMAQ to include predictions of NTSOA formed from aircraft emissions of S/IVOC using a parameterization developed by Jathar et al. (2012) and based on smog chamber data (Miracolo et al., 2012) (Chapter 3); and

3. by combining plume-in-grid model techniques to remove spatial uncertainty introduced from modeled grid resolution with alternative emission estimates based on a 1-D plume scale model, while simultaneously quantifying both fine scale (subgrid) and regional scale aviation-attributable $PM_{2.5}$ (Chapter 4).

5.1 Non-Linear Response to SOA From Aircraft

Regarding the non-linear response to SOA from aircraft, CMAQ model results indicated that the modeled sensitivity of Atlanta (ATL) aircraft emissions to form SOA concentrations varied depending on the modeled grid resolution. Process analysis was used to successfully diagnose this varying sensitivity and explain the relevant atmospheric process that led to this result. At the 36-km and 12-km model grid cells containing the ATL airport, modeled NO_x emissions from aircraft reacted and reduced NO_3^-, OH, and HOO radical concentrations. The reduction in NO_3^- lowered the amount of biogenic SOA precursors oxidized during nighttime hours. Similarly, reductions in OH radicals

lowered the amount of anthropogenic SOA precursors oxidized during daytime hours while the reduction in HOO radicals lowered the amount of anthropogenic SOA formed through the low-NO_x pathway both during daytime and nighttime hours. At the 4-km grid resolution however, modeled SOA formation was influenced more by concentrations of POA than NO_x chemistry. Modeled POA concentrations reached significantly higher levels due to emissions from aircraft (max concentration of 1.00 μg m^{-3} at the 4-km grid resolution compared to 0.29 μg m^{-3} and 0.08 μg m^{-3} at the 12-km and 36-km grid resolutions, respectively). This increase in organic aerosol mass promoted partitioning of semi-volatile organic carbon gas phase species into the particle phase. Furthermore, the change in modeled SOA concentrations at the 4-km grid resolution was dominated by biogenic SOA, indicating this was the result of interaction between aircraft emissions and biogenic SOA precursors and not caused by anthropogenic SOA precursors contained in aircraft emissions.

Results from this work demonstrated clearly the model sensitivities of SOA formation as it pertains to aircraft emissions and the identification of the relevant processes that cause them. However, further research is needed to determine if a particular grid resolution is a more accurate representation of the actual effects of aircraft emissions on SOA production. Further complicating the problem is the lack of ambient SOA measurements from aircraft emissions, making comparisons against ambient data difficult. Given the current modeling limitations for SOA from aircraft, care must be taken when interpreting aircraft contributions for other types of studies (e.g. health impacts) considering that the SOA component is likely underpredicted.

5.2 NTSOA from Aircraft

For NTSOA, an aircraft-specific parameterization of NTSOA formed from aircraft engine emissions of S/IVOC and based on smog chamber data was successfully incorporated into CMAQ with VBS using the SAPRC-07 chemical mechanism. The newly represented NTSOA, a heretofore unaccounted for $PM_{2.5}$ component in most air quality models, was generally confined to near the airport and increased monthly average $PM_{2.5}$ contributions by 2.4 ng m^{-3} in January and 9.1 ng m^{-3} in July, 2002. These values represent a 1.7% (of 140 ng m^{-3}) and 7.4% (of 122 ng m^{-3}) increase in aircraft-attributable $PM_{2.5}$, respectively, and were approximately 6 times higher than traditional SOA

contributions from aircraft emissions. Downwind of the airport, NTSOA as a percentage of aircraft-attributable $PM_{2.5}$ was higher, where NTSOA averaged as much as 17.9% in January (55–102 km downwind) and 11.8% in July (6–30 km downwind). These results suggest that grid-based air quality models may underestimate the impacts of aircraft emissions on $PM_{2.5}$ by 2–7% near airports and 4–18% downwind due to missing contributions from NTSOA, and could be as high as 10% near the airport and 20–24% downwind when considering uncertainty associated with the NTSOA parameterization.

The increased contributions from secondary organic aerosols (as NTSOA) from aircraft are of potential importance for future emission control strategies or other policies related to aircraft emission impacts on air quality. Traditionally, AQM predictions have been dominated by inorganic species (Woody et al., 2012) and therefore have been the primary focus. However, this work suggests NTSOA, which was previously unaccounted for, is a significant component of aviation-attributable $PM_{2.5}$. As efforts are made to reduce the inorganic portion of aviation-attributable $PM_{2.5}$, such as the desulfurization of jet fuel (Barrett et al., 2012), the importance of aircraft NTSOA will only rise.

5.3 Combination of Plume-in-Grid Model Techniques with Alternative Emission Estimates for Aircraft

In combining modeling techniques for aircraft, the CMAQ-APT model was successfully used to model a large number of aircraft sources as PinG emission sources ($\sim$2,000 PinG sources across 99 airports) on a large scale (contiguous U.S.), simultaneously providing model based estimates at fine (subgrid) scales and regional scales. Additionally, a 1-D plume scale model for aircraft emission estimates was successfully incorporated into the modeling framework to provide alternative emission estimates. These updated emission estimates account for variations in emissions based on ambient conditions (temperature and relative humidity) and include volatility based S/IVOC emissions along with traditional aircraft PM emissions (elemental carbon, primary organic aerosol, and primary sulfate aerosol).

Utilizing ADSC emissions with PinG, we estimated monthly and contiguous U.S. average aviation-attributable $PM_{2.5}$ to be 2.7 ng m^{-3} in January and 2.6 ng m^{-3} in July. This represents a 40% increase in January $PM_{2.5}$ and 12% increase in July $PM_{2.5}$ over estimates using traditional AEDT emissions

and without the use of PinG and was primarily attributed to increased EC emissions and ammonium nitrate formation. Subgrid scale impacts were also much higher in ADSC, with a maximum receptor-based impact of 23.7 μg m^{-3} in January (5-km downwind of the airport) and 59.3 μg m^{-3} in July (1-km downwind of the airport). These values were 5.5 μg m^{-3} higher in January and 33.9 μg m^{-3} higher in July compared to the maximum subgrid scale impacts using AEDT emissions and PinG and 19.4 μg m^{-3} higher in January and 58.8 μg m^{-3} higher in July compared to the maximum AEDT grid-based impacts (without PinG). The higher subgrid impacts in ADSC were largely attributable to the higher primary emissions of EC and POA.

The use of PinG alone increased aircraft-attributable $PM_{2.5}$ concentrations in January, 2005 both locally and regionally, primarily due to an increase in ammonium nitrate concentrations. For example, over the contiguous U.S., aviation-attributable $PM_{2.5}$ concentrations increased by 27% (from 1.9 ng m^{-3} to 2.5 ng m^{-3}) due to PinG. In July, 2005, however, the use of PinG only slightly altered aircraft-attributable $PM_{2.5}$ (increase of 2%) since warm temperatures in summer present less favorable conditions to form ammonium nitrate compared to winter.

Subgrid scale impacts at and around airports (without altering emissions) were approximately an order of magnitude higher than grid-based impacts, with concentrations reaching as high as 8.4 μg m^{-3} in January and 25.4 μg m^{-3} in July, or approximately 2 and 50 times higher than grid-based impacts, respectively. Furthermore, the use of PinG prevented the interaction of aircraft NO_x emissions and biogenic SOA precursors at ATL. Where previous model results indicated aircraft NO_x emissions lowered biogenic SOA concentrations at coarse model grid resolutions (Chapter 2), this was no longer the case when using PinG.

Comparisons of ADSC against measurements made by Kinsey et al. (2010) and Agrawal et al. (2008) suggest that ADSC EC emission indices compare favorably across a range of power settings for two aircraft engines. Also, ADSC provides EC emission estimates for all aircraft engines and power settings, unlike FOA3 which estimates an EC emission index of zero for engine and power settings when Smoke Numbers are not available in the ICAO engine database (Stettler et al., 2011). This also suggests that the ADSC EC emissions are a better indicator of total EC emissions. However, the ADSC emission comparison against measurements was only performed for two engines with

available measurements. While these two engines compared favorably, its possible that other engines (or the mapping of ADSC emission indices to other engines) could bias the ADSC inventory high or low. Additional comparisons of the ADSC (and AEDT) PM emission indices are needed to provide additional certainty in the aircraft emission inventories used in AQMs.

Finally, when considering $PM_{2.5}$ from all emission sources, grid-based results would suggest that aviation-attributable $PM_{2.5}$ comprises only a small ($<1\%$) fraction of total $PM_{2.5}$. From this, one may conclude that air quality impacts (and health related impacts) from aircraft emissions are negligible. However, higher aviation-attributable $PM_{2.5}$ concentrations at the subgrid scale would suggest otherwise. Typical concentrations ranged from 0.1 μg m^{-3} to 1.0 μg m^{-3} several km away from airports which could negatively impact public health and attainment demonstration downwind of the airport. Therefore, while considerations of grid-based impacts do well in providing overall impacts from aircraft, they could potentially miss "hot spots" of impacts near airports.

5.4 Future Considerations

AQMs traditionally underpredict SOA (De Gouw et al., 2005; Volkamer et al., 2006), including CMAQ (Foley et al., 2010). NTSOA from S/IVOC emissions represent a formation pathway which, until recently, was not considered in AQMs. While there is a significant amount of uncertainty associated with NTSOA, both in emissions of S/IVOCs and yields, this pathway could potentially improve AQM predictions of SOA. Aircraft represent a small percentage of total anthropogenic emissions and therefore NTSOA from aircraft is relatively small compared to total $PM_{2.5}$ from all sources. However, other major combustion sources, such as gas and diesel vehicles similarly emit S/IVOCs, and improving NTSOA predictions from these sources in AQMs, as was done in this work for aircraft, would likely significantly increase the amount of SOA mass formed in AQMs.

Future considerations of the PinG work could explore how sensitive model estimates are to the number and location of emitters used to represent aircraft. Specifically, this would include incorporating higher resolution AEDT aircraft locations from single airport AEDT simulations into CMAQ-APT, providing radar based aircraft locations near the airport. Additional considerations include developing ADSC look-up tables for additional aircraft engines to provide a broader base of engines to pull from when developing an ADSC based emission inventory. And finally, considerations should

be made to compare grid-based and subgrid-based aircraft impacts to measurements from field campaigns, though currently a limited number of measurement studies appropriate for comparison to these model results currently exist.

5.5 Uncertainty

Uncertainty still remains in model predictions of aviation-attributable $PM_{2.5}$. For example, the S/IVOC emission estimates used in this work (both AEDT and ADSC emissions) are based on one set of measurements and experiments for a single aircraft engine and extrapolated to other engines. Moreover, considerations of S/IVOC emissions from all sources is a relatively new area and the science is continually evolving. Measurement techniques are still being developed to accurately quantify S/IVOCs emissions and their chemistry and both of which would have direct implications for how S/IVOC and their products are represented in AQMs. Furthermore, aircraft PM emissions on a whole remain uncertain. There are currently approximately 500 active aircraft engines in the ICAO aircraft engine database, each with a unique emission profile. However, ICAO only certifies those engines for NO_x, CO, hydrocarbons, and smoke number, a proxy for EC emissions. Uncertainty will likely remain until measurements of S/IVOC and POA emissions become available for a broader base of aircraft engines. This work provides a step in the right direction but as is the case with any modeling application, results are limited by the accuracy of the model inputs.

Furthermore, evaluations of model predictions of aviation-attributable PM against measurements would help to provide additional certainty in model estimates. Limited measurements are currently available for aircraft and there are no PM measurement standards for aircraft (though a measurement standard for EC is currently being developed). Additionally, measurements are made at a wide range of distances from aircraft (ranging from 1 m behind the engine to 10's of meters) and typically do not provide detailed speciation, reporting total PM, total primary vs. secondary PM, or a single component (e.g. EC). Finally, these types of measurements are commonly made in conjunction with the development of emissions. Therefore, the measurements are reported in terms of mass of pollutant per mass of fuel burned (e.g. gram per kg fuel). While useful for emissions, this type of measurement is difficult to use in a comparison of ambient concentrations, which are reported as a mass per

unit volume (e.g. μg m^{-3}) and more appropriate for model evaluations. These limitations in measurements thereby limit the ability to evaluate model results and indicate the need for comprehensive field measurement campaigns to be conducted at varying spatial scales (near aircraft/runways as well as downwind to assess evolution of aircraft emissions) for speciated PM components to effectively corroborate model results.

APPENDIX A SUPPLEMENTAL MATERIAL: SECONDARY ORGANIC AEROSOL PRODUCED FROM AIRCRAFT EMISSIONS AT THE ATLANTA AIRPORT – AN ADVANCED DIAGNOSTIC INVESTIGATION USING PROCESS ANALYSIS

A.1 CMAQ v4.7 Carbon Bond 05 SOA Precursor Reactions

adapted from CMAQs mech.def file and Carlton et al. (2010)

A.1.1 Biogenic Precursors

$$\mathrm{TERP} + \mathrm{O} \longrightarrow \mathrm{TERPRXN} \tag{A.1}$$

$$\mathrm{TERP} + \mathrm{OH} \longrightarrow \mathrm{TERPRXN} \tag{A.2}$$

$$\mathrm{TERP} + \mathrm{O3} \longrightarrow \mathrm{TERPRXN} \tag{A.3}$$

$$\mathrm{TERP} + \mathrm{NO3} \longrightarrow \mathrm{TERPRXN} \tag{A.4}$$

$$\mathrm{SESQ} + \mathrm{O3} \longrightarrow \mathrm{SESQRXN} \tag{A.5}$$

$$\mathrm{SESQ} + \mathrm{OH} \longrightarrow \mathrm{SESQRXN} \tag{A.6}$$

$$\mathrm{SESQ} + \mathrm{NO3} \longrightarrow \mathrm{SESQRXN} \tag{A.7}$$

A.1.2 Anthropogenic Precursors

$$\mathrm{TOL} + \mathrm{OH} \longrightarrow \mathrm{TOLRO2} \tag{A.8}$$

$$\mathrm{TOLRO2} + \mathrm{NO} \longrightarrow \mathrm{TOLNRXN} \tag{A.9}$$

$$\mathrm{TOLRO2} + \mathrm{HO2} \longrightarrow \mathrm{TOLHRXN} \tag{A.10}$$

$$\mathrm{XYL} + \mathrm{OH} \longrightarrow \mathrm{XYLRO2} \tag{A.11}$$

$$\mathrm{XYLRO2} + \mathrm{NO} \longrightarrow \mathrm{XYLNRXN} \tag{A.12}$$

$$\mathrm{TOLRO_2} + \mathrm{HO2} \longrightarrow \mathrm{XYLHRXN} \tag{A.13}$$

$$\mathrm{BENZENE} + \mathrm{OH} \longrightarrow \mathrm{BENZRO2} \tag{A.14}$$

$$\mathrm{BENZRO2} + \mathrm{NO} \longrightarrow \mathrm{BNZNRXN} \tag{A.15}$$

$$\mathrm{BENZRO2} + \mathrm{HO2} \longrightarrow \mathrm{BNZHRXN} \tag{A.16}$$

RXN species represent oxidized SOA precursors and are used to estimate semi-volatile SOA species in gas/aerosol partitioning. Similarly, NRXN and HRXN species represent oxidized SOA precursors for high NO_x and low NO_x SOA formation pathways, respectively. Some other products in the above reactions not involved in SOA formation were removed for brevity, and to keep the focus on SOA.

A.2 Modeled Aircraft Emissions

A.2.1 Emission Totals

Table A.1: Average monthly total aircraft emissions for 2002 and total aircraft emissions for June 6, 2002; and June 7, 2002 (identical for all 3 grid resolutions) in tons.

	CO	NO_x	SO_2	VOCs	$PM_{2.5}$
Average Monthly Total	481.9	631.9	62.3	81.5	13.8
June 6, 2002	18.8	24.5	2.4	3.9	0.6
June 7, 2002	16.4	21.4	2.1	3	0.5

Table A.2: Surface level aircraft emissions in the airport grid cell for June 6 and 7, 2002 in tons. Note emissions are slightly lower in the 12-km and 4-km grid resolutions due to portions of the airport extending into adjacent grid cells.

	Model Resolution	CO	NO_x	SO_2	VOCs	$PM_{2.5}$
June 6, 2002	36-km	16.2	6.7	1.1	3.6	0.2
	12-km	15.8	6.5	1.1	3.6	0.2
	4-km	12.3	4.3	0.8	1.5	0.2
June 7, 2002	36-km	14.1	6	1	2.8	0.2
	12-km	13.9	5.9	1	2.8	0.2
	4-km	12.1	4.9	0.8	1.3	0.2

A.2.2 Vertical Profile of Emissions

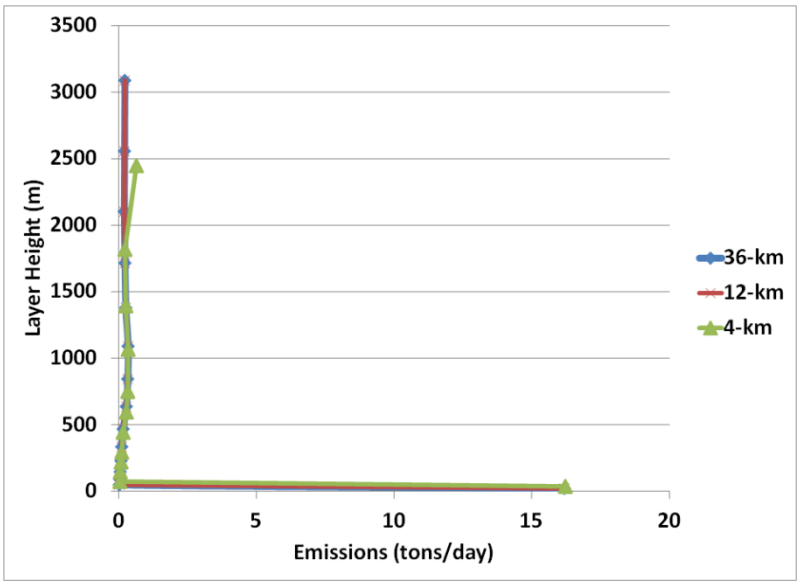

Figure A.1: Vertical aircraft emission profile for CO at the 36-km, 12-km, and 4-km grid resolutions on June 6, 2002.

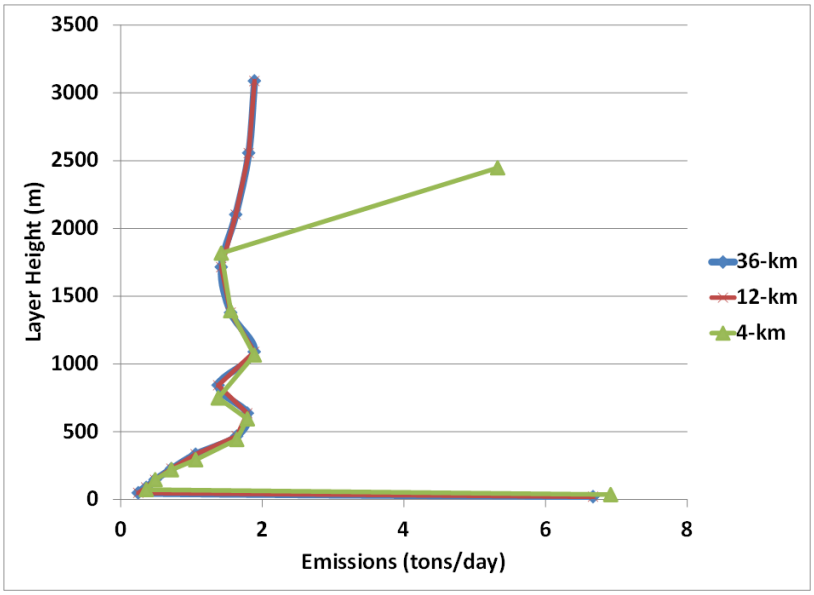

Figure A.2: Vertical aircraft emission profile for NO_x at the 36-km, 12-km, and 4-km grid resolutions on June 6, 2002.

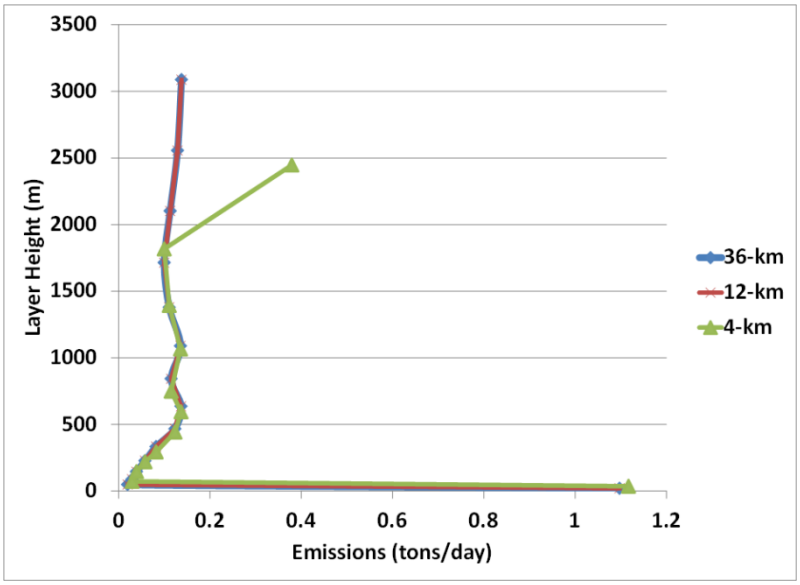

Figure A.3: Vertical aircraft emission profile for SO_2 at the 36-km, 12-km, and 4-km grid resolutions on June 6, 2002.

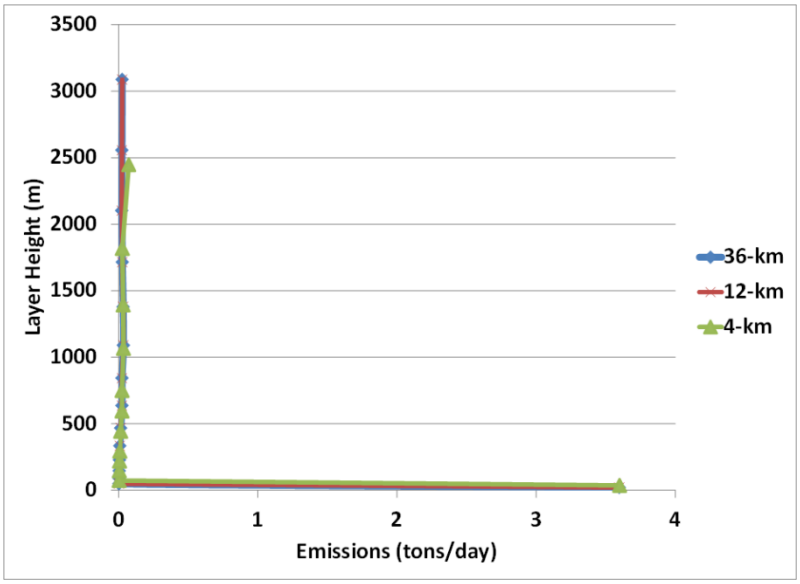

Figure A.4: Vertical aircraft emission profile for VOCs at the 36-km, 12-km, and 4-km grid resolutions on June 6, 2002.

A.3 Meteorological Data

A.3.1 Modeled and Observed Wind Speeds and Direction

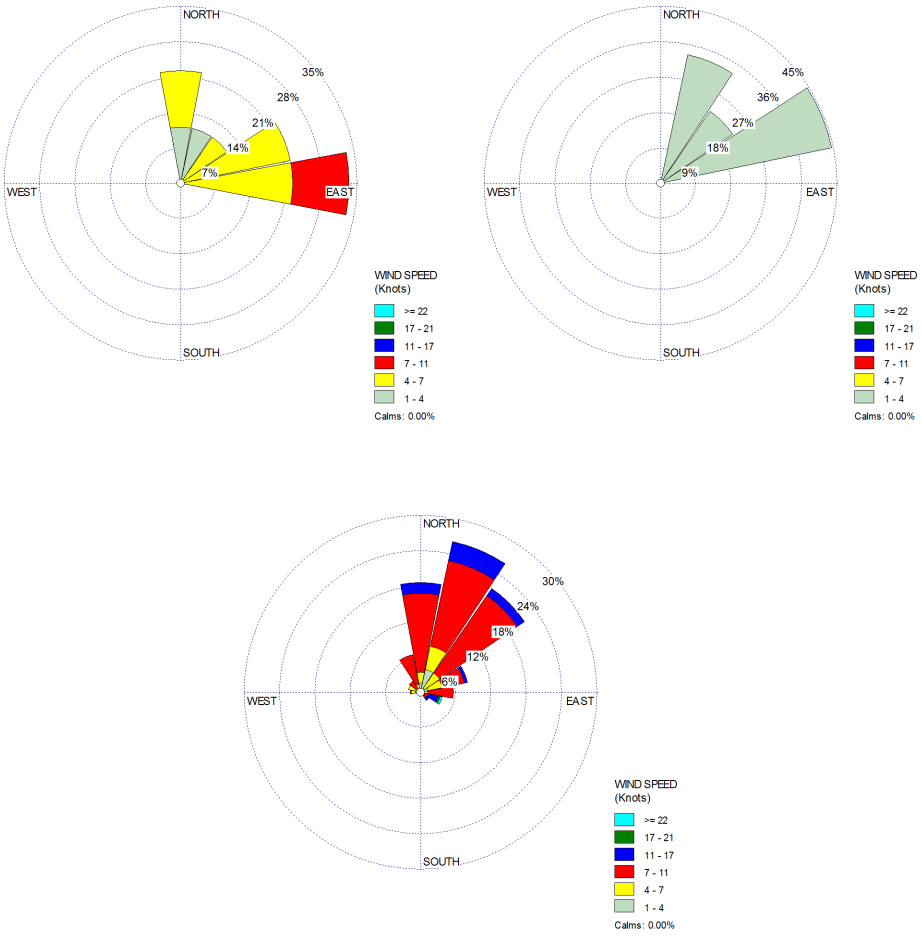

Figure A.5: Modeled surface wind direction and speed at the 36-km grid resolution for nighttime hours (0 to 8 GMT or 8 PM to 4AM LST) on June 6 (top left), June 7 (top right), and June and July (bottom).

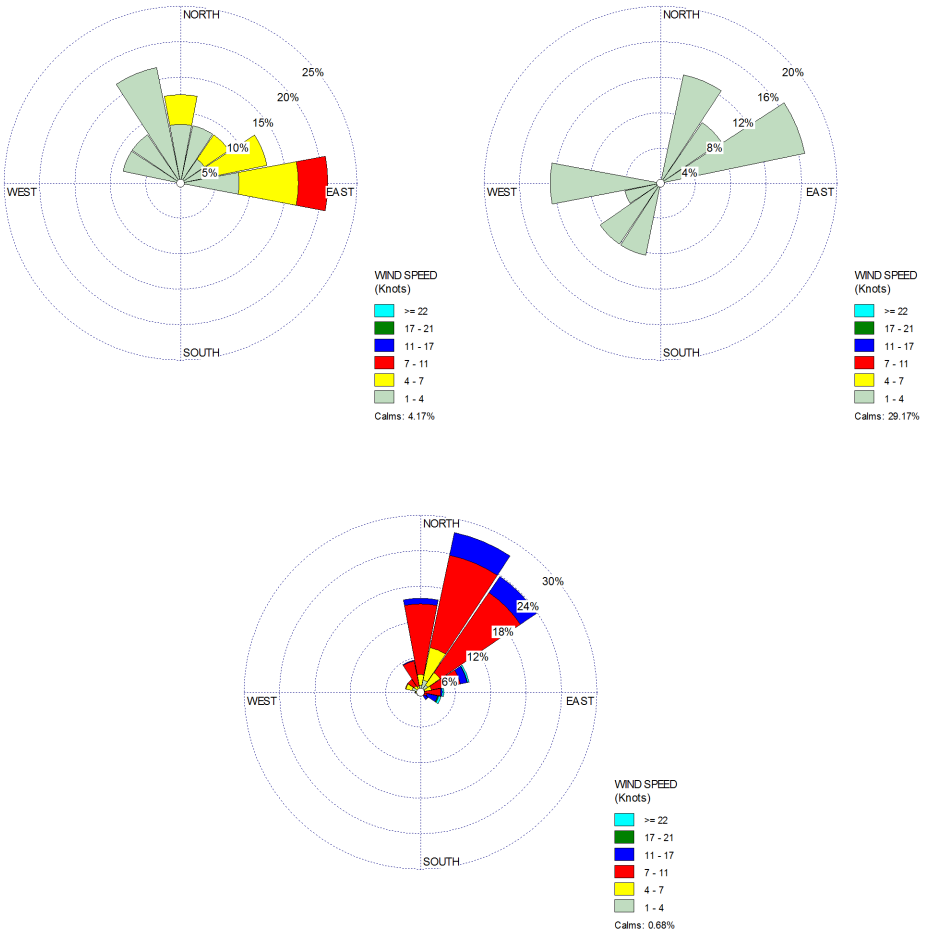

Figure A.6: Modeled surface wind direction and speed at the 36-km grid resolution for all hours on June 6 (top left), June 7 (top right), and June and July (bottom).

Figure A.7: Modeled surface wind direction and speed at the 12-km grid resolution for nighttime hours (0 to 8 GMT or 8 PM to 4AM LST) on June 6 (top left), June 7 (top right), and June and July (bottom).

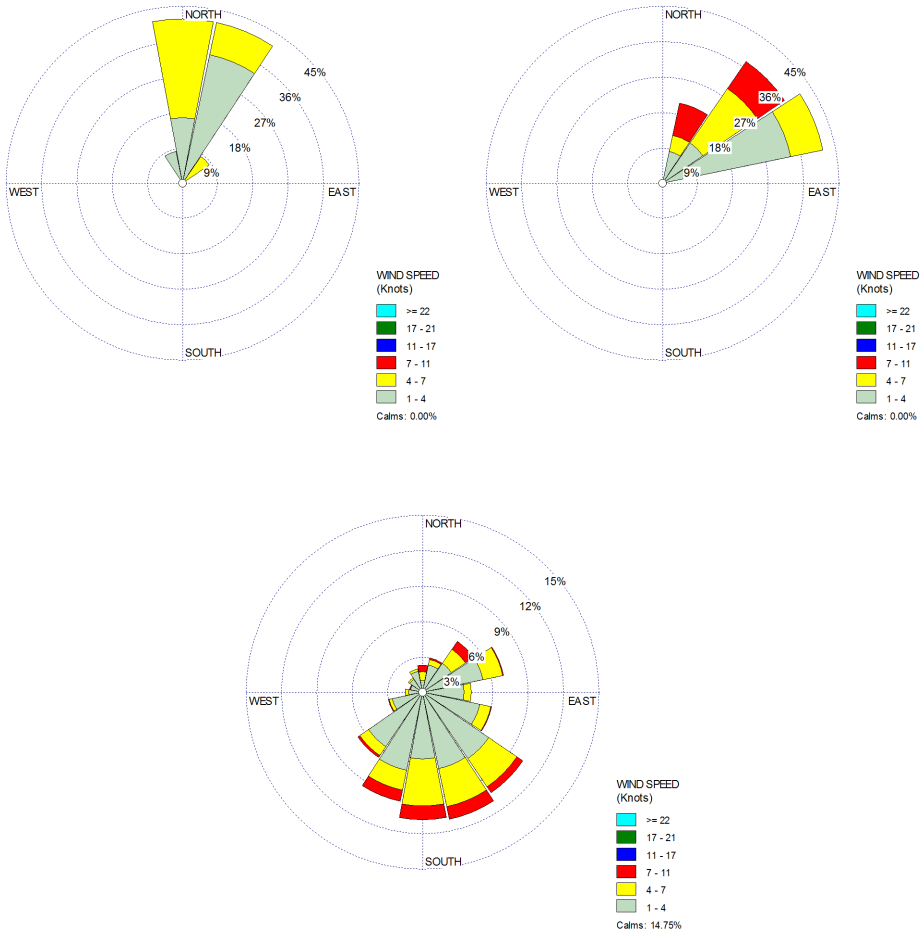

Figure A.8: Modeled surface wind direction and speed at the 12-km grid resolution all hours on June 6 (top left), June 7 (top right), and June and July (bottom).

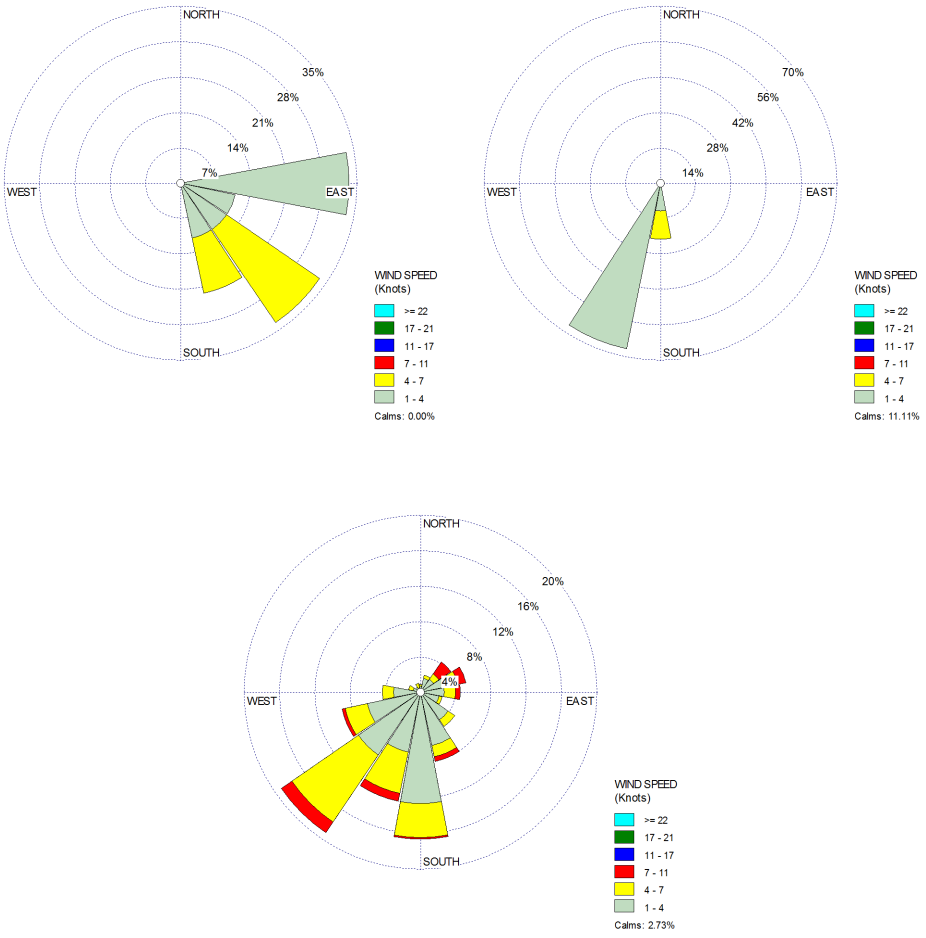

Figure A.9: Modeled surface wind direction and speed at the 4-km grid resolution for nighttime hours (0 to 8 GMT or 8 PM to 4AM LST) on June 6 (top left), June 7 (top right), and June and July (bottom).

Figure A.10: Modeled surface wind direction and speed at the 4-km grid resolution for all hours on June 6 (top left), June 7 (top right), and June and July (bottom).

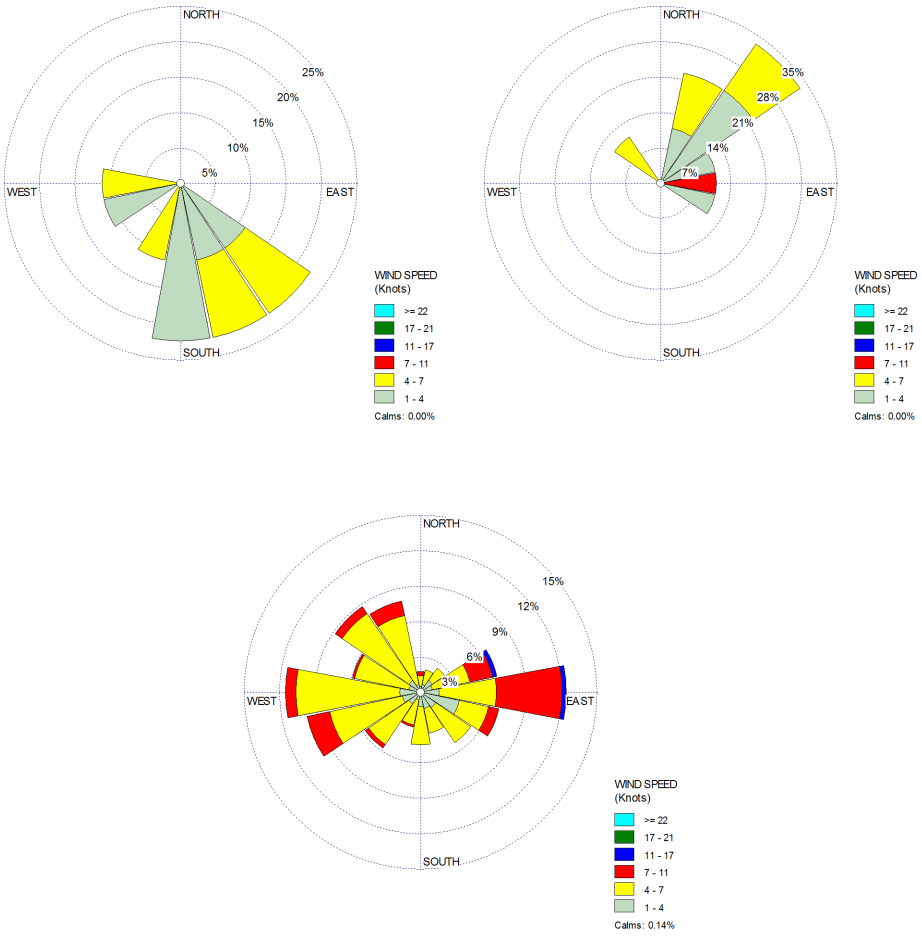

Figure A.11: Measured surface wind direction and speed at ATL for nighttime hours (0 to 8 GMT or 8 PM to 4AM LST) on June 6 (top left), June 7 (top right), and June and July (bottom).

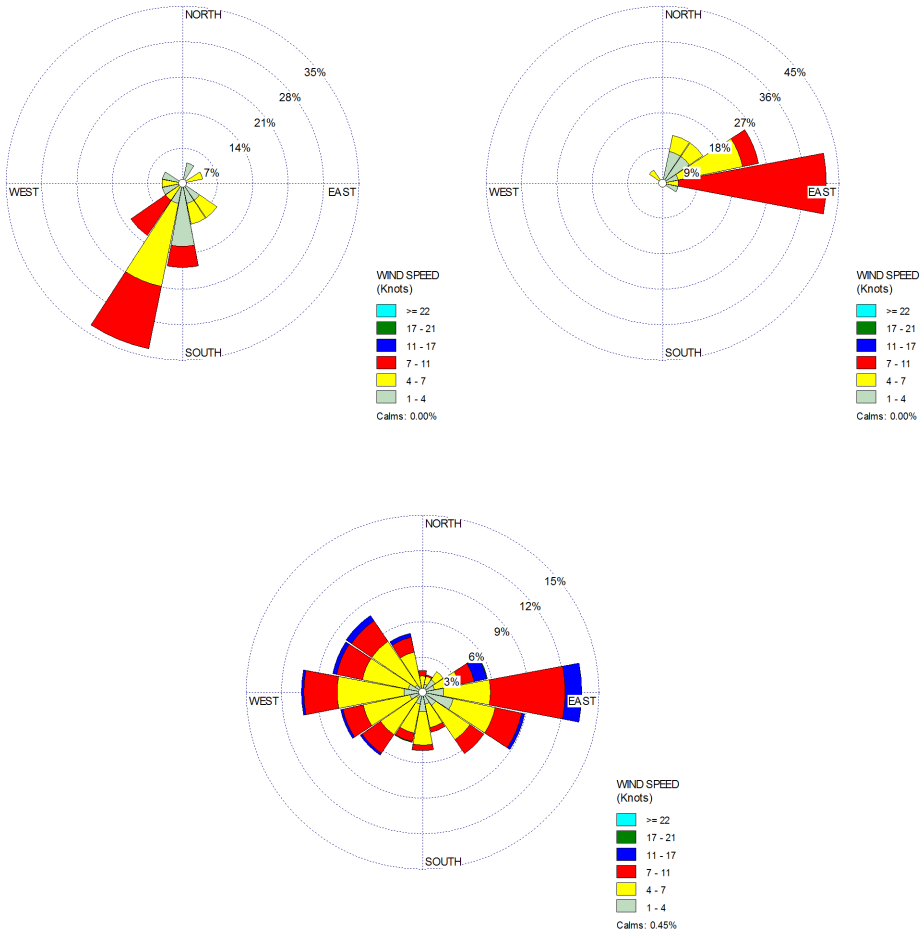

Figure A.12: Observed surface wind direction and speed at ATL for all hours on June 6 (top left), June 7 (top right), and June and July (bottom).

A.3.2 Modeled Planetary Boundary Layer Heights

Figure A.13 indicates planetary boundary layer (PBL) heights in meters and layers for the three modeled grid resolutions. There is good agreement in PBL heights between the 12-km and 4-km resolutions on June 6 and in the 36-km and 12-km on June 7. Additionally, changes in SOA concentrations due to aircraft emissions presented here were small during daytime hours (13–21 GMT) on June 7 (relative to other hours) when the maximum variation in PBL heights occurred between the 36-km/12-km and 4-km grid resolutions. Therefore, differences in vertical resolution associated with using separate meteorological inputs to derive the 36-km/12-km and 4-km meteorology do not appear to serve a role in the variation of model response from aircraft emissions to SOA concentrations between the three grid resolutions with additional details provided in the results section.

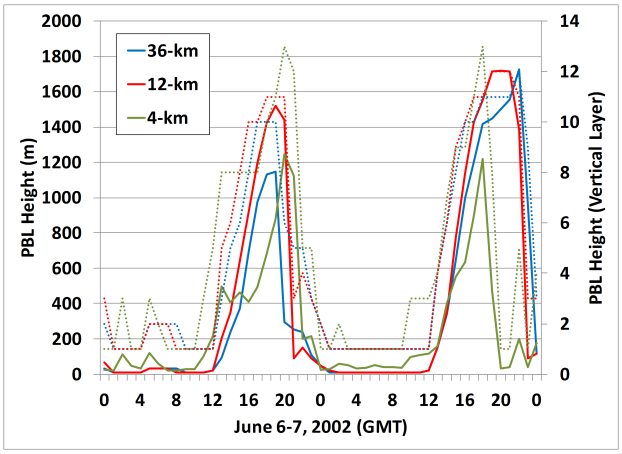

Figure A.13: Planetary Boundary Layer heights for the 36-km, 12-km, and 4-km grid resolutions. Solid lines indicate heights in meters while dotted lines indicate model vertical layers.

A.4 CMAQ v4.6 vs. v4.7 Model Performance

The Arunachalam et al. (2011) work, which provides the basis for this study, was modeled using CMAQ v4.6. Conversely, CMAQ v4.7 includes a number of SOA updates which include additional SOA precursors and formation pathways, updated enthalpy of vaporizations, effective saturation concentrations, and stoichiometric yield values (Carlton et al., 2010; Foley et al., 2010) and was therefore the preferred choice for assessing changes in SOA due to aircraft emissions. Since results were available from CMAQ v4.6 and v4.7, this provided the opportunity to test how SOA updates in CMAQ v4.7 influence the impacts of aircraft emissions on SOA. However, to test the updates in CMAQ v4.7

on overall model performance and prior to examining the changes of model sensitivity to SOA concentrations from aircraft emissions, overall model performance was first considered for both CMAQ v4.6 and 4.7. Hourly total carbon (TC) concentrations from the CMAQ v4.6 (aerosol 4 module) and CMAQ v4.7 (aerosol 5 module) model runs were compared against observations at the Jefferson Street (JST) Southeastern Aerosol Research and Characterization (SEARCH) monitor (Hansen et al., 2003) located in downtown Atlanta approximately 15 km north of the airport (Table A.3 and Figure A.14a). TC is defined as the sum of organic (both primary and secondary) aerosols and EC aerosols predicted by CMAQ. For the 36-km and 12-km grid resolutions, both model versions typically overpredicted TC during this episode. However, for the 4-km grid resolution, v4.7 appears to have exhibited better model performance lowering both model error and bias (Table A.3), particularly on the second episode day (Figure A.14a). This improved agreement for TC for the 4-km grid resolution was not attributed to changes in SOA concentrations or to updates to the SOA mechanism in the new version of CMAQ. Instead, it is associated with another update to CMAQ: the convective and resolved cloud models (Carlton et al., 2008; Foley et al., 2010). Process analysis results (Figures A.15a and A.15b) indicated that both POA and AEC concentrations are reduced on June 7 for the 4-km grid resolution by cloud processes in CMAQ v4.7. While this modeled reduction in the other components of TC (besides SOA) led to better agreement with the SEARCH monitor, it did not appear to influence the modeled impacts of aviation emissions on SOA concentrations.

Table A.3: CMAQ v4.6 and v4.7 TC model error and model bias at the Jefferson Street SEARCH monitoring site.

	36-km		12-km		4-km	
	v4.6	v4.7	v4.6	v4.7	v4.6	v4.7
Model Bias (μg m^{-3})	1.72	1.72	2.96	3.08	1.76	1.09
Model Error (μg m^{-3})	1.74	1.82	2.96	3.08	1.87	1.34

A.5 Modeled Aircraft Contributions

A.5.1 CMAQ v4.6 vs. v4.7 Aircraft Contributions

Comparing the impacts of aviation emissions on SOA formation between CMAQ v4.6 and CMAQ v4.7, the two models predicted similar diurnal patterns (Figure A.14b). The comparison also indicated that the same model processes contributed to the changes in biogenic SOA concentrations in both

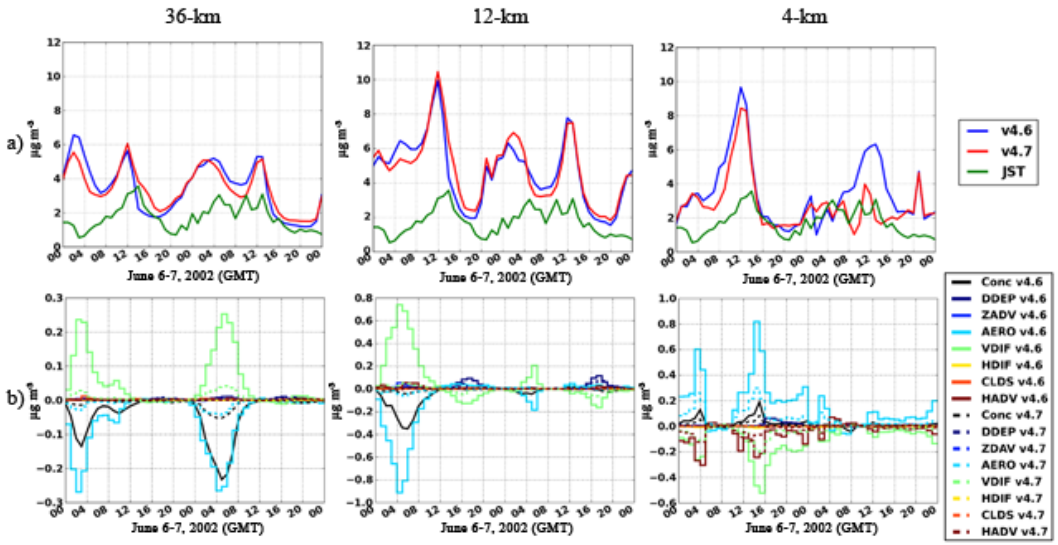

Figure A.14: (a) Comparison of CMAQ v4.6 and v4.7 TC concentrations to the Jefferson Street SEARCH monitoring site, and (b) changes in SOA IPR rates in CMAQ v4.6 (solid lines) and v4.7 (dashed lines).

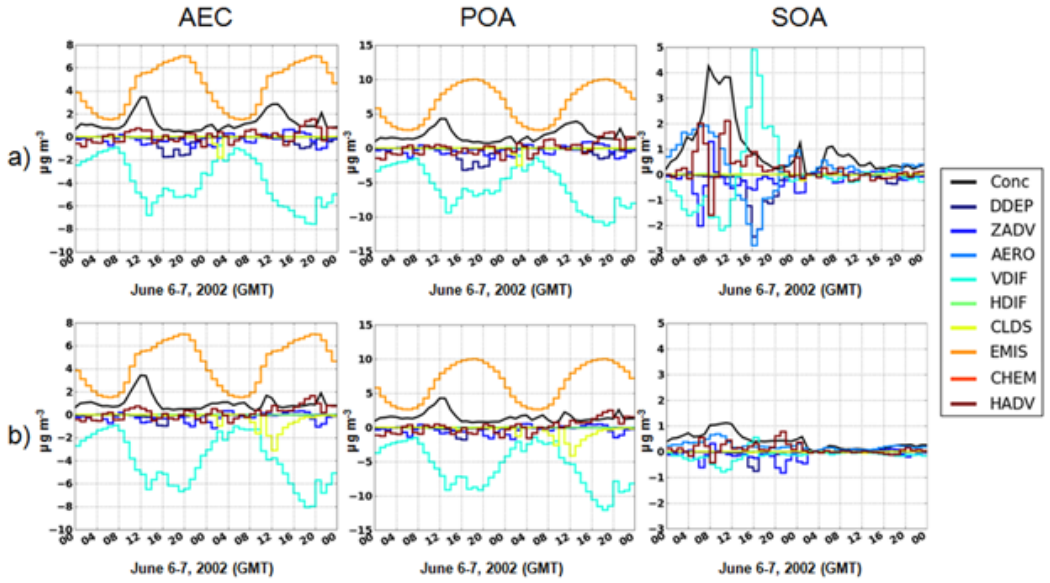

Figure A.15: CMAQ IPR outputs for AEC, POA, and SOA at grid cell containing the Jefferson Street SEARCH monitoring site at the 4-km grid resolution for (a) v4.6 and (b) v4.7.

versions. However, two primary differences between the two versions are the magnitude of the change in biogenic SOA (v4.7 predicts a smaller change to SOA) and the reduction of anthropogenic SOA concentrations. The change in biogenic SOA was attributed to parameter updates to the SOA modeling mechanism in v4.7—specifically, the enthalpy of vaporization, effective saturation concentration, and stoichiometric yield values (Carlton et al., 2010; Foley et al., 2010). Stoichiometric yields for aromatic SOA precursors as well as enthalpies of vaporization and effective saturation concentrations for all SOA precursors were updated to reflect more recent laboratory experiments (Offenberg et al., 2006; Edney et al., 2007; Ng et al., 2007b; Carlton et al., 2008). Additionally, a correction factor of 1.3 was applied to stoichiometric yields for biogenic SOA precursors reported by Griffin et al. (1999), which was based on the assumption of a density of 1.0 g/cc for monoterpene, while more recent work has suggested a density of 1.3 g/cc (Bahreini et al., 2005; Alfarra et al., 2006; Kostenidou et al., 2007; Ng et al., 2007a; Offenberg et al., 2007). To test the effect of these model updates, a model sensitivity analysis was performed in which CMAQ v4.7 was run using SOA parameter values taken from CMAQ v4.6 for enthalpies of vaporization, effective saturation concentrations (c*), and stoichiometric yields. Figure A.16 presents the results of that sensitivity analysis, indicating that when using v4.6 parameters in v4.7, SOA concentrations predicted by the two model versions (v4.6 and v4.7s) follow nearly identical diurnal patterns, with differences attributed to updated SOA pathways in v4.7.

A.5.2 Equivalent Spatial Extents Comparison

To extend the analysis beyond the single 36-km, 12-km, or 4-km grid cell containing the airport and to determine the role of spatial extents when assessing how modeled airport emissions influence SOA concentrations, results for equivalent spatial extents for the three grid resolutions were compared. Results were compared for the 36-km grid cell to average concentrations from the 9 grid cells in the 12-km domain and from the 81 grid cells in the 4-km domain corresponding to the same spatial extent as the 36-km grid cell containing the airport. Figure A.17a presents the time series of changes in anthropogenic and biogenic components of SOA for the equivalent spatial extents comparison due to aircraft emissions, and similarly Figure A.17b presents the similar comparisons for total SOA. Results for the 12-km and 4-km resolutions from the equivalent spatial extents comparison more closely

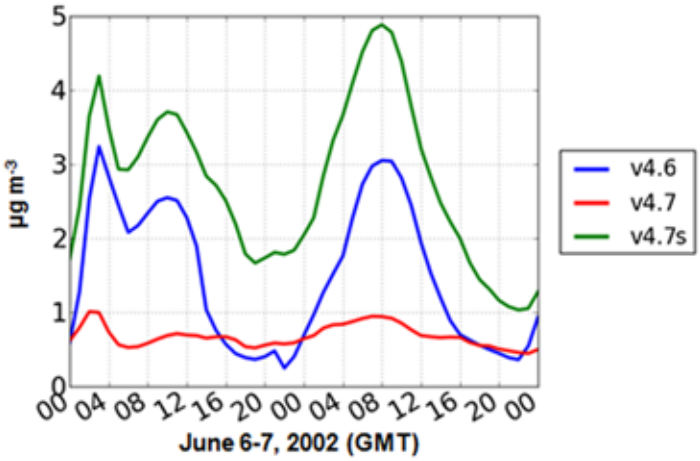

Figure A.16: Base case SOA concentrations at the ATL airport grid cell in CMAQ v4.6, v4.7, and v4.7 updated to use enthalpies of vaporization, effective saturation concentrations, and stoichiometric yields taken from v4.6 (referred to as v4.7s).

resemble the time series from the 36-km individual grid cell containing the ATL airport than do the 12-km and 4-km single-cell results, indicating that the modeled gas-phase chemistry dominated the changes in SOA concentrations from aircraft at the extended spatial extents. In the case of the 4-km grid resolution, while aircraft emissions increased SOA concentrations at the airport, they reduced SOA concentrations at grid cells surrounding the airport. The modeling mechanism which led to the reduction of SOA concentrations from aircraft emissions in these neighboring cells was the same as in the 36-km and 12-km grid cell containing the airport. NO_2 emissions from aircraft aloft were emitted and advected into neighboring grid cells where they removed nitrate radicals and ultimately reduced SOA production. However, the overall reduction of SOA concentrations in the 12-km and 4-km extents was lower than in the grid cell containing the airport at the 36-km resolution because a smaller proportion of the grid cells composing the average were influenced by aircraft emissions aloft.

A.5.3 36-km Nitrate Aerosol Contributions

Contributions from aircraft in the grid cell containing the ATL airport lowered daily average nitrate aerosol (ANO3) concentrations on June 6 and 7, 2002 at the 4-km and 12-km resolutions but only on June 7, 2002 for the 36-km resolution. The processes responsible for the reductions were similar to those for SOA, aircraft NO_x emissions lowered NO_3 radical concentrations, inhibiting the formation of ANO3. The unique feature on June 6, 2002 in the 36-km grid containing the airport

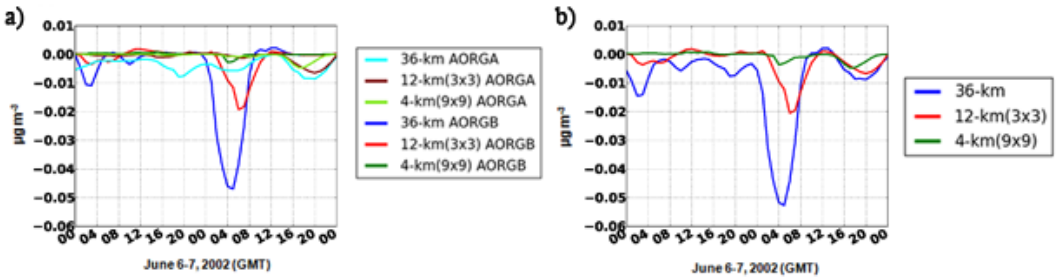

Figure A.17: Changes in (a) anthropogenic (AORGA), biogenic (AORGB), and (b) total SOA concentrations due to aircraft emissions for equivalent spatial extents to 36-km grid cell containing the ATL airport. Note changes to biogenic SOA dominate total changes to SOA and therefore the AORGB results in (a) are nearly identical to the total SOA results in (b).

was a precipitation event, which converted N_2O_5 to HNO_3 (which goes on to form ANO3) via the heterogeneous chemistry pathway. The increased HNO_3 concentrations via this heterogeneous pathway offset the reductions due to NO_x chemistry and thus led to an overall positive contribution from aircraft to ANO3 concentrations. Note that while the precipitation event also occurred in the 12-km grid resolution, it did not occur in the grid cell containing the airport and therefore did not impact results at the airport in the 12-km grid resolution.

A.5.4 Spatial Plots of Monthly Average Modeled Aircraft Contributions

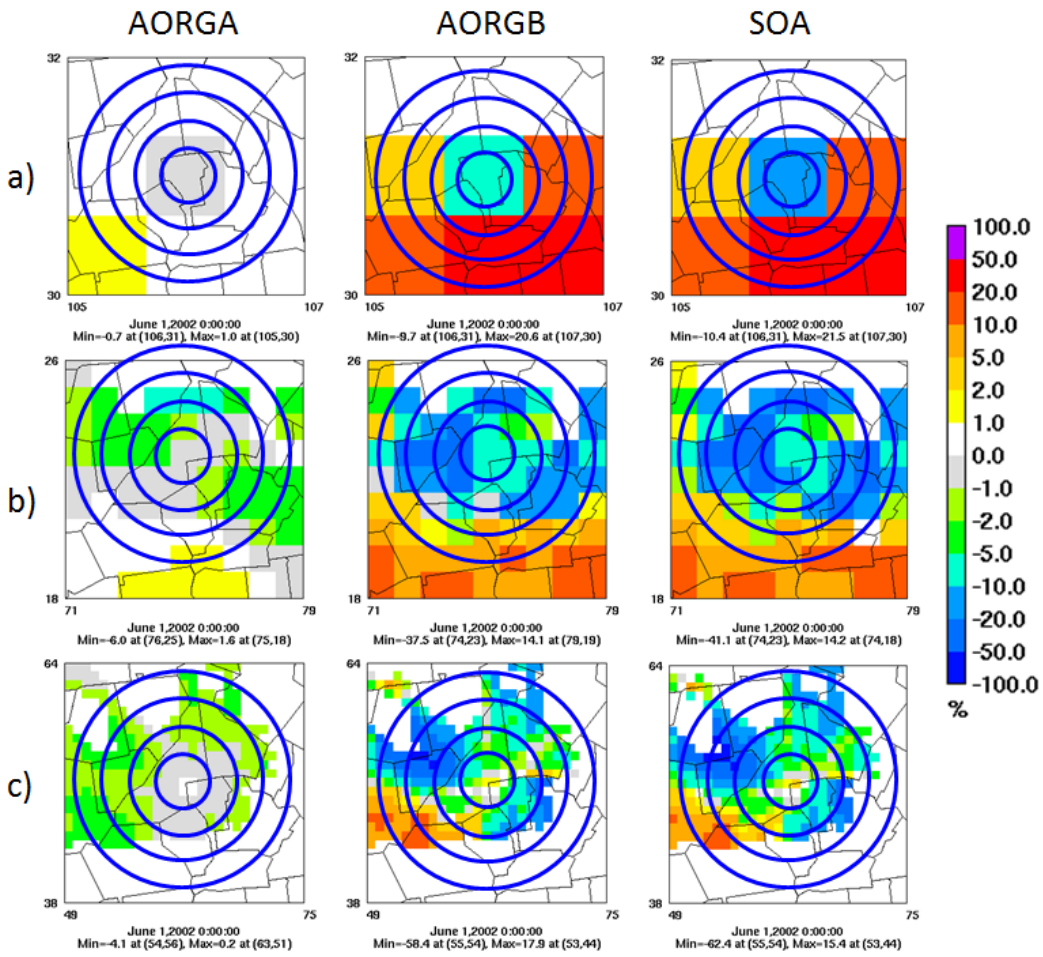

Figure A.18: CMAQ v4.6 monthly average incremental contributions (change in individual species divided by total change in $PM_{2.5}$) of anthropogenic (AORGA), biogenic (AORGB), and total SOA due to aircraft emissions at (a) 36-km, (b) 12-km, and (c) 4-km grid resolutions for June 2002 adapted from Arunachalam et al. (2011). Rings denote radii of 12-km, 24-km, 36-km, and 48-km from ATL airport.

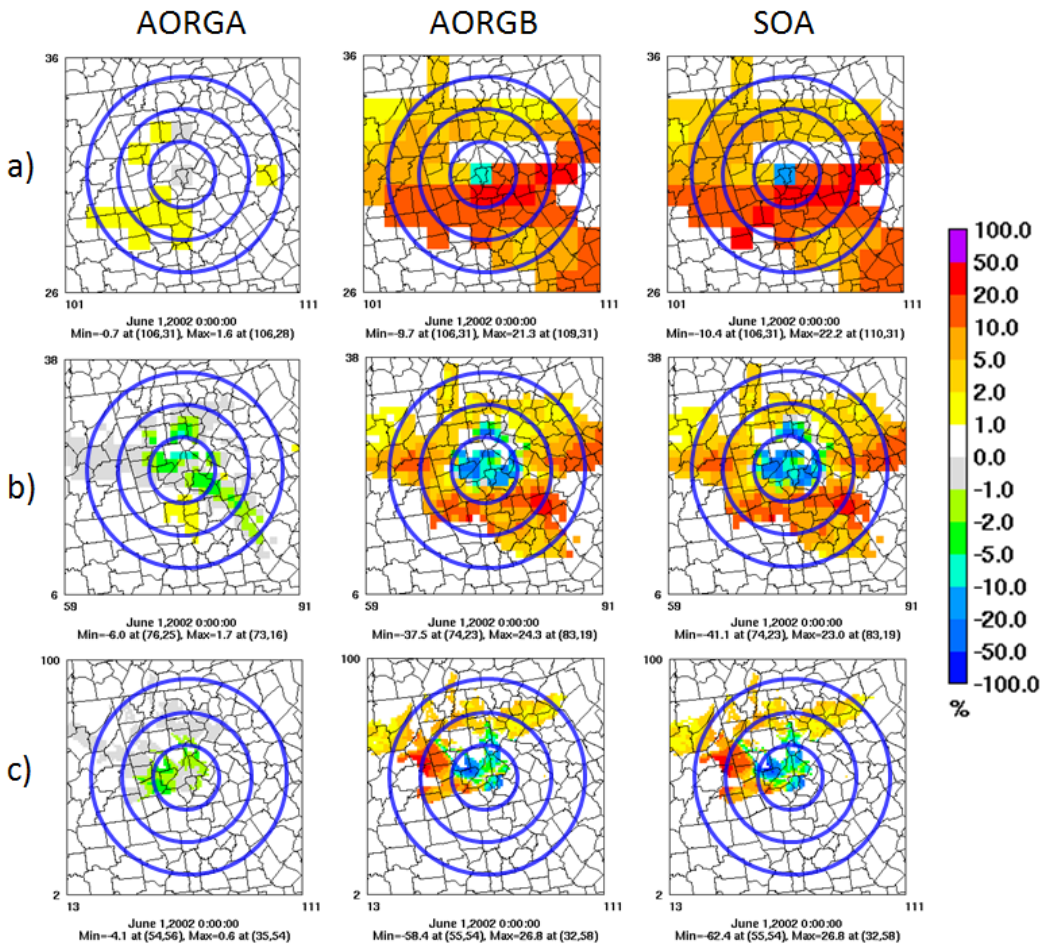

Figure A.19: CMAQ v4.6 monthly average incremental contributions (change in individual species divided by total change in $PM_{2.5}$) of anthropogenic (AORGA), biogenic (AORGB), and total SOA due to aircraft emissions at (a) 36-km, (b) 12-km, and (c) 4-km grid resolutions for June 2002 adapted from Arunachalam et al. (2011). Rings denote radii of 50-km, 100-km, and 150-km from ATL airport. (Note that the information is the same as in Figure A.18, but for a larger domain around the airport)

APPENDIX B SUPPLEMENTAL MATERIAL: ESTIMATES OF NON-TRADITIONAL SECONDARY ORGANIC AEROSOLS FROM AIRCRAFT SVOC AND IVOC EMISSIONS IN CMAQ

B.1 VBS vs. AE6 in CMAQ

B.1.1 Description of VBS in CMAQ

VBS in CMAQ, implemented by Koo et al. (2014) for the Carbon Bond 2005 (CB05) chemical mechanism (Yarwood et al., 2005), includes four distinct organic aerosol groups: primary anthropogenic (representing hydrocarbon-like OA), secondary anthropogenic and biogenic (representing oxygenated OA), and primary biogenic (biomass burning). Five volatility bins are used to represent the four semi-volatile groups, with the lowest bin being non-volatile and the other four bins representing particles with C* values ranging from 10^0 to 10^3 μg m^{-3}. Stoichiometric yields representing semi-volatile products of SOA gas-phase precursors are based on Murphy and Pandis (2009) except for toluene, which is based on Hildebrandt et al. (2009) and are summarized in Table B.1. Formation of SOA from aromatics, isoprene, and monoterpenes precursors include both high and low-NO_x yields. Anthropogenic SOA is aged by reactions with OH using a rate constant of 2 x 10^{-11} cm^3 $molecules^{-1}$ s^{-1}, with each aging reaction reducing volatility by an order of magnitude and adding approximately 3% to the SOA mass (Murphy and Pandis, 2009). Biogenic SOA is not aged (Murphy and Pandis, 2009), though the exclusion of biogenic aging reactions may not be a good assumption based on smog chamber data (Donahue et al., 2012). POA is aged by OH with a rate constant of 4 x 10^{-11} cm^3 $molecules^{-1}$ s^{-1} (Robinson et al., 2007), lowering volatility by a order of magnitude with 87–90% of the mass (depending on the volatility of the parent POA oxidized) retained as POA and 7–9% transfered to SOA (Koo et al., 2014). The conversion of a portion of POA (hydrocarbon-like OA) to SOA (oxidized OA), is based on carbon and oxygen balances (Koo et al., 2014). SVOCs emissions, which partition between the particle and gas phase, replace POA emissions. To account for the loss of particles to the gas phase, particle formation from IVOC emissions are added. The VBS implementation includes two options to internally estimate SVOC and IVOC emissions at runtime based on traditional POA emission inventories, a conservative and a high case both within the uncertainty range of S/IVOC emissions. In the conservative case, the total mass of SVOC emissions

Table B.1: CMAQ mass based VBS yields for the CB05 (Koo et al., 2012) and SAPRC-07 (this work) chemical mechanisms.

	CB05 and SAPRC-07 Mechanism							
	High NOx Yields				Low NOx Yields			
Model Species	10^0	10^1	10^2	10^3	10^0	10^1	10^2	10^3
BENZ[a]	0.0030	0.1659	0.3000	0.4350	0.0750	0.2250	0.3750	0.5250
TOL[b]	0.0110	0.2480	0.4660	0.6940[d]	0.0110	0.2480	0.7250	0.4520[d]
XYL[a,c]	0.0015	0.1950	0.3000	0.4350	0.0750	0.3000	0.3750	0.5250
ISOP[a]	0.0000	0.0225	0.0150	0.0000	0.0090	0.0300	0.0150	0.0000
TERP[a]	0.0120	0.1215	0.2010	0.5070	0.1073	0.0918	0.3587	0.6075
SESQ[a]	0.0750	0.1500	0.7500	0.5090[d]	0.0750	0.1500	0.7500	0.5090[d]
	SAPRC-07 Mechanism Only							
	High NOx Yields				Low NOx Yields			
	10^0	10^1	10^2	10^3	10^0	10^1	10^2	10^3
ARO1[b]	0.0110	0.2480	0.4660	0.6940	0.0110	0.2480	0.7250	0.4520
ARO2[a]	0.0015	0.1950	0.3000	0.4350	0.0750	0.3000	0.3750	0.5250
TRIMETH_BENZ124[a]	0.0015	0.1950	0.3000	0.4350	0.0750	0.3000	0.3750	0.5250
ALK5[a]	0.0000	0.1500	0.0000	0.0000	0.0000	0.3000	0.0000	0.0000
APIN[a]	0.0120	0.1215	0.2010	0.5070	0.1073	0.0918	0.3587	0.6075

[a] Murphy and Pandis (2009)
[b] Hildebrandt et al. (2009)
[c] SAPRC-07 includes MXYL, OXYL, and PXYL
[d] Adjusted to meet a mass balance check (Bonyoung Koo, personal communication, March 13, 2013)

Table B.2: Fraction of POA emissions allocated to SVOC volatility bins.

		C*			
	Non-Vol	10^0	10^1	10^2	10^3
VBS	0.09	0.09	0.14	0.18	0.5
high S/IVOC VBS	0.4	0.26	0.4	0.51	1.43

are estimated to be equal to traditional POA emissions while IVOC emissions are estimated as twice POA emissions (Robinson et al., 2007). In the high SVOC and IVOC emission case, SVOC emissions are estimated as 3 times POA emissions while IVOCs are estimated as 4.5 times POA emissions (Shrivastava et al., 2011). Table B.2 indicates the fraction of POA mass assigned to each volatility bin of SVOC emissions.

B.1.2 Methodology

In this study, the CMAQ v5.0.1 VBS implementation developed by Koo et al. (2014) was expanded for use with the more explicit SAPRC-07 chemical mechanism (Carter, 2010). Updated and added reactions are listed in Tables B.4 and B.5 of Section B.2. In CMAQ, our VBS implementation for SAPRC-07 includes 150 gas phase species [13 representing SOA precursors — 9 anthropogenic (8

contained in aircraft emissions) and 4 biogenic] and 413 reactions compared to 80 gas phase species (6 representing SOA precursors — 3 anthropogenic and 3 biogenic) and 205 reactions in CB05. SAPRC-07 oxidation products of gas-phase SOA precursors were updated from traditional Odum 2-product (Odum et al., 1996) species to VBS species with yields taken from Murphy and Pandis (2009) and Hildebrandt et al. (2009) and identical to Koo et al. (2014) (Table B.1), while the aerosol module remained unchanged from Koo et al. (2014).

Three different scenarios were modeled for January and July, 2002 over a nested 12-km Eastern U.S. domain: 1) CMAQ with the traditional model for organic aerosols (AE6), 2) CMAQ with VBS and conservative estimates of S/IVOC emissions (VBS) and 3) CMAQ with VBS and high estimates of S/IVOC emissions (high S/IVOC VBS). Model inputs are based on those used in Hutzell et al. (2012). Briefly, meteorological inputs were generated using the Pennsylvania State University/NCAR mesoscale (MM5) model (Grell et al., 1994). Emissions were generated using the Sparse Matrix Operator Kernel Emissions (SMOKE) model (Houyoux et al., 2000) and estimated using the U.S. EPAs 2002 National Emissions Inventory (NEI) (U.S. EPA, 2004). Table B.3 summarizes CMAQ domain and monthly total POA emissions in January and July 2002 for AE6 [where POA is the sum of primary organic carbon (POC) and primary non-carbon organic mass (PNCOM)], VBS, and high S/IVOC VBS (where SVOC emissions represent POA emissions). Because the CMAQ boundary conditions do not currently include gas- or particle-phase VBS species, three 36-km contiguous U.S. simulations, one each for AE6, VBS, and high S/IVOC VBS, were performed for January and July, 2002 and the results used to generate boundary conditions for the 12-km domain. For each nested 12-km simulation, the coarser domain used the identical OA scheme as the nested simulations.

Model estimates of total fine particulate matter ($PM_{2.5}$) and organic carbon (OC) concentrations were compared against observations at Chemical Speciation Network (CSN) (http://www.epa.gov/ttn/amtic/speciepg.html) and Interagency Monitoring of Protected Visual Environments (IMPROVE) network sites (http://vista.cira.colostate.edu/improve) and OC observations at Southeastern Aerosol Research and Characterization (SEARCH) network sites (http://www.atmospheric-research.com/studies/SEARCH). Additional information about the monitoring sites, such as the number of

Table B.3: Primary organic carbon (POC), primary non-carbon organic mass (PNCOM), primary organic aerosol (POA, where POA = POC + PNCOM), SVOC, and IVOC emissions for CMAQ with AE6, VBS, and high S/IVOC VBS (VBSh).

		AE6			
		Jan		Jul	
	POC	86,737		53,763	
	PNCOM	34,695		21,505	
	POA	121,432		75,268	
		VBS		VBSh	
	C*	Jan	Jul	Jan	Jul
SVOCs	Non-Vol	10,929	6,774	48,573	30,107
	10^0	10,929	6,774	31,572	19,570
	10^1	17,000	10,538	48,573	30,107
	10^2	21,858	13,548	61,930	38,387
	10^3	60,716	37,634	173,648	107,34
	Total SVOCs	121,432	75,268	363,296	225,806
	IVOCs	150,537	242,864	546,444	337,709

sites in the domain (Table B.7), their locations (Figure B.5), and performance at sites located closest to ATL (Tables B.8 and B.9) are provided in Section B.2. Note that the VBS implementation in CMAQ does not track primary organic carbon and primary non-carbon organic matter separately as in AE6, only estimating primary organic aerosols. Therefore, primary OC was estimated assuming an OM/OC ratio of 1.4, similar to Lane et al. (2008); Murphy and Pandis (2009, 2010). PNCOM emission estimates were adjusted to account for this assumption and to maintain consistency between the model scenarios. For SOA, the EPA recommended precursor-specific OC/OM ratios, which range from 1.4 to 2.7, were used to calculate AE6 OC. VBS, however, does not track mass formed from each parent precursor separately as in AE6 and therefore an OC/OM ratio of 2 was assumed for all secondary species, similar to Murphy and Pandis (2009, 2010).

B.1.3 Results

Organic Carbon

In both January and July 2002, VBS predicted lower OC concentrations compared to AE6, primarily due to the evaporation of POA from the particle phase to the gas phase (Figures B.1b and e). This effect was more pronounced in winter (Figure B.1b), when POA emissions were approximately 1.6 times higher than in summer (Figure B.1e and Table B.3). While differences in summer appear

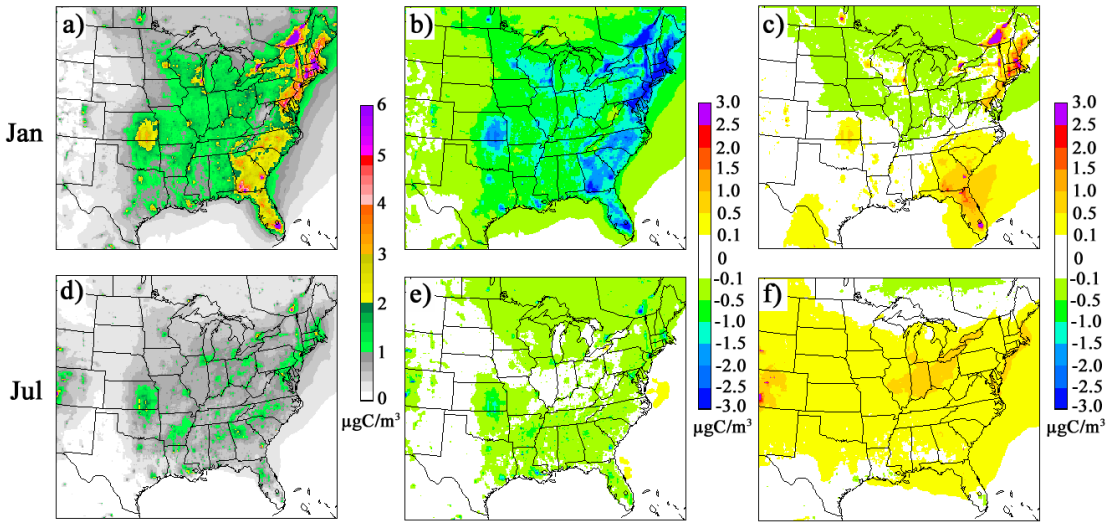

Figure B.1: Monthly average OC concentrations for CMAQ with AE6 in a) January and d) July, CMAQ with VBS minus CMAQ with AE6 in b) January and e) July, and CMAQ with VBS and High S/IVOC emissions minus CMAQ with AE6 in c) January and f) July.

relatively small on an absolute change basis (Figure B.1) compared to winter, low overall concentrations of OC in summer somewhat obscure the differences between AE6 and VBS, which are actually similar to those in winter on a percent change basis. Compared to AE6, high S/IVOC VBS predicted higher OC concentrations in the south and portions of the northeast in winter, and near the Great Lakes and in Colorado in summer (Figures B.1c,f) largely due to anthropogenic SOA formed from oxidative aging of S/IVOCs from sources of POA emissions (e.g. wildfire in Colorado in July). Evaporation of POA, which impacted VBS OC results, was generally offset by the increased emissions of S/IVOCs.

Comparing individual components of OC (anthropogenic SOA, biogenic SOA, and POA), VBS predicted higher concentrations of anthropogenic SOA than AE6, but lower concentrations of biogenic SOA (with the exception of slightly higher concentrations in the South during July) and POA (Figures B.2a-c and e-g). Lower POA concentrations far to have shifted gas-particle partitioning of SOA from the particle phase to the gas phase in VBS, effectively lowering SOA concentrations throughout the domain. Aging, changes in yields, and conversion of POA to anthropogenic SOA appear to have counteracted this effect to produce higher anthropogenic SOA concentrations, with aging and the conversion of POA likely more important in summer due to the additional photo-oxidation which

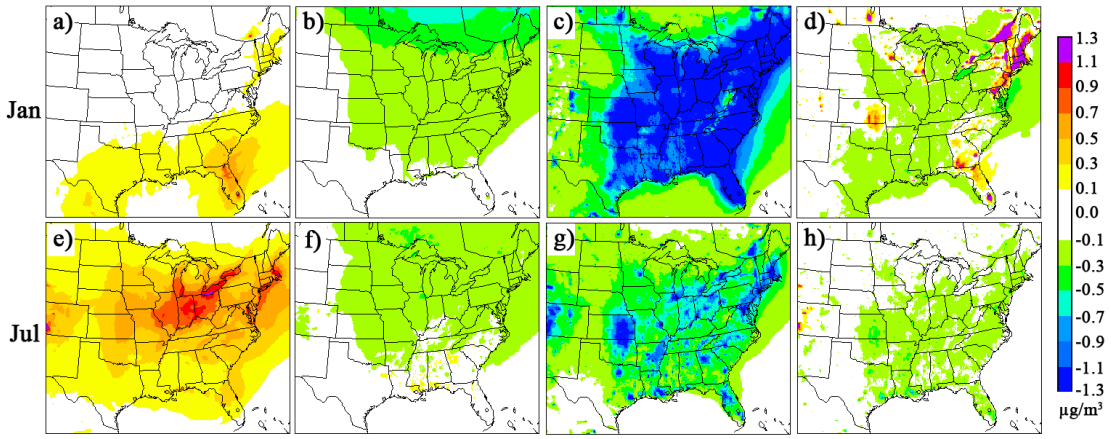

Figure B.2: Monthly average absolute difference of CMAQ with VBS minus CMAQ with AE6 in January for a) anthropogenic SOA b) biogenic SOA c) and POA and in July for e) anthropogenic SOA f) biogenic SOA g) and POA. Monthly average absolute difference of CMAQ with VBS and high S/IVOC emissions minus CMAQ with AE6 for POA concentrations in d) January and h) July.

occurs during warmer months. For biogenic SOA, differences in yields appear to have counteracted the shift in partitioning to produce higher concentrations in the South, where biogenic emissions are highest (despite lower overall organic mass available for particle partitioning), but not in other areas. Compared to VBS, the high S/IVOC VBS predictions were similar for biogenic SOA (slightly higher concentrations in the South during July likely due to additional organic mass shifting gas-particle partitioning to the particle phase), and a similar spatial pattern for anthropogenic SOA but with a larger magnitude. POA concentrations in the high S/IVOC case were higher than AE6 near POA emission sources due to the increase in S/IVOC emissions in winter but slightly lower in other areas due to partitioning to the gas phase (Figure B.2d). In summer, POA concentrations were likely lowered by aging reactions, which shifted a portion of POA mass to anthropogenic SOA (Figure B.2h).

Figure B.3 indicates the normalized mean bias (NME) and normalized mean error (NME) for all PM species, including OC, and Tables B.6–B.9 indicate the fractional error (FE) and fractional bias (FB), the recommended model performance metrics for PM (Boylan and Russell, 2006), for OC and $PM_{2.5}$. OC model performance comparisons indicate that in general, the VBS treatment performed worse at CSN and IMPROVE monitor locations compared to AE6 (Figure B.3, Tables B.6 and B.8). Lower concentrations in VBS led to more severe underpredictions of OC at CSN sites in January

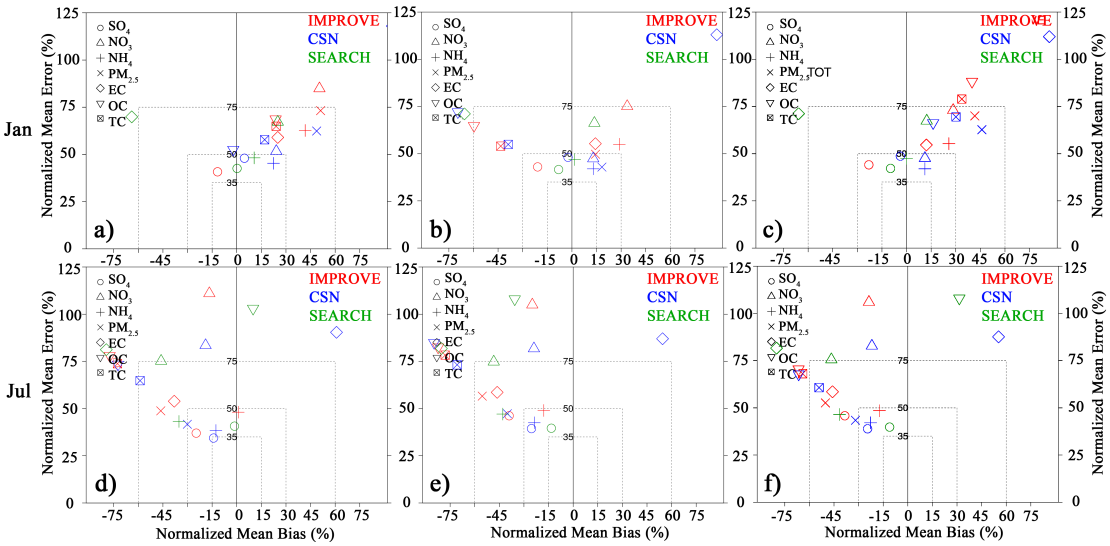

Figure B.3: Normalized mean bias and normalized mean error at CSN, IMPROVE, and SEARCH monitor sites in January for a) CMAQ, b) CMAQ with VBS, and c) CMAQ with VBS and high S/IVOCs and in July for d) CMAQ, e) CMAQ with VBS, and f) CMAQ with VBS and high S/IVOCs. PM species include sulfate (SO_4), nitrate (NO_3), ammonium (NH_4), $PM_{2.5}$, elemental carbon (EC), organic carbon (OC), and total carbon (TC).

and July and at IMPROVE sites in January where AE6 also underpredicted OC. At IMPROVE sites in January, the underprediction of OC using VBS [FB of -106%] was worse than using AE6 (FB of -5.9%) (Table B.6). At SEARCH sites, VBS generally performed better than AE6 in January where AE6 overpredicted OC. Lower OC concentrations in VBS slightly improved FB (150 %) compared to AE6 (166%) while FE was slightly worse (from 174% in AE6 to 185% in VBS). However, these values are considered rather poor model performance overall. Performance using VBS with high S/IVOCs estimates was, in general, similar to AE6. FBs were slightly higher at CSN and SEARCH sites using high S/IVOC VBS compared to AE6 (Table B.6). In instances where AE6 underpredicted OC (CSN in July), high S/IVOC VBS improved FB whereas when AE6 overpredicted OC (SEARCH in January and July), high S/IVOC VBS tended to more severely overpredict OC. The poor model performance in VBS was largely attributable to the semi-volatile treatment of POA, as a portion of the POA emissions were partitioned into the gas phase. This effect was somewhat counteracted by the higher POA emissions in the high S/IVOC emission case.

To test the sensitivity of POA aging on OC concentrations in VBS, an alternative aging scheme proposed by Pye and Seinfeld (2010) was implemented over the same modeling domain and time

periods. The Pye and Seinfeld (2010) aging scheme uses a rate constant of 2 x 10^{-11} cm^3 $molecules^{-1}$ s^{-1} (vs. 4 x 10^{-11} cm^3 $molecules^{-1}$ s^{-1}), lowers volatility by two orders of magnitude (vs. one order of magnitude), only allows for one oxidation step per parent hydrocarbon (vs. multi-generational aging), and assumes that oxidation produces a product 50% heavier than the parent hydrocarbon (vs. no increase). Model predictions of OC using the alternative aging scheme were nearly identical during the summer at CSN (0.454 μgC m^{-3} in the alternative aging scheme vs. 0.452 μgC m^{-3} in the CMAQ aging scheme) and IMPROVE (0.747 vs. 0.743 μgC m^{-3}) monitoring locations and marginally higher in winter (0.479 vs. 0.441 μgC m^{-3} at CSN sites and 0.936 vs. 0.884 μgC m^{-3} at IMPROVE sites). The slight increase in OC concentrations did little to improve model performance given the underpredictions of OC (0.7 to 4.2 μgC m^{-3}) with VBS.

Koo et al. (2014) reported similar OC model performance at CSN and IMPROVE monitoring locations in the Eastern U.S. using CMAQ v5.0.1 with CB05 and VBS; VBS model performance was markedly worse in winter and marginally worse in summer compared to AE6. In the high S/IVOC, Koo et al. (2014) indicated similar results in winter (performance similar to AE6) but with significant improvements to performance in summer. In a separate study, Koo et al. (2013) showed that the high S/IVOC case in CMAQ generally improved performance in February and August, 2005. The traditional aerosol treatment in CMAQ [AE5 in Koo et al. (2013)] generally underpredicted OC and therefore the higher predictions of the high S/IVOC case improved performance [note that Koo et al. (2013) did not report results for CMAQ with VBS and conservative estimates of S/IVOC emissions).

Koo et al. (2014) also reported results for an implementation of VBS in the Comprehensive Air Quality Model with Extensions (CAMx) (ENVIRON, 2013). In CAMx, model performance between the traditional OA modeling scheme, VBS, and high S/IVOC VBS were mixed depending on the time of year and network. In the Weather Research and Forecasting model coupled with Chemistry (WRF-Chem) (Grell et al., 2005), Li et al. (2011) reported that VBS with high estimates of S/IVOC emissions generally improved model performance in Mexico City, where the traditional 2-product OA treatment previously underpredicted OA. Given the mixed model performance in CMAQ (as well as CAMx), future efforts are needed to refine the VBS treatment, particularly the S/IVOC emission inputs, to improve CMAQ model performance. With the variation in seasonal performance, one

possible improvement would be to use seasonally specific S/IVOC emission estimates as proposed by Koo et al. (2014). Another improvement would be to use source-specific S/IVOC emission inputs. The CMAQ v5.0.2 implementation of VBS provides the flexibility to estimate S/IVOC emissions using different scaling factors applied to gas vehicle POA emissions, diesel vehicle POA emissions, and all other anthropogenic POA emissions. However, the default approach used in this study applies the same S/IVOC scaling factor to POA emissions from all sources, as source specific scaling factors for CMAQ were not available at the time this study was performed.

$PM_{2.5}$

VBS lowered total $PM_{2.5}$ concentrations throughout the Eastern U.S. in both January and July (Figures B.4b,e). The same was true for the high S/IVOC case with the exception of Florida and portions of the Northeast in January and Colorado in the summer (Figures B.4c,f). The reduction of $PM_{2.5}$ concentrations with VBS led to mixed impacts on model performance (Figure B.3). Instances where CMAQ previously overpredicted total PM (CSN and IMPROVE in January) (Table B.7), VBS improved performance though due to compensating bias. Alternatively, in cases where CMAQ previously underpredicted total PM (CSN and IMPROVE in July) (Table B.7), VBS worsened model performance.

Comparing total $PM_{2.5}$ concentrations between organic aerosol schemes, it is worth noting that the total change in $PM_{2.5}$ concentrations was not completely attributable to changes in organics. For example, reductions in summertime $PM_{2.5}$ concentrations in the VBS case (or summer and winter concentrations in the high S/IVOC case) did not agree spatially with changes in OC concentrations (Figures B.1c,e,f and B.4e,c,f). Comparisons of mean concentrations also support this finding, e.g. mean OC concentrations in January of 2.8 μgC m^{-3} and 0.9 μgC m^{-3} for AE6 and VBS respectively (difference of 1.9 μgC m^{-3}) vs. total $PM_{2.5}$ concentrations of 18.4 μg m^{-3} and 14.7 μg m^{-3} (difference of 3.7 μg m^{-3}). The additional differences were due to an increase in dry deposition of $PM_{2.5}$ species, which reduced non-organic PM concentrations in VBS by 9–17.5%.

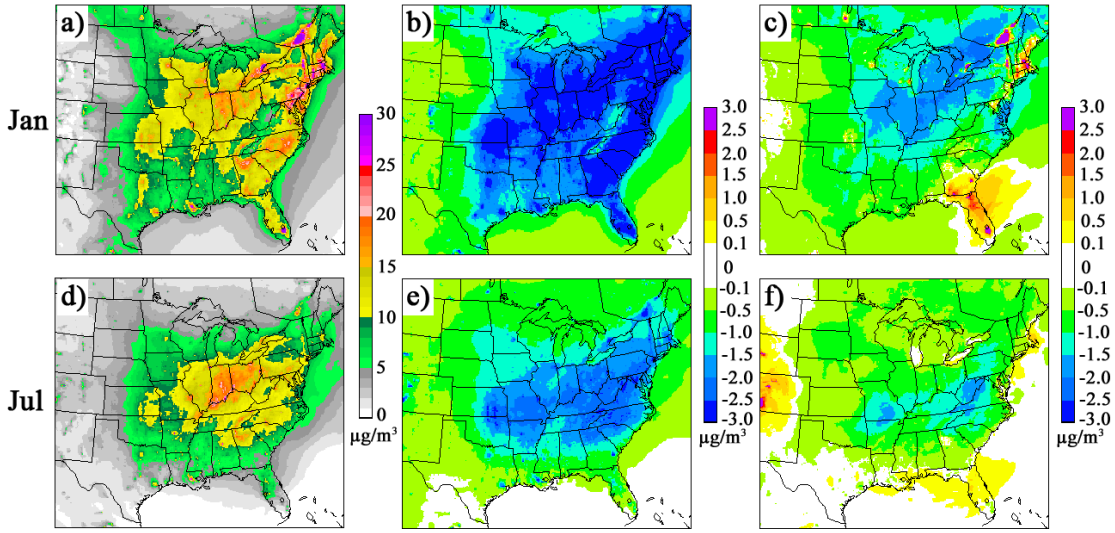

Figure B.4: Monthly average $PM_{2.5}$ concentrations for CMAQ with AE6 in a) January and d) July. Monthly average absolute difference in CMAQ with AE6 minus CMAQ with VBS in b) January and e) July and CMAQ with AE6 minus CMAQ with VBS and high S/IVOC emissions in c) January and f) July.

B.2 Additional Figures and Tables

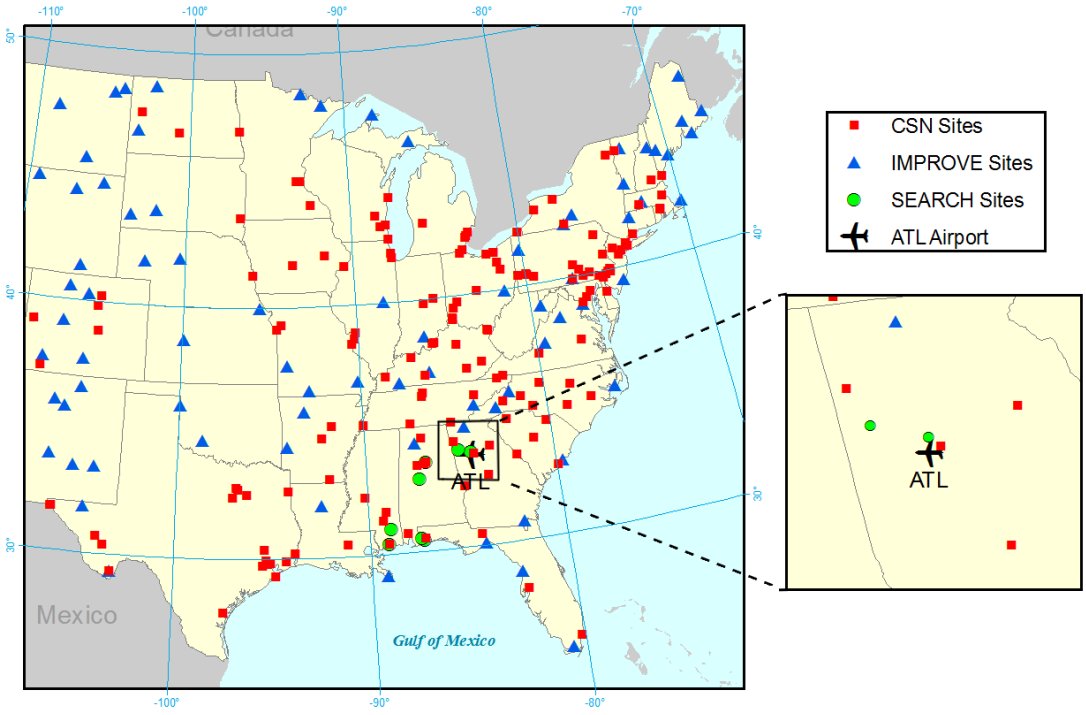

Figure B.5: Locations of CSN, IMPROVE, and SEARCH ambient monitors in the domain as well as the Atlanta Airport.

Table B.4: Updates to existing CMAQ SAPRC-07 reactions for VBS based on Koo et al. (2014). Where RXN products are replaced by RO2, high and low NO_x yields replace NO_x independent yields. SV_BVB and SV_AVB correspond to semi-volatile biogenic and anthropogenic SOA species, respectively. Newly added reactions (those without a corresponding reaction in SAPRC-07 without VBS) are listed in Table B.5.

Reactants	Default Product	Updated VBS CMAQ Product(s)
ISOPRENE + OH	ISOPRXN	ISOPRO2
APIN + OH	TRPRXN	TRPRO2
APIN + O3	TRPRXN	TRPRO2
APIN + NO3	TRPRXN	TRPRO2
TERP + OH	TRPRXN	TRPRO2
TERP + O3	TRPRXN	TRPRO2
TERP + NO3	TRPRXN	TRPRO2
ALK5 + OH	ALK5RXN	ALK5RO2
SESQ + OH	SESQRXN	0.092*SV_BVB1 + 0.188*SV_BVB2 + 0.968*SV_BVB3 + 0.679*SV_BVB4
SESQ + O3	SESQRXN	0.092*SV_BVB1 + 0.188*SV_BVB2 + 0.968*SV_BVB3 + 0.679*SV_BVB4
SESQ + NO3	SESQRXN	0.092*SV_BVB1 + 0.188*SV_BVB2 + 0.968*SV_BVB3 + 0.679*SV_BVB4
SESQ + O3P	SESQRXN	0.092*SV_BVB1 + 0.188*SV_BVB2 + 0.968*SV_BVB3 + 0.679*SV_BVB4
BENZRO2 + NO	BNZNRXN	0.001*SV_AVB1 + 0.079*SV_AVB2 + 0.148*SV_AVB3 + 0.222*SV_AVB4
BENZRO2 + HO2	BNZHRXN	0.035*SV_AVB1 + 0.108*SV_AVB2 + 0.185*SV_AVB3 + 0.268*SV_AVB4
XYLRO2 + NO	XYLNRXN	0.001*SV_AVB1 + 0.127*SV_AVB2 + 0.201*SV_AVB3 + 0.301*SV_AVB4
XYLRO2 + HO2	XYLHRXN	0.048*SV_AVB1 + 0.195*SV_AVB2 + 0.252*SV_AVB3 + 0.364*SV_AVB4
TOLRO2 + NO	TOLNRXN	0.006*SV_AVB1 + 0.145*SV_AVB2 + 0.281*SV_AVB3 + 0.432*SV_AVB4
TOLRO2 + HO2	TOLHRXN	0.006*SV_AVB1 + 0.145*SV_AVB2 + 0.437*SV_AVB3 + 0.281*SV_AVB4

Table B.5: Newly added reactions for SAPRC-07 for CMAQ with VBS based on Koo et al. (2014). SV_BVB, SV_AVB, SV_PVB, and SV_FVB correspond to semi-volatile biogenic SOA, anthropogenic SOA, anthropogenic POA, and biogenic POA (biomass burning), respectively and similarly IVOC_P and IVOC_F correspond to anthropogenic and biogenic IVOCs.

Reactants	Product(s)
ISOPRENE + O3	ISOPRO2
ISOPRENE + NO3	ISOPRO2
ISOPRO2 + NO	0.000*SV_BVB1 + 0.009*SV_BVB2 + 0.006*SV_BVB3 + 0.000*SV_BVB4
ISOPRO2 + HO2	0.004*SV_BVB1 + 0.013*SV_BVB2 + 0.006*SV_BVB3 + 0.000*SV_BVB4
TRPRO2 + NO	0.010*SV_BVB1 + 0.101*SV_BVB2 + 0.173*SV_BVB3 + 0.451*SV_BVB4
TRPRO2 + HO2	0.087*SV_BVB1 + 0.077*SV_BVB2 + 0.309*SV_BVB3 + 0.540*SV_BVB4
ALK5RO2 + NO	0.000*SV_AVB1 + 0.109*SV_AVB2 + 0.000*SV_AVB3 + 0.000*SV_AVB4
ALK5RO2 + HO2	0.000*SV_AVB1 + 0.219*SV_AVB2 + 0.000*SV_AVB3 + 0.000*SV_AVB4
SV_AVB1 + OH	SV_AVB0
SV_AVB2 + OH	SV_AVB1
SV_AVB3 + OH	SV_AVB2
SV_AVB4 + OH	SV_AVB3
SV_PVB1 + OH	0.864*SV_PVB0 + 0.142*SV_AVB0
SV_PVB2 + OH	0.877*SV_PVB1 + 0.129*SV_AVB1
SV_PVB3 + OH	0.889*SV_PVB2 + 0.116*SV_AVB2
SV_PVB4 + OH	0.869*SV_PVB3 + 0.137*SV_AVB3
SV_FVB1 + OH	0.538*SV_FVB0 + 0.464*SV_BVB0
SV_FVB2 + OH	0.689*SV_FVB1 + 0.313*SV_BVB1
SV_FVB3 + OH	0.783*SV_FVB2 + 0.220*SV_BVB2
SV_FVB4 + OH	0.846*SV_FVB3 + 0.156*SV_BVB3
IVOC_P + OH	0.033*SV_AVB1 + 0.216*SV_AVB2 + 0.304*SV_AVB3 + 0.447*SV_AVB4
IVOC_F + OH	0.033*SV_BVB1 + 0.216*SV_BVB2 + 0.304*SV_BVB3 + 0.447*SV_BVB4

Table B.6: Mean organic carbon concentrations, fractional bias (FB) and fractional error (FE) for CMAQ (AE6), CMAQ with VBS (VBS), and CMAQ with VBS and high S/IVOC emissions (VBSh) for CSN, IMPROVE, and SEARCH monitor sites located within the model domain.

Network (# of sites)		Mean Conc. (μg m^{-3}) Obs.	AE6	VBS	VBSh	FB (%) AE6	VBS	VBSh	FE (%) AE6	VBS	VBSh
CSN	Jan	2.9	2.8	0.9	3.4	-3.3	-105	0.4	53.0	111	58.4
(173)	Jul	4.9	1.3	0.7	1.6	-103	-140	-92.3	107	142	95.8
IMPROVE	Jan	1.1	1.4	0.4	1.5	-5.9	-106	-14.6	59.6	109	67.8
(83)	Jul	2.6	0.6	0.5	0.9	-118	-132	-93.7	119	132	97.4
SEARCH	Jan	0.7	2.0	0.7	2.3	166	150	168	174	185	173
(8)	Jul	1.2	1.3	0.8	1.6	121	105	124	158	174	155

Table B.7: Mean $PM_{2.5}$ concentrations, fractional bias (FB) and fractional error (FE) for CMAQ (AE6), CMAQ with VBS (VBS), and CMAQ with VBS and high S/IVOC emissions (VBSh) for CSN, IMPROVE, and SEARCH monitor sites located within the model domain.

Network (# of sites)		Mean Conc. (μg m^{-3}) Obs.	AE6	VBS	VBSh	FB (%) AE6	VBS	VBSh	FE (%) AE6	VBS	VBSh
CSN	Jan	12.4	18.4	14.7	18.1	27.8	5.5	23.0	47.0	39.4	46.8
(173)	Jul	18.4	12.9	11.0	12.5	-39.9	-53.3	-44.6	53.1	62.2	57.5
IMPROVE	Jan	5.4	8.2	6.2	7.7	24.6	0.5	14.4	53.8	47.9	53.1
(83)	Jul	12.5	6.7	5.6	6.2	-69.1	-82.8	-81.4	72.7	85.0	84.3

Table B.8: Mean organic concentrations, fractional bias (FB) and fractional error (FE) for CMAQ (AE6), CMAQ with VBS (VBS), and CMAQ with VBS and high S/IVOC emissions (VBSh) for the CSN monitor (Site No. 130890002, located approximately 15 km northeast of the airport in Decatur, GA) and SEARCH monitor [Jefferson Street Site (JST), located approximately 15 km north of the airport in downtown Atlanta, GA] closest to the Atlanta Airport.

Network		Mean Conc. (μg m^{-3}) Obs.	AE6	VBS	VBSh	FB (%) AE6	VBS	VBSh	FE (%) AE6	VBS	VBSh
Decatur	Jan	4.6	3.1	1.0	3.5	-29.5	-127	-21.2	34.1	127	25.4
	Jul	4.6	1.2	0.8	1.5	-112	105	-99.4	112	195	99.4
JST	Jan	4.5	3.5	1.1	4.1	-18.0	-115	-5.2	34.0	118	27.6
	Jul	4.0	2.1	1.1	2.5	-53.1	-105	-43.5	66.4	118	57.3

Table B.9: Mean $PM_{2.5}$ concentrations, fractional bias (FB) and fractional error (FE) for CMAQ (AE6), CMAQ with VBS (VBS), and CMAQ with VBS and high S/IVOC emissions (VBSh) for the CSN monitor (Site No. 130890002, located approximately 15 km northeast of the airport in Decatur, GA) closest to the Atlanta Airport.

Network		Mean Conc. (μg m^{-3})				FB (%)			FE (%)		
		Obs.	AE6	VBS	VBSh	AE6	VBS	VBSh	AE6	VBS	VBSh
Decatur	Jan	13.7	19.4	15.6	19.2	35.2	12.2	32.8	36.0	23.4	36.6
	Jul	18.2	11.9	10.5	12.0	-56.2	-69.9	-52.0	56.2	69.9	53.9

APPENDIX C SUPPLEMENTAL MATERIAL: MULTISCALE PREDICTIONS OF AIRCRAFT-ATTRIBUTABLE $PM_{2.5}$ MODELED USING CMAQ-APT FOR U.S. AIRPORTS

Table C.1: List of the 99 airports included in this study and their tier classification, which is based on activity.

Code	Tier	Name	City	State
ABQ	III	Albuquerque Intl. Sunport	Albuquerque	NM
ALB	III	Albany Intl.	Albany	NY
ATL	I	Hartsfield-Jackson Atlanta Intl.	Atlanta	GA
AUS	III	Austin-Bergstrom Intl.	Austin	TX
BDL	III	Bradley Intl.	Windsor Locks	CT
BFL	III	Meadows Field	Bakersfield	CA
BHM	III	Birmingham Intl.	Birmingham	AL
BNA	III	Nashville Intl.	Nashville	TN
BOI	III	Boise Air Terminal-Gowen Field	Boise	ID
BOS	II	General Edward Lawrence Logan Intl.	Boston	MA
BTR	III	Baton Rouge Metropolitan-Ryan Field	Baton Rouge	LA
BUF	III	Buffalo Niagara Intl.	Buffalo	NY
BUR	III	Bob Hope	Burbank	CA
BWI	II	Baltimore-Washington Intl.	Baltimore	MD
CHS	III	Charleston Air Force Base/Intl.	Charleston	SC
CLE	III	Cleveland-Hopkins Intl.	Cleveland	OH
CLT	I	Charlotte Douglas Intl.	Charlotte	NC
CMH	III	Port Columbus Intl.	Columbus	OH
COS	III	City of Colorado Springs Municipal	Colorado Springs	CO
CRP	III	Corpus Christi Intl.	Corpus Christi	TX
CVG	II	Cincinnati Northern Kentucky Intl.	Covington	OH
DAB	III	Daytona Beach Intl.	Daytona Beach	FL
DAL	III	Dallas Love Field	Dallas	TX
DAY	III	James M. Cox Dayton Intl.	Dayton	OH
DCA	II	Ronald Reagan Washington National	Washington	DC
DEN	I	Denver Intl.	Denver	CO

(Continued on next page)

Table C.1: 99 airports – continued from previous page

Code	Tier	Name	City	State
DFW	I	Dallas-Fort Worth Intl.	Dallas-Fort Worth	TX
DSM	III	Des Moines Intl.	Des Moines	IA
DTW	I	Detroit Metropolitan Wayne County	Detroit	MI
ELP	III	El Paso Intl.	El Paso	TX
EUG	III	Mahlon Sweet Field	Eugene	OR
EWR	II	Newark Liberty Intl.	Newark	NJ
FAT	III	Fresno Yosemite Intl.	Fresno	CA
FLL	II	Fort Lauderdale Hollywood Intl.	Fort Lauderdale	FL
FNT	III	Bishop Intl.	Flint	MI
GFK	III	Grand Forks Intl.	Grand Forks	ND
GRR	III	Gerald R. Ford Intl.	Grand Rapids	MI
GSO	III	Piedmont Triad Intl.	Greensboro	NC
HOU	III	William P. Hobby	Houston	TX
HPN	III	Westchester County	White Plains	NY
IAD	I	Washington Dulles Intl.	Washington	DC
IAH	I	George Bush Intercontinental-Houston	Houston	TX
ICT	III	Wichita Mid-Continent	Wichita	KS
IND	III	Indianapolis Intl.	Indianapolis	IN
ISP	III	Long Island MacArthur	Islip	NY
JAX	III	Jacksonville Intl.	Jacksonville	FL
JFK	II	John F. Kennedy Intl.	New York	NY
LAN	III	Capital City	Lansing	MI
LAS	II	McCarran Intl.	Las Vegas	NV
LAX	I	Los Angeles Intl.	Los Angeles	CA
LGA	II	La Guardia	New York	NY
LGB	III	Long Beach-Daugherty Field	Long Beach	CA
LIT	III	Adams Field	Little Rock	AR
MCI	III	Kansas City Intl.	Kansas City	MI
MCO	II	Orlando Intl.	Orlando	FL
MDW	II	Chicago Midway Intl.	Chicago	IL

(Continued on next page)

Table C.1: 99 airports – continued from previous page

Code	Tier	Name	City	State
MEM	II	Memphis Intl.	Memphis	TN
MIA	II	Miami Intl.	Miami	FL
MKE	III	General Mitchell Intl.	Milwaukee	WI
MLB	III	Melbourne Intl.	Melbourne	FL
MSN	III	Dane County Regional-Truax Field	Madison	WI
MSP	I	Minneapolis-St Paul Intl.	Minneapolis	MN
MSY	III	Louis Armstrong New Orleans Intl.	New Orleans	LA
OAK	III	Metropolitan Oakland Intl.	Oakland	CA
OKC	III	Will Rogers World	Oklahoma City	OK
OMA	III	Eppley Airfield	Omaha	NE
ONT	III	Ontario Intl.	Ontario	CA
ORD	I	Chicago O'Hare Intl.	Chicago	IL
ORF	III	Norfolk Intl.	Norfolk	VA
PBI	III	Palm Beach Intl.	West Palm Beach	FL
PDX	III	Portland Intl.	Portland	OR
PHF	III	Newport News Williamsburg Intl.	Newport News	VA
PHL	I	Philadelphia Intl.	Philadelphia	PA
PHX	I	Phoenix Sky Harbor Intl.	Phoenix	AR
PIT	III	Pittsburgh Intl.	Pittsburgh	PA
PVD	III	Theodore Francis Green State	Providence	RI
RDU	III	Raleigh-Durham Intl.	Raleigh-Durham	NC
RIC	III	Richmond Intl.	Richmond	ViA
RNO	III	Reno Tahoe Intl.	Reno	NV
ROC	III	Greater Rochester Intl.	Rochester	NY
RSW	III	Southwest FL Intl.	Fort Myers	FL
SAN	III	San Diego Intl.	San Diego	CA
SAT	III	San Antonio Intl.	San Antonio	TX
SBA	III	Santa Barbara Municipal	Santa Barbara	CA
SDF	III	Louisville Intl.-Standiford Field	Louisville	KY
SEA	II	Seattle-Tacoma Intl.	Seattle	WA

(Continued on next page)

Table C.1: 99 airports – continued from previous page

Code	Tier	Name	City	State
SFO	II	San Francisco Intl.	San Francisco	CA
SJC	III	Norman Y. Mineta San Jose Intl.	San Jose	CA
SLC	II	Salt Lake City Intl.	Salt Lake City	UT
SMF	III	Sacramento Intl.	Sacramento	CA
SNA	III	John Wayne Airport-Orange County	Santa Ana	CA
STL	II	Lambert-St Louis Intl.	St Louis	MI
SWF	III	Stewart Intl.	Newburgh	NY
SYR	III	Syracuse Hancock Intl.	Syracuse	NY
TPA	III	Tampa Intl.	Tampa	FL
TUL	III	Tulsa Intl.	Tulsa	OK
TUS	III	Tucson Intl.	Tucson	AR
TVC	III	Cherry Capital	Traverse City	MI
TYS	III	McGhee Tyson	Knoxville	TN

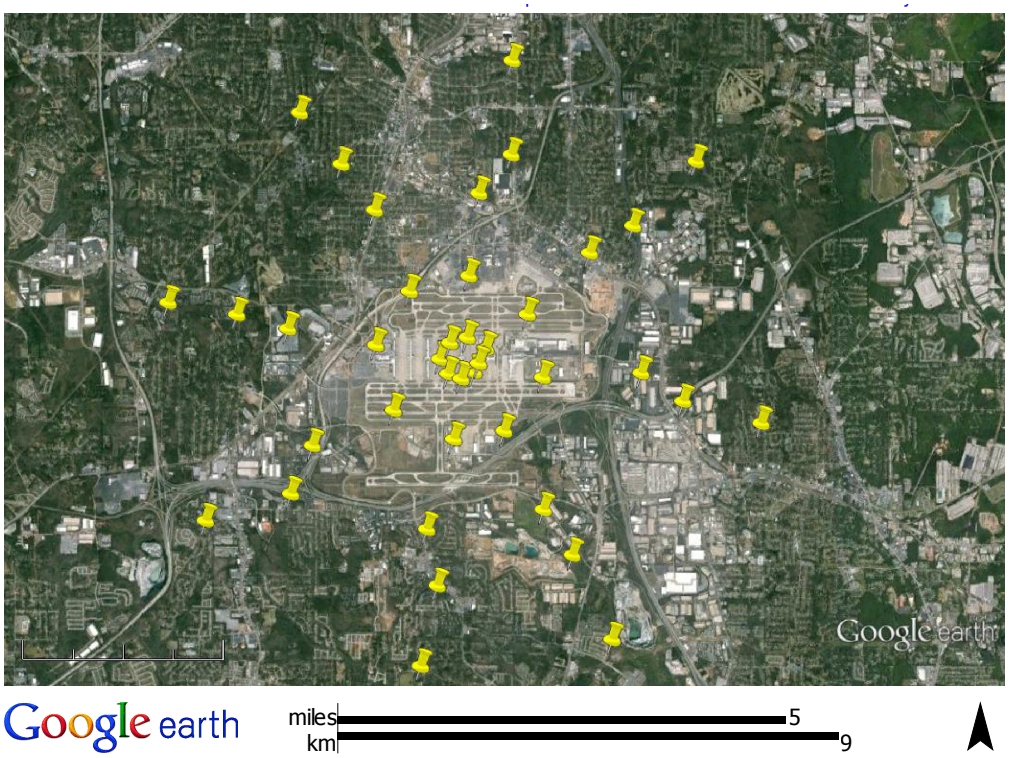

Figure C.1: Example of emitter placement for the Hartsfield-Jackson Atlanta International Airport.

Figure C.2: Illustrative example of puff locations in CMAQ-APT using puff centroid locations at 12 GMT on July 1.

	Input Parameters								Emissions						
	Engine Type	Power	FSC	ε	Hydrocarbon Concentration	Sigma	Ambient Temperature	Ambient RH	Total Emissions Rates		PM Emissions Rates				
									SO_4	HC	Black Carbon	SO_4 Nuc	SO_4 Soot	SO_4 Total	
	-	%	ppm	%	ppm	-	K	%	mg/s	mg/s	mg/s	mg/s	mg/s	mg/s	
	CFM56-2C1	7	600	1	400	8	275	10	2.2203	23.4022	0.5445	0.0025	0.2722	0.2747	
							275	20	2.2203	23.4083	0.5446	0.0066	0.2796	0.2862	
							275	30	2.2203	23.4141	0.5448	0.0409	0.2930	0.3339	

Figure C.3: Exert from ADSC look-up table.

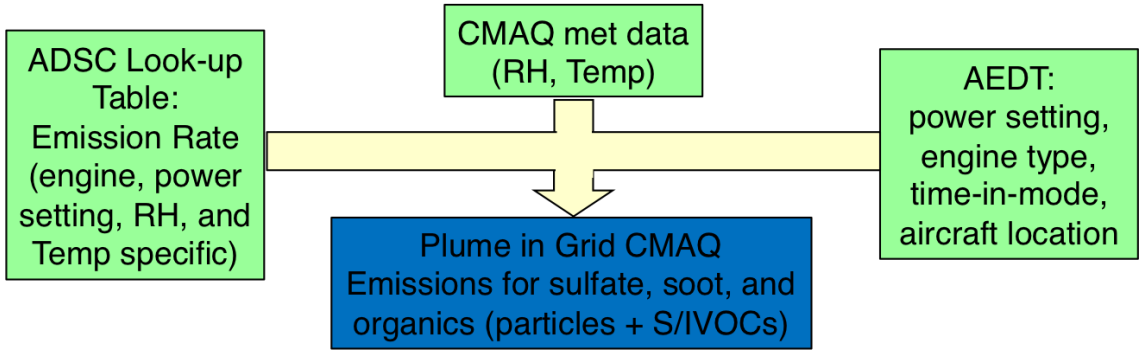

Figure C.4: Schematic indicating the flow of data used to create ADSC-based CMAQ plume-in-grid emissions. Note AEDT-based CMAQ plume-in-grid emissions only utilize AEDT data.

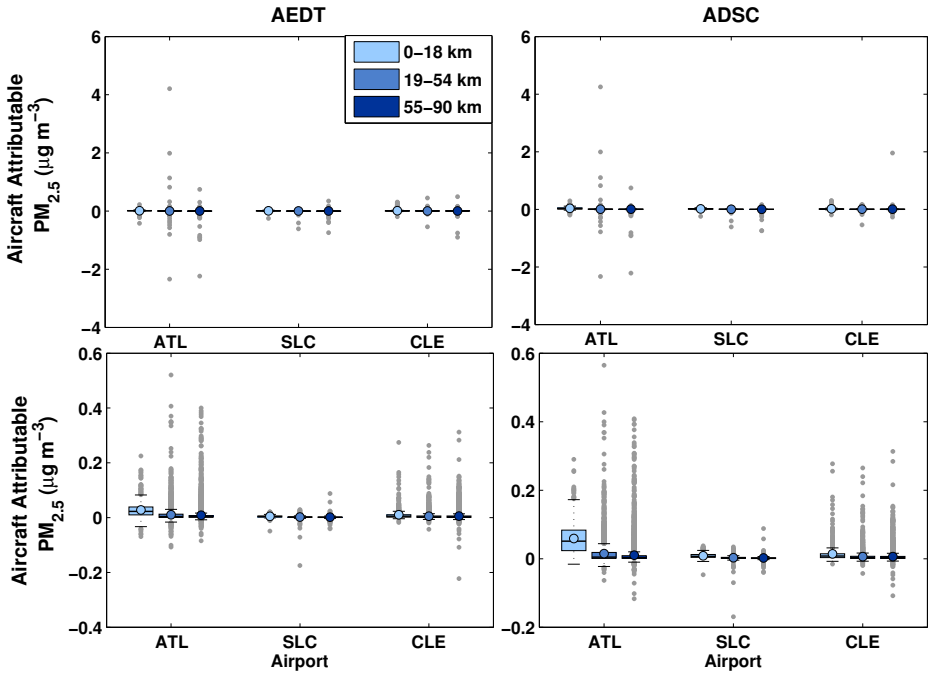

Figure C.5: Box-and-whisker plots of grid-based aircraft-attributable $PM_{2.5}$ (scenarios without PinG) in the grid cell containing the Atlanta (ATL), Salt Lake City (SLC), and Cleveland (CLE) airports (0-18 km) and grid cells located 19-54 km and 55-90 km downwind of the airports in January (top) and July (bottom). Grey dots represent outliers which are defined as values more than 1.5 times the inter-quartile range above the 75th percentile and below the 25th percentile.

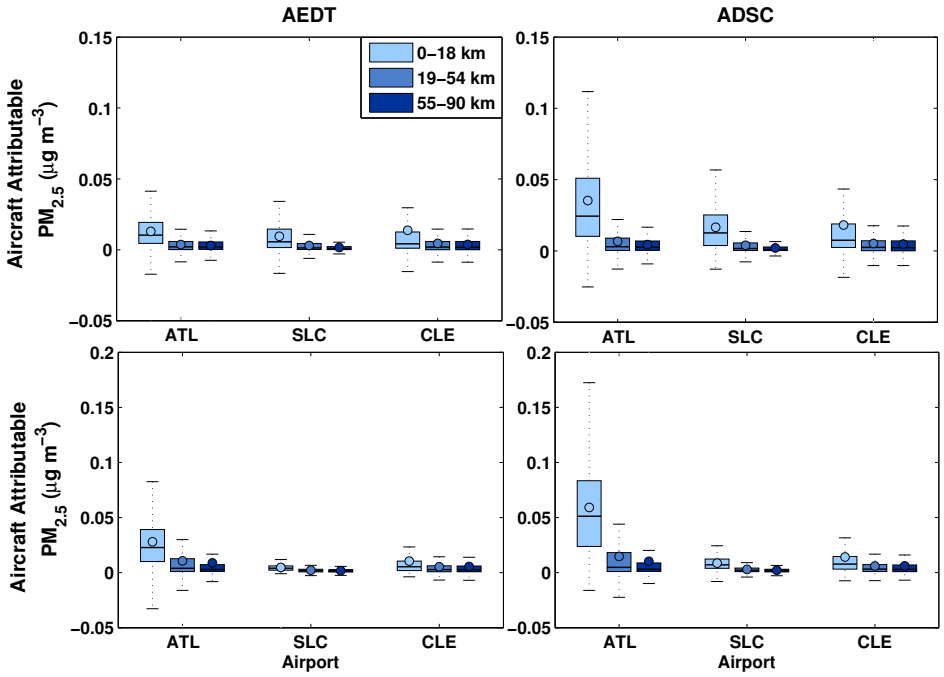

Figure C.6: The same as with Figure C.5 but with outliers removed.

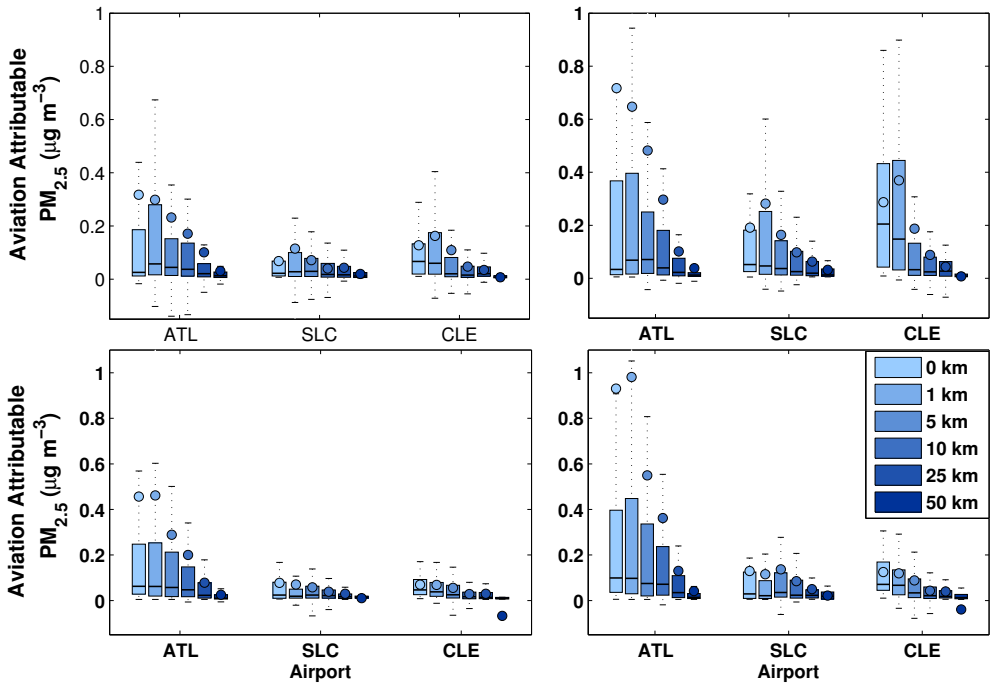

Figure C.7: Box-and-whisker plots of aircraft-attributable $PM_{2.5}$ (grid plus puff) at receptors located at the Atlanta (ATL), Salt Lake City (SLC), and Cleveland (CLE) airports and at distances of 1 km, 5 km, 10 km, 25 km and 50 km away in January (top) and July (bottom) with outliers removed, i.e. the same as with Figure 4.5 but with outliers removed.

REFERENCES

Agrawal, H., Sawant, A. A., Jansen, K., Wayne Miller, J., and Cocker III, D. R.: Characterization of chemical and particulate emissions from aircraft engines, Atmospheric Environment, 42, 4380–4392, 2008.

Alfarra, M. R., Paulsen, D., Gysel, M., Garforth, A. A., Dommen, J., Prévôt, A. S., Worsnop, D. R., Baltensperger, U., and Coe, H.: A mass spectrometric study of secondary organic aerosols formed from the photooxidation of anthropogenic and biogenic precursors in a reaction chamber, Atmospheric Chemistry and Physics, 6, 5279–5293, 2006.

Allen, D., Pickering, K., Pinder, R., Henderson, B., Appel, K., and Prados, A.: Impact of lightning-NO on eastern United States photochemistry during the summer of 2006 as determined using the CMAQ model, Atmospheric Chemistry and Physics, 12, 1737–1758, 2012.

Arunachalam, S., Holland, A., Do, B., and Abraczinskas, M.: A quantitative assessment of the influence of grid resolution on predictions of future-year air quality in North Carolina, USA, Atmospheric Environment, 40, 5010–5026, 2006.

Arunachalam, S., Wang, B., Davis, N., Baek, B. H., and Levy, J. I.: Effect of chemistry-transport model scale and resolution on population exposure to $PM_{2.5}$ from aircraft emissions during landing and takeoff, Atmospheric Environment, 45, 3294–3300, 2011.

Baek, B. H., Arunachalam, S., Holland, A., Adelman, Z., Hanna, A., Thrasher, T., and Philip, S.: Development of an Interface for the Emissions and Dispersion Modeling System (EDMS) with the SMOKE Modeling System, in: 16th Annual Emissions Inventory Conference, 2007.

Baek, B. H., Arunachalam, S., Woody, M., Vennam, L. P., Omary, M., Binkowski, F., and Fleming, G.: A New Interface to Model Global Commercial Aircraft Emissions from the FAA Aviation Environmental Design Tool (AEDT) in Air Quality Models, in: 11th Annual Emissions Inventory Conference, 2012.

Bahreini, R., Keywood, M., Ng, N., Varutbangkul, V., Gao, S., Flagan, R., Seinfeld, J., Worsnop, D., and Jimenez, J.: Measurements of secondary organic aerosol from oxidation of cycloalkenes, terpenes, and m-xylene using an Aerodyne aerosol mass spectrometer, Environmental Science & Technology, 39, 5674–5688, 2005.

Barrett, S. R., Britter, R. E., and Waitz, I. A.: Global mortality attributable to aircraft cruise emissions, Environmental Science & Technology, 44, 7736–7742, 2010.

Barrett, S. R., Yim, S. H., Gilmore, C. K., Murray, L. T., Kuhn, S. R., Tai, A. P., Yantosca, R. M., Byun, D. W., Ngan, F., Li, X., et al.: Public health, climate, and economic impacts of desulfurizing jet fuel, Environmental science & technology, 46, 4275–4282, 2012.

Bauer, S. E. and Menon, S.: Aerosol direct, indirect, semidirect, and surface albedo effects from sector contributions based on the IPCC AR5 emissions for preindustrial and present-day conditions,

Journal of Geophysical Research: Atmospheres (1984–2012), 117, 2012.

Bergin, M. S., Russell, A. G., Odman, M. T., Cohan, D. S., and Chameides, W. L.: Single-source impact analysis using three-dimensional air quality models, Journal of the Air & Waste Management Association, 58, 1351–1359, 2008.

Beyersdorf, A., Timko, M., Ziemba, L., Bulzan, D., Corporan, E., Herndon, S., Howard, R., Miake-Lye, R., Thornhill, K., Winstead, E., et al.: Reductions in aircraft particulate emissions due to the use of Fischer–Tropsch fuels, Atmospheric Chemistry and Physics, 14, 11–23, 2014.

Bhave, P. V., Pouliot, G. A., and Zheng, M.: Diagnostic model evaluation for carbonaceous $PM_{2.5}$ using organic markers measured in the southeastern US, Environmental Science & Technology, 41, 1577–1583, 2007.

Binkowski, F. S. and Roselle, S. J.: Models-3 Community Multiscale Air Quality (CMAQ) model aerosol component 1. Model description, Journal of Geophysical Research: Atmospheres (1984–2012), 108, 2003.

Boylan, J. W. and Russell, A. G.: PM and light extinction model performance metrics, goals, and criteria for three-dimensional air quality models, Atmospheric Environment, 40, 4946–4959, 2006.

Brasseur, G., Cox, R., Hauglustaine, D., Isaksen, I., Lelieveld, J., Lister, D., Sausen, R., Schumann, U., Wahner, A., and Wiesen, P.: European scientific assessment of the atmospheric effects of aircraft emissions, Atmospheric Environment, 32, 2329–2418, 1998.

Brunelle-Yeung, E., Masek, T., Rojo, J. J., Levy, J. I., Arunachalam, S., Miller, S. M., Barrett, S. R., Kuhn, S. R., and Waitz, I. A.: Assessing the impact of aviation environmental policies on public health, Transport Policy, 2014.

Byun, D. and Schere, K. L.: Review of the governing equations, computational algorithms, and other components of the Models-3 Community Multiscale Air Quality (CMAQ) modeling system, Applied Mechanics Reviews, 59, 51–77, 2006.

Byun, D. W. and Ching, J.: Science algorithms of the EPA Models-3 community multiscale air quality (CMAQ) modeling system, US Environmental Protection Agency, Office of Research and Development Washington, DC, USA, 1999.

Cameron, M. A., Jacobson, M. Z., Naiman, A. D., and Lele, S. K.: Effects of plume-scale versus grid-scale treatment of aircraft exhaust photochemistry, Geophysical Research Letters, 40, 5815–5820, 2013.

Carlton, A. G., Turpin, B. J., Altieri, K. E., Seitzinger, S. P., Mathur, R., Roselle, S. J., and Weber, R. J.: CMAQ model performance enhanced when in-cloud secondary organic aerosol is included: Comparisons of organic carbon predictions with measurements, Environmental Science & Technology, 42, 8798–8802, 2008.

Carlton, A. G., Bhave, P. V., Napelenok, S. L., Edney, E. O., Sarwar, G., Pinder, R. W., Pouliot, G. A., and Houyoux, M.: Model representation of secondary organic aerosol in CMAQv4.7,

Environmental Science & Technology, 44, 8553–8560, 2010.

Carslaw, D. C., Beevers, S. D., Ropkins, K., and Bell, M. C.: Detecting and quantifying aircraft and other on-airport contributions to ambient nitrogen oxides in the vicinity of a large international airport, Atmospheric Environment, 40, 5424–5434, 2006.

Carter, W. P.: Development of the SAPRC-07 chemical mechanism, Atmospheric Environment, 44, 5324–5335, 2010.

Cross, E. S., Hunter, J. F., Carrasquillo, A. J., Franklin, J. P., Herndon, S. C., Jayne, J. T., Worsnop, D. R., Miake-Lye, R. C., and Kroll, J. H.: Online measurements of the emissions of intermediate-volatility and semi-volatile organic compounds from aircraft, Atmospheric Chemistry and Physics, 13, 7845–7858, 2013.

De Gouw, J., Middlebrook, A., Warneke, C., Goldan, P., Kuster, W., Roberts, J., Fehsenfeld, F., Worsnop, D., Canagaratna, M., Pszenny, A., et al.: Budget of organic carbon in a polluted atmosphere: Results from the New England Air Quality Study in 2002, Journal of Geophysical Research: Atmospheres, 110, 2005.

Dockery, D. W. and Pope, C. A.: Acute respiratory effects of particulate air pollution, Annual Review of Public Health, 15, 107–132, 1994.

Donahue, N., Robinson, A., Stanier, C., and Pandis, S.: Coupled partitioning, dilution, and chemical aging of semivolatile organics, Environmental Science & Technology, 40, 2635–2643, 2006.

Donahue, N. M., Henry, K. M., Mentel, T. F., Kiendler-Scharr, A., Spindler, C., Bohn, B., Brauers, T., Dorn, H. P., Fuchs, H., Tillmann, R., et al.: Aging of biogenic secondary organic aerosol via gas-phase OH radical reactions, Proceedings of the National Academy of Sciences, 109, 13 503–13 508, 2012.

DuBois, D. and Paynter, G. C.: "Fuel Flow Method2" for Estimating Aircraft Emissions, SAE TRANSACTIONS, 115, 1, 2007.

Edney, E., Kleindienst, T., Lewandowski, M., and Offenberg, J.: Updated SOA chemical mechanism for the community multi-scale air quality model, US Environmental Protection Agency, Research Triangle Park, North Carolina, 2007.

Electric Power Research Institute: Review, Testing and Evaluation of SCICHEM (Second-Order Closure Integrated Puff Model with Chemistry) and CMAQ-APT (Community Multiscale Air Quality Model-Advanced Plume Treatment), Palo Alto, CA, URL http://www.epri.com/abstracts/Pages/ProductAbstract.aspx?ProductId=000000000001005241, 2003.

ENVIRON: User's Guide to the Comprehensive Air Quality Model with Extensions (CAMx) Version 6.0, ENVIRON International Corporation, Novato, CA, URL http://www.camx.com/files/camxusersguide_v6-00.pdf, 2013.

Farina, S. C., Adams, P. J., and Pandis, S. N.: Modeling global secondary organic aerosol formation and processing with the volatility basis set: Implications for anthropogenic secondary organic

aerosol, Journal of Geophysical Research: Atmospheres (1984–2012), 115, 2010.

Federal Aviation Administration: 2011 Passenger boarding (enplanement) and all-cargo data for U.S. airports, http://www.faa.gov/airports/planning_capacity/passenger_allcargo_stats/passenger/index.cfm?year=2011, 2012a.

Federal Aviation Administration: FAA Aerospace Forecast Fiscal Years 2012-2032, URL http://www.faa.gov/about/office_org/headquarters_offices/apl/aviation_forecasts/aerospace_forecasts/2012-2032/media/Forecast%20Highlights.pdf, 2012b.

Federal Aviation Administration: Aviation Performance Metrics (APM), https://aspm.faa.gov/apm/sys/, 2013.

Federal Aviation Administration: Passenger boarding (enplanement) and all-cargo data for U.S. airports, http://www.faa.gov/airports/planning_capacity/passenger_allcargo_stats/passenger/, 2014a.

Federal Aviation Administration: Voluntary Airport Low Emissions Program (VALE), http://www.faa.gov/airports/environmental/vale, 2014b.

Federal Register Notice: Emissions and Dispersion Modeling System Policy for Airport Air Quality Analysis; Interim Guidance for FAA Orders 1050.1D and 5050.4A, Federal Aviation Administration, 63, 18 068, http://www.faa.gov/about/office_org/headquarters_offices/aep/models/edms_model, 1998.

Foley, K., Roselle, S., Appel, K., Bhave, P., Pleim, J., Otte, T., Mathur, R., Sarwar, G., Young, J., Gilliam, R., et al.: Incremental testing of the Community Multiscale Air Quality (CMAQ) modeling system version 4.7, Geoscientific Model Development, 3, 205–226, 2010.

Grell, G. A., Dudhia, J., and Stauffer, D. R.: A description of the fifth-generation Penn State/NCAR mesoscale model (MM5), Tech. rep., Mesoscale and Microscale Meteorology Division, National Center for Atmospheric Research, 1994.

Grell, G. A., Peckham, S. E., Schmitz, R., McKeen, S. A., Frost, G., Skamarock, W. C., and Eder, B.: Fully coupled online chemistry within the WRF model, Atmospheric Environment, 39, 6957–6975, 2005.

Griffin, R. J., Cocker, D. R., Flagan, R. C., and Seinfeld, J. H.: Organic aerosol formation from the oxidation of biogenic hydrocarbons, Journal of Geophysical Research: Atmospheres, 104, 3555–3567, 1999.

Hallquist, M., Wenger, J., Baltensperger, U., Rudich, Y., Simpson, D., Claeys, M., Dommen, J., Donahue, N., George, C., Goldstein, A., et al.: The formation, properties and impact of secondary organic aerosol: current and emerging issues, Atmospheric Chemistry and Physics, 9, 5155–5236, 2009.

Hansen, D. A., Edgerton, E. S., Hartsell, B. E., Jansen, J. J., Kandasamy, N., Hidy, G. M., and Blanchard, C. L.: The southeastern aerosol research and characterization study: Part 1Overview,

Journal of the Air & Waste Management Association, 53, 1460–1471, 2003.

Henderson, B., Vizuete, W., Jeffries, H., and Pinder, R.: Python-based Environment for Reaction Mechanisms, in: 8th Annual Emissions Inventory Conference, 2009.

Henderson, B. H., Kimura, Y., McDonald-Buller, E., Allen, D. T., and Vizuete, W.: Comparison of Lagrangian Process Analysis tools for Eulerian air quality models, Atmospheric Environment, 45, 5200–5211, 2011.

Herndon, S. C., Jayne, J. T., Lobo, P., Onasch, T. B., Fleming, G., Hagen, D. E., Whitefield, P. D., and Miake-Lye, R. C.: Commercial aircraft engine emissions characterization of in-use aircraft at Hartsfield-Jackson Atlanta International Airport, Environmental Science & Technology, 42, 1877–1883, 2008.

Herndon, S. C., Wood, E. C., Northway, M. J., Miake-Lye, R., Thornhill, L., Beyersdorf, A., Anderson, B. E., Dowlin, R., Dodds, W., and Knighton, W. B.: Aircraft hydrocarbon emissions at Oakland International Airport, Environmental Science & Technology, 43, 1730–1736, 2009.

Hildebrandt, L., Donahue, N., and Pandis, S.: High formation of secondary organic aerosol from the photo-oxidation of toluene, Atmospheric Chemistry and Physics, 9, 2973–2986, 2009.

Hodzic, A., Madronich, S., Bohn, B., Massie, S., Menut, L., and Wiedinmyer, C.: Wildfire particulate matter in Europe during summer 2003: meso-scale modeling of smoke emissions, transport and radiative effects, Atmospheric Chemistry and Physics, 7, 4043–4064, 2007.

Hogrefe, C., Werth, D., Avissar, R., Lynn, B., Rosenzweig, C., Goldberg, R., Rosenthal, J., Knowlton, K., and Kinney, P.: Analyzing the impacts of climate change on ozone and particulate matter with tracer species, process analysis, and multiple regional climate scenarios, Developments in Environmental Science, 6, 648–660, 2007.

Houyoux, M. R., Vukovich, J. M., Coats, C. J., Wheeler, N. J., and Kasibhatla, P. S.: Emission inventory development and processing for the Seasonal Model for Regional Air Quality (SMRAQ) project, Journal of Geophysical Research: Atmospheres, 105, 9079–9090, 2000.

Hutzell, W., Luecken, D., Appel, K., and Carter, W.: Interpreting predictions from the SAPRC07 mechanism based on regional and continental simulations, Atmospheric Environment, 46, 417–429, 2012.

Jacobson, M. Z., Wilkerson, J. T., Naiman, A. D., and Lele, S. K.: The effects of aircraft on climate and pollution. Part II: 20-year impacts of exhaust from all commercial aircraft worldwide treated individually at the subgrid scale, Faraday Discussions, 165, 369–382, 2013.

Jang, J.-C. C., Jeffries, H. E., and Tonnesen, S.: Sensitivity of ozone to model grid resolutionII. Detailed process analysis for ozone chemistry, Atmospheric Environment, 29, 3101–3114, 1995.

Jathar, S., Farina, S., Robinson, A., and Adams, P.: The influence of semi-volatile and reactive primary emissions on the abundance and properties of global organic aerosol, Atmospheric Chemistry and

Physics, 11, 7727–7746, 2011.

Jathar, S., Miracolo, M., Presto, A., Donahue, N., Adams, P., and Robinson, A.: Modeling the formation and properties of traditional and non-traditional secondary organic aerosol: problem formulation and application to aircraft exhaust, Atmospheric Chemistry and Physics, 12, 9025–9040, 2012.

Jathar, S., Donahue, N., Adams, P., and Robinson, A.: Testing secondary organic aerosol models using smog chamber data for complex precursor mixtures: influence of precursor volatility and molecular structure, Atmospheric Chemistry and Physics, 14, 5771–5780, 2014.

Jeffries, H. E. and Tonnesen, S.: A comparison of two photochemical reaction mechanisms using mass balance and process analysis, Atmospheric Environment, 28, 2991–3003, 1994.

Kanakidou, M., Seinfeld, J. H., Pandis, S. N., Barnes, I., Dentener, F. J., Facchini, M. C., Van Dingenen, R., Ervens, B., Nenes, A., Nielsen, C. J., Swietlicki, E., Putaud, J. P., Balkanski, Y., Fuzzi, S., Horth, J., Moortgat, G. K., Winterhalter, R., Myhre, C. E. L., Tsigaridis, K., Vignati, E., Stephanou, E. G., and Wilson, J.: Organic aerosol and global climate modelling: a review, Atmospheric Chemistry and Physics, 5, 1053–1123, http://www.atmos-chem-phys.net/5/1053/2005/, 2005.

Karamchandani, P., Johnson, J., Yarwood, G., and Knipping, E.: Implementation and Application of Sub-Grid Scale Plume Treatment in the Latest Version of EPA's Third-Generation Air Quality Model, CMAQ 5.01, Journal of the Air & Waste Management Association, 64, 2014.

Kinsey, J. S., Dong, Y., Williams, D. C., and Logan, R.: Physical characterization of the fine particle emissions from commercial aircraft engines during the Aircraft Particle Emissions eXperiment (APEX) 1–3, Atmospheric Environment, 44, 2147–2156, 2010.

Koo, B., Yarwood, G., and Knipping, E.: Implementing VBS Algorithm for OA Formation in CMAQ v5, in: AAAR 31st Annual Conference, 2012.

Koo, B., Knipping, E., and Yarwood, G.: An Improved Volatility Basis Set for Modeling Organic Aerosol in both CAMx and CMAQ, in: 33rd International Technical Meeting on Air Pollution Modelling and its Application, 2013.

Koo, B., Knipping, E., and Yarwood, G.: 1.5-Dimensional Volatility Basis Set Approach for Modeling Organic Aerosol in CAMx and CMAQ, Atmospheric Environment, 95, 158–164, 2014.

Kostenidou, E., Pathak, R. K., and Pandis, S. N.: An algorithm for the calculation of secondary organic aerosol density combining AMS and SMPS data, Aerosol Science and Technology, 41, 1002–1010, 2007.

Kroll, J. H. and Seinfeld, J. H.: Chemistry of secondary organic aerosol: Formation and evolution of low-volatility organics in the atmosphere, Atmospheric Environment, 42, 3593–3624, 2008.

Kumar, P., Pirjola, L., Ketzel, M., and Harrison, R. M.: Nanoparticle emissions from 11 non-vehicle

exhaust sources–a review, Atmospheric Environment, 67, 252–277, 2013.

Lamarque, J.-F., Emmons, L., Hess, P., Kinnison, D. E., Tilmes, S., Vitt, F., Heald, C., Holland, E. A., Lauritzen, P., Neu, J., et al.: CAM-chem: description and evaluation of interactive atmospheric chemistry in the Community Earth System Model, Geoscientific Model Development, 5, 369–411, 2012.

Lane, T. E., Donahue, N. M., and Pandis, S. N.: Simulating secondary organic aerosol formation using the volatility basis-set approach in a chemical transport model, Atmospheric Environment, 42, 7439–7451, 2008.

Lee, D. S., Fahey, D. W., Forster, P. M., Newton, P. J., Wit, R. C., Lim, L. L., Owen, B., and Sausen, R.: Aviation and global climate change in the 21st century, Atmospheric Environment, 43, 3520–3537, 2009.

Lee, H., Olsen, S., Wuebbles, D., and Youn, D.: Impacts of aircraft emissions on the air quality near the ground, Atmospheric Chemistry and Physics, 13, 5505–5522, 2013.

Levy, J. I., Woody, M., Baek, B. H., Shankar, U., and Arunachalam, S.: Current and Future Particulate-Matter-Related Mortality Risks in the United States from Aviation Emissions During Landing and Takeoff, Risk Analysis, 32, 237–249, 2012.

Li, G., Zavala, M., Lei, W., Tsimpidi, A., Karydis, V., Pandis, S., Canagaratna, M., and Molina, L.: Simulations of organic aerosol concentrations in Mexico City using the WRF-CHEM model during the MCMA-2006/MILAGRO campaign, Atmospheric Chemistry and Physics, 11, 3789–3809, 2011.

Liu, P., Zhang, Y., Yu, S., and Schere, K. L.: Use of a process analysis tool for diagnostic study on fine particulate matter predictions in the US-Part II: Analyses and sensitivity simulations., Atmospheric Pollution Research, 2, 2011.

Lobo, P., Hagen, D. E., and Whitefield, P. D.: Measurement and analysis of aircraft engine PM emissions downwind of an active runway at the Oakland International Airport, Atmospheric Environment, 61, 114–123, 2012.

Miracolo, M., Hennigan, C., Ranjan, M., Nguyen, N., Gordon, T., Lipsky, E., Presto, A., Donahue, N., and Robinson, A.: Secondary aerosol formation from photochemical aging of aircraft exhaust in a smog chamber, Atmospheric Chemistry and Physics, 11, 4135–4147, 2011.

Miracolo, M. A., Drozd, G. T., Jathar, S. H., Presto, A. A., Lipsky, E. M., Corporan, E., and Robinson, A. L.: Fuel composition and secondary organic aerosol formation: Gas-turbine exhaust and alternative aviation fuels, Environmental Science & Technology, 46, 8493–8501, 2012.

Morris, R. E., Koo, B., Guenther, A., Yarwood, G., McNally, D., Tesche, T., Tonnesen, G., Boylan, J., and Brewer, P.: Model sensitivity evaluation for organic carbon using two multi-pollutant air quality models that simulate regional haze in the southeastern United States, Atmospheric

Environment, 40, 4960–4972, 2006.

Moussiopoulos, N., Sahm, P., Karatzas, K., Papalexiou, S., and Karagiannidis, A.: Assessing the impact of the new Athens airport to urban air quality with contemporary air pollution models, Atmospheric Environment, 31, 1497–1511, 1997.

Murphy, B. N. and Pandis, S. N.: Simulating the formation of semivolatile primary and secondary organic aerosol in a regional chemical transport model, Environmental Science & Technology, 43, 4722–4728, 2009.

Murphy, B. N. and Pandis, S. N.: Exploring summertime organic aerosol formation in the eastern United States using a regional-scale budget approach and ambient measurements, Journal of Geophysical Research: Atmospheres, 115, 2010.

Nam, J., Kimura, Y., Vizuete, W., Murphy, C., and Allen, D. T.: Modeling the impacts of emission events on ozone formation in Houston, Texas, Atmospheric Environment, 40, 5329–5341, 2006.

Ng, N., Chhabra, P., Chan, A., Surratt, J., Kroll, J., Kwan, A., McCabe, D., Wennberg, P., Sorooshian, A., Murphy, S., et al.: Effect of NO x level on secondary organic aerosol (SOA) formation from the photooxidation of terpenes, Atmospheric Chemistry and Physics, 7, 5159–5174, 2007a.

Ng, N., Kroll, J., Chan, A., Chhabra, P., Flagan, R., and Seinfeld, J.: Secondary organic aerosol formation from m-xylene, toluene, and benzene, Atmospheric Chemistry and Physics, 7, 3909–3922, 2007b.

Odum, J. R., Hoffmann, T., Bowman, F., Collins, D., Flagan, R. C., and Seinfeld, J. H.: Gas/particle partitioning and secondary organic aerosol yields, Environmental Science & Technology, 30, 2580–2585, 1996.

Offenberg, J. H., Kleindienst, T. E., Jaoui, M., Lewandowski, M., and Edney, E. O.: Thermal properties of secondary organic aerosols, Geophysical Research Letters, 33, 2006.

Offenberg, J. H., Lewis, C. W., Lewandowski, M., Jaoui, M., Kleindienst, T. E., and Edney, E. O.: Contributions of toluene and α-pinene to SOA formed in an irradiated toluene/α-pinene/NO x/air mixture: Comparison of results using 14C content and SOA organic tracer methods, Environmental Science & Technology, 41, 3972–3976, 2007.

Olsen, S., Wuebbles, D., and Owen, B.: Comparison of global 3-D aviation emissions datasets, Atmospheric Chemistry and Physics, 13, 429–441, 2013.

Orville, R. E., Huffines, G. R., Burrows, W. R., Holle, R. L., and Cummins, K. L.: The North American Lightning Detection Network (NALDN)-First Results: 1998-2000, Monthly Weather Review, 130, 2098–2109, 2002.

Pacsi, A. P., Alhajeri, N. S., Zavala-Araiza, D., Webster, M. D., and Allen, D. T.: Regional air quality

impacts of increased natural gas production and use in Texas, Environmental Science & Technology, 47, 3521–3527, 2013.

Pison, I. and Menut, L.: Quantification of the impact of aircraft traffic emissions on tropospheric ozone over Paris area, Atmospheric Environment, 38, 971–983, 2004.

Presto, A. A., Miracolo, M. A., Kroll, J. H., Worsnop, D. R., Robinson, A. L., and Donahue, N. M.: Intermediate-volatility organic compounds: A potential source of ambient oxidized organic aerosol, Environmental Science & Technology, 43, 4744–4749, 2009.

Presto, A. A., Nguyen, N. T., Ranjan, M., Reeder, A. J., Lipsky, E. M., Hennigan, C. J., Miracolo, M. A., Riemer, D. D., and Robinson, A. L.: Fine particle and organic vapor emissions from staged tests of an in-use aircraft engine, Atmospheric Environment, 45, 3603–3612, 2011.

Pye, H. O. and Seinfeld, J. H.: A global perspective on aerosol from low-volatility organic compounds, Atmospheric Chemistry and Physics, 10, 4377–4401, 2010.

Ratliff, G., Sequeira, C., Waitz, I., Ohsfeldt, M., Thrasher, T., Graham, G., Thompson, T., Graham, M., and Thompson, T.: Aircraft Impacts on Local and Regional Air Quality in the United States, PARTNER Project 15 Final Report, http://web.mit.edu/aeroastro/partner/reports/proj15/proj15finalreport.pdf, 2009.

Rienecker, M. M., Suarez, M. J., Gelaro, R., Todling, R., Bacmeister, J., Liu, E., Bosilovich, M. G., Schubert, S. D., Takacs, L., Kim, G.-K., et al.: MERRA: NASA's modern-era retrospective analysis for research and applications, Journal of Climate, 24, 3624–3648, 2011.

Rissman, J., Arunachalam, S., Woody, M., West, J., BenDor, T., and Binkowski, F.: A plume-in-grid approach to characterize air quality impacts of aircraft emissions at the Hartsfield-Jackson Atlanta International Airport, Atmospheric Chemistry and Physics, 13, 2013.

Robinson, A. L., Donahue, N. M., Shrivastava, M. K., Weitkamp, E. A., Sage, A. M., Grieshop, A. P., Lane, T. E., Pierce, J. R., and Pandis, S. N.: Rethinking organic aerosols: Semivolatile emissions and photochemical aging, Science, 315, 1259–1262, 2007.

Rollins, A., Browne, E., Min, K.-E., Pusede, S., Wooldridge, P., Gentner, D., Goldstein, A., Liu, S., Day, D., Russell, L., et al.: Evidence for NOx control over nighttime SOA formation, Science, 337, 1210–1212, 2012.

Schell, B., Ackermann, I. J., Hass, H., Binkowski, F. S., and Ebel, A.: Modeling the formation of secondary organic aerosol within a comprehensive air quality model system, Journal of Geophysical Research. D. Atmospheres, 106, 28, 2001.

Schürmann, G., Schäfer, K., Jahn, C., Hoffmann, H., Bauerfeind, M., Fleuti, E., and Rappenglück, B.: The impact of NO_x, CO and VOC emissions on the air quality of Zurich airport, Atmospheric Environment, 41, 103–118, 2007.

Shrivastava, M., Fast, J., Easter, R., Gustafson Jr, W., Zaveri, R. A., Jimenez, J. L., Saide, P., and

Hodzic, A.: Modeling organic aerosols in a megacity: comparison of simple and complex representations of the volatility basis set approach, Atmospheric Chemistry and Physics, 11, 6639–6662, 2011.

Sisler, J. F. and Malm, W. C.: Interpretation of Trends of PM25 and Reconstructed Visibility from the IMPROVE Network, Journal of the Air & Waste Management Association, 50, 775–789, 2000.

Skamarock, W. C. and Klemp, J. B.: A time-split nonhydrostatic atmospheric model for weather research and forecasting applications, Journal of Computational Physics, 227, 3465–3485, 2008.

Stettler, M., Eastham, S., and Barrett, S.: Air quality and public health impacts of UK airports. Part I: Emissions, Atmospheric Environment, 45, 5415–5424, 2011.

Tarrasón, L., Jonson, J. E., Berntsen, T. K., and Rypdal, K.: Study on air quality impacts of non-LTO emissions from aviation, Norwegian Meteorological Institute, 2004.

Timko, M. T., Knighton, W. B., Herndon, S. C., Wood, E. C., Onasch, T. B., Northway, M. J., Jayne, J. T., Canagaratna, M. R., and Miake-Lye, R. C.: Gas turbine engine emissionspart I: volatile organic compounds and nitrogen oxides, Journal of Engineering for Gas Turbines and Power, 132, 061 504, 2010.

Timko, M. T., Albo, S. E., Onasch, T. B., Fortner, E. C., Yu, Z., Miake-Lye, R. C., Canagaratna, M. R., Ng, N. L., and Worsnop, D. R.: Composition and Sources of the Organic Particle Emissions from Aircraft Engines, Aerosol Science and Technology, 48, 61–73, 2014.

Unal, A., Hu, Y., Chang, M. E., Talat Odman, M., and Russell, A. G.: Airport related emissions and impacts on air quality: Application to the Atlanta International Airport, Atmospheric Environment, 39, 5787–5798, 2005.

U.S. Department of Transportation: Freight in America: A New National Picture, Research and Innovative Technology Administration, Bureau of Transportation Statistics, 2006.

U.S. Department of Transportation: Transportations role in reducing US greenhouse gas emissions, US Department of Transportation, Washington, DC, http://ntl.bts.gov/lib/32000/32700/32779/DOT_Climate_Change_Report_-_April_2010_-_Volume_1_and_2.pdf, 2010.

U.S. Environmental Protection Agency: New Emission Standards for New Commercial Aircraft Engines , EPA420-F-05-015, 2005.

U.S. Environmental Protection Agency: Air Trends: Particulate Matter, http://www.epa.gov/airtrends/pm.html, 2013.

U.S. Environmental Protection Agency: Evaluation of Air Pollutant Emissions from Subsonic Commercial Jet Aircraft, EPA420-R-99-013, http://www.epa.gov/oms/regs/nonroad/aviation/r99013.pdf, 1999.

U.S. Environmental Protection Agency: 2002 National Emission Inventory, http://www.epa.gov/ttn/

chief/net/2002inventory.html, 2004.

U.S. Environmental Protection Agency: 2005 National Emission Inventory, http://www.epa.gov/ttn/chief/net/2005inventory.html, 2007.

U.S. Environmental Protection Agency: Recommended Best Practice for Quantifying Speciated Organic Gas Emissions from Aircraft Equipped with Turbofan, Turbojet, and Turboprop Engines, EPA-420-R-09901, 2009a.

U.S. Environmental Protection Agency: Aircraft Engine Speciated Organic Gases: Speciation of Unburned Organic Gases in Aircraft Exhaust, EPA-420-R-09902, 2009b.

Volkamer, R., Jimenez, J. L., San Martini, F., Dzepina, K., Zhang, Q., Salcedo, D., Molina, L. T., Worsnop, D. R., and Molina, M. J.: Secondary organic aerosol formation from anthropogenic air pollution: Rapid and higher than expected, Geophysical Research Letters, 33, 2006.

Wayson, R. L., Fleming, G. G., and Iovinelli, R.: Methodology to estimate particulate matter emissions from certified commercial aircraft engines, Journal of the Air & Waste Management Association, 59, 91–100, 2009.

Wilkerson, J., Jacobson, M. Z., Malwitz, A., Balasubramanian, S., Wayson, R., Fleming, G., Naiman, A., and Lele, S.: Analysis of emission data from global commercial aviation: 2004 and 2006, Atmospheric Chemistry and Physics, 10, 6391–6408, 2010.

Wong, H.-W., Yelvington, P. E., Timko, M. T., Onasch, T. B., Miake-Lye, R. C., Zhang, J., and Waitz, I. A.: Microphysical modeling of ground-level aircraft-emitted aerosol formation: Roles of sulfur-containing species, Journal of Propulsion and Power, 24, 590–602, 2008.

Wood, E. C., Herndon, S. C., Timko, M. T., Yelvington, P. E., and Miake-Lye, R. C.: Speciation and chemical evolution of nitrogen oxides in aircraft exhaust near airports, Environmental science & technology, 42, 1884–1891, 2008.

Woody, M., Baek, B. H., Adelman, Z., Omary, M., Lam, Y. F., West, J. J., and Arunachalam, S.: An assessment of Aviations contribution to current and future fine particulate matter in the United States, Atmospheric Environment, 45, 3424–3433, 2011.

Woody, M., West, J. J., Jathar, S., Robinson, A. L., and Arunachalam, S.: Estimates of Non-traditional Secondary Organic Aerosols from Aircraft SVOC and IVOC Emissions Using CMAQ, Atmospheric Chemistry and Physics Discussions, 14, 30667-30703, 2014.

Woody, M. C. and Arunachalam, S.: Secondary Organic Aerosol Produced from Aircraft Emissions at the Atlanta Airport: An Advanced Diagnostic Investigation Using Process Analysis, Atmospheric Environment, 2013.

Xu, J., Zhang, Y., Fu, J. S., Zheng, S., and Wang, W.: Process analysis of typical summertime ozone

episodes over the Beijing area, Science of the Total Environment, 399, 147–157, 2008.

Yarwood, G., Rao, S., Yocke, M., and Whitten, G. Z.: Updates to the Carbon Bond chemical mechanism: CB05, ENVIRON International Corporation, Novato, CA, 2005.

Yim, S. H., Stettler, M. E., and Barrett, S. R.: Air quality and public health impacts of UK airports. Part II: Impacts and policy assessment, Atmospheric Environment, 67, 184–192, 2013.

Yu, S., Mathur, R., Schere, K., Kang, D., Pleim, J., Young, J., Tong, D., Pouliot, G., McKeen, S. A., and Rao, S.: Evaluation of real-time $PM_{2.5}$ forecasts and process analysis for $PM_{2.5}$ formation over the eastern United States using the Eta-CMAQ forecast model during the 2004 ICARTT study, Journal of Geophysical Research: Atmospheres, 113, 2008.

Zhang, Q., Jimenez, J. L., Canagaratna, M. R., Allan, J. D., Coe, H., Ulbrich, I., Alfarra, M. R., Takami, A., Middlebrook, A. M., Sun, Y. L., Dzepina, K., Dunlea, E., Docherty, K., DeCarlo, P. F., Salcedo, D., Onasch, T., Jayne, J. T., Miyoshi, T., Shimono, A., Hatakeyama, S., Takegawa, N., Kondo, Y., Schneider, J., Drewnick, F., Borrmann, S., Weimer, S., Demerjian, K., Williams, P., Bower, K., Bahreini, R., Cottrell, L., Griffin, R. J., Rautiainen, J., Sun, J. Y., Zhang, Y. M., and Worsnop, D. R.: Ubiquity and dominance of oxygenated species in organic aerosols in anthropogenically-influenced Northern Hemisphere midlatitudes, Geophysical Research Letters, 34, 2007.

Zhu, Y., Fanning, E., Yu, R. C., Zhang, Q., and Froines, J. R.: Aircraft emissions and local air quality impacts from takeoff activities at a large International Airport, Atmospheric Environment, 45, 6526–6533, 2011.